UNIVERSIDADE DE SÃO PAULO
INSTITUTO DE FÍSICA DE SÃO CARLOS

João Carlos de Andrade Getelina

A compilation of studies on random systems:

measurements of correlation functions and localization properties

São Carlos

2021

João Carlos de Andrade Getelina

A compilation of studies on random systems:

measurements of correlation functions and localization properties

Thesis presented to the Graduate Program in Physics at the Instituto de Física de São Carlos da Universidade de São Paulo, to obtain the degree of Doctor in Science.

Concentration area: Basic Physics

Advisor: Prof. Dr. José Abel Hoyos Neto

Original version

São Carlos

2021

Getelina, João Carlos de Andrade
A compilation of studies on random systems: measurements of correlation functions and localization properties / João Carlos de Andrade Getelina; advisor José Abel Hoyos Neto -- São Carlos 2021.
69 p.

Thesis (Doctorate - Graduate Program in Basic Physics) -- Instituto de Física de São Carlos, Universidade de São Paulo - Brasil , 2021.

1. Random systems. 2. Critical behavior. 3. Numerical methods. I. Hoyos Neto, José Abel, advisor. II. Title.

FOLHA DE APROVAÇÃO

João Carlos de Andrade Getelina

Tese apresentada ao Instituto de Física de São Carlos da Universidade de São Paulo para obtenção do título de Doutor em Ciências. Área de Concentração: Física Teórica e Experimental.

Aprovado(a) em: 15/03/2021

Comissão Julgadora

Dr(a). José Abel Hoyos Neto

Instituição: (IFSC/USP)

Dr(a). André de Pinho Vieira

Instituição: (IF/USP)

Dr(a). Tobias Micklitz

Instituição: (CBPF/Rio de Janeiro)

Dr(a). Ricardo Luís Doretto

Instituição: (UNICAMP/Campinas)

Dr(a). Leonardo Paulo Maia

Instituição: (IFSC/USP)

ACKNOWLEDGEMENTS

This work came to fruition thanks to the great tutoring by my advisor Dr. José Abel Hoyos Neto, and also by my internship supervisor Dr. Thomas Vojta. Their remarkable knowledge of physics, allied with an eagerness to explain and assist, have been defining to my maturing as a scientist. I also thank Dr. Martin Puschmann for his fundamental help in the development of part of this work.

Despite not being directly involved in the making of this thesis, I would like to thank my parents Luiz Darci Getelina and Maria Joana Machado de Andrade, and my wife Alessandra Marjorie Schon, who were always there to provide emotional support. I also show gratitude to my truest friends Matheus de Oliveira Schossler and Rogério Capobianco. In addition, I thank my friends who live in the USA, Eric and Amanda Ansley (and also the boys Graham, Lleyton and Sutton), Alireza, and Mahla, for making my internship abroad much more enjoyable.

Lastly, I would also like to show my gratitude to IFSC and its employees for providing everything I needed for my work, and to CAPES for the financial support.

ABSTRACT

GETELINA, J. C. A. **A compilation of studies on random systems:** measurements of correlation functions and localization properties. 2021. 69p. Thesis (Doctor in Science) - Instituto de Física de São Carlos, Universidade de São Paulo, São Carlos, 2021.

We present a collection of studies about several properties of two random systems, namely (*i*) the random one-dimensional spin-1/2 chain, and (*ii*) the random two-dimensional Bose-Hubbard model. In study (*i*), we consider two variants of random spin chains: the usual case with uncorrelated random couplings, and the correlated case, in which the even and odd sublattices are identical to each other. Using the Jordan-Wigner transformation, we map the spin-1/2 chain Hamiltonian into a noninteracting fermionic model. On this new basis, we perform an exact diagonalization routine, which allows us to compute spin-spin correlation functions and related observables. Our results are presented here as a reproduction of two published papers. In the first one, we measure entanglement properties and the violation of Bell inequalities. We show that the correlated case does not violate the Bell inequality up to a small degree of randomness, thus contradicting the prior belief that any amount of disorder should lead to a violation of Bell inequalities and, equivalently, the existence of nonlocal states. In the second paper, we confirm the strong-disorder renormalization group predictions about the scaling of spin-spin correlation functions for the uncorrelated disorder case. We show that results suggesting a possible correction to the scaling function may be consequence of either a lack of numerical precision or a relatively large crossover length. In addition, we show that much of the nonuniversal properties of the spin-spin correlation functions can be understood from a single parameter scaling perspective. In study (*ii*), we consider the two-dimensional Bose-Hubbard model with disorder introduced either as random site dilution or as onsite interactions generated from a uniform probability distribution. We investigate the localization properties of collective modes by employing a multifractal analysis and a recursive Green's function method. Using a variational mean-field approach, we obtain noninteracting Hamiltonians for the Goldstone (phase) and Higgs (amplitude) modes. Our results show that only the lowest-excitation Goldstone mode undergoes a localization-delocalization transition close to the superfluid-Mott insulator phase transition; higher-excitation phase modes and all amplitude modes remain localized. This behavior is observed for the two types of disorder investigated.

Keywords: Random systems. Critical behavior. Numerical methods.

RESUMO

GETELINA, J. C. A. **Uma coletânea de estudos em sistemas desordenados:** medidas de funções de correlação e propriedades de localização. 2021. 69p. Tese (Doutorado em Ciências) - Instituto de Física de São Carlos, Universidade de São Paulo, São Carlos, 2021.

Apresentamos uma coletânea de estudos sobre diversas propriedades referentes a dois sistemas desordenados, (*i*) a cadeia unidimensional de spin-1/2 desordenada, e (*ii*) o modelo de Bose-Hubbard bidimensional desordenado. No estudo (*i*), nós consideramos duas variantes da cadeia de spin randômica: o caso usual com acoplamentos randômicos descorrelacionados, e o caso correlacionado, em que as sub-redes par e ímpar são idênticas entre si. Utilizando-se da transformação de Jordan-Wigner, nós mapeamos o Hamiltoniano da cadeia de spin-1/2 em um modelo fermiônico não-interagente. Nesta nova base, realizamos uma rotina de diagonalização exata, que nos permite calcular as funções de correlação spin-spin e observáveis relacionados. Nossos resultados são apresentados aqui na forma de reprodução de dois artigos publicados. No primeiro artigo, medimos as propriedades de emaranhamento e a violação das desigualdades de Bell. Nós demonstramos que o caso correlacionado não viola a desigualdade de Bell até um certo grau de desordem pequeno, contradizendo assim a crença anterior de que qualquer grau de desordem deveria ocasionar na violação de desigualdades de Bell e, equivalentemente, a existência de estados não-locais. No segundo artigo, nós confirmamos as previsões do método do grupo de renormalização de desordem forte acerca do escalonamento das funções de correlação spin-spin para o caso com desordem descorrelacionada. Mostramos que resultados sugerindo uma possível correção na função de escala podem ser consequência tanto de uma falta de precisão numérica, como de um comprimento de transição relativamente longo. Além disso, demonstramos que grande parte das propriedades não-universais das funções de correlação spin-spin podem ser compreendidas a partir de um escalonamento de parâmetro único. No estudo (*ii*), consideramos o modelo de Bose-Hubbard bidimensional com desordem introduzida tanto na forma de diluição aleatória de sítios, como na forma de interações no sítio geradas a partir de uma distribuição de probabilidade uniforme. Investigamos as propriedades de localização de modos coletivos através de uma análise multifractal e pelo método da função de Green recursiva. Utilizando-se de um método de campo médio variacional, nós obtemos Hamiltonianos não-interagentes para os modos de Goldstone (fase) e de Higgs (amplitude). Nossos resultados mostram que apenas o modo de Goldstone de energia mais baixa sofre uma transição localização-deslocalização nas proximidades da transição de fase superfluida-isolante de Mott; modos de fase de energia mais alta e todos os modos de amplitude permanecem localizados. Este comportamento é observado para os dois tipos de desordem investigados.

Palavras-chave: Sistemas desordenados. Comportamento crítico. Métodos numéricos.

CONTENTS

1 INTRODUCTION

The numerous discoveries and theories developed over the past century have consolidated condensed matter as one of the major areas of physics. Consequently, the building of such a solid foundation in condensed matter physics (CMP) has led to the publication of many textbooks on the subject.[1–7] However, one feature that most CMP textbooks have in common is the absence of a thorough discussion about a feature responsible for many fascinating phenomena: the introduction of disorder, i.e., impurities or defects, in materials.

One of the main reasons why disordered (or random, interchangeably) systems do not appear in CMP textbooks is the lack of a general analytical theory that can describe them. Introducing randomness breaks translational symmetry, which is the starting point for the vast majority of analytical approaches. Hence, straightforward analytical methods, such as a Fourier transform, become non-applicable to random systems.

Nevertheless, despite the increased challenge, several reasons justify pursuing investigations on disordered systems. The first reason is the ubiquitousness of disorder in materials that are very important in our day-to-day lives. Two of the principal examples are glasses and semiconductor devices. One can find these materials everywhere, in the form of many different applications, and most of their properties are due to the effects of their inherent randomness.[8–14] Glasses and semiconductors, however, differ with respect to the source of disorder: glasses exhibit a so-called structural disorder, while semiconductors have (most of the time) substitutional disorder.

Structural disorder here means a lack of a perfect crystalline structure. Even though glasses are solid materials, their microscopic structure resembles more of a frozen-in liquid; the spacing between neighboring atoms or molecules varies randomly across the system. Semiconductors, on the other hand, usually maintain a perfectly organized microscopic structure, but the atoms forming the crystal lattice are either randomly removed or randomly replaced by a dopant (hence the expression substitutional disorder).

Most of the time, the theory of translationally invariant systems suffices to provide a fair understanding of the physics of many systems. Sometimes, however, experimental observations strongly disagree with the theoretical prediction, thus suggesting an incomplete or utterly wrong theory. In some cases, these inconsistencies can be resolved by introducing randomness to the original translationally invariant theory. Conversely, in other problems, introducing disorder may yield completely novel behavior that could not be anticipated from the original theory.

One relevant phenomenon that could finally be understood thanks to the investiga-

tion of disorder effects is the existence of insulators in noninteracting electronic systems. These systems are commonly described via the so-called tight-binding model. In this model, the system atoms are at fixed sites, and they are represented as sharp potentials that rapidly go to zero as one moves away from the corresponding position. The electrons from the outermost atomic layer are thus bound to these potentials, except that they have a nonzero probability of hopping (i.e., tunneling) to their nearest neighbors. One can solve this problem by casting the so-called Bloch theorem, which takes advantage of the potential periodicity to solve the Schorödinger equation, ultimately obtaining a plane-wave solution for the electron wave function.

However, describing the electrons as plane waves cannot account for the existence of insulators, since these wave functions spread themselves throughout the system and, thus, always lead to a finite conduction from one end of the system to the other. In his seminal paper [Ref. (15)], Anderson has solved this problem by recasting the potentials in the tight-binding model as site-dependent and randomly distributed. Anderson has shown that the introduction of disorder yields a destructive quantum interference in the electronic plane waves, ultimately leading to electrons completely confined (i.e., localized) to a certain region of the system. This phenomenon has become known as Anderson localization, and a series of remarkable works[16–18] have established it as one of the cornerstones of CMP [for reviews see Refs. (19, 20)].

In addition to phenomena that can only be understood under the presence of disorder, the introduction of randomness in some systems can either lead to novel exotic behavior or completely suppress the homogeneous system behavior. This feature is especially true for systems that undergo a quantum phase transition (QPT). Differently from a classical phase transition, a QPT happens at zero temperature, due to the tuning of a given control parameter in the system Hamiltonian. The effects of such phase transitions can, however, be observed at finite temperatures, as long as the energy related to thermal fluctuations do not surpass the typical energy scale of the system.[21,22]

Regarding the effects caused by disorder in QPTs, there are two known criteria, namely the Harris[23] and the Imry-Ma,[24] which tells one whether or not introducing randomness modifies the critical behavior (i.e., the behavior close to a QPT) of a homogeneous system. These elegant criteria can determine the relevance of disorder based solely on the homogeneous system universality class. Each criterion accounts for a different type of disorder; randomness introduced in the kinetic part of the Hamiltonian is dubbed as random mass or random-T_c disorder. This class of disordered systems is subject to the Harris criterion. Conversely, disorder introduced in the potential part of the Hamiltonian is known as random field disorder, and such systems are subject to the Imry-Ma criterion.

As it was aforementioned, the usual analytical methods employed in the study of homogeneous systems are in general inapplicable to random systems. Therefore, another

reason that makes the study of random systems valuable is the urge for developing new methods that may become useful for other problems. An example of an approach developed especially for random systems is the so-called strong-disorder renormalization group (SDRG). This approach was first envisioned by Ma, Dasgupta, and Hu,[25,26] as an alternative method to study random spin chains, based on a real-space renormalization group procedure. However, these early works did not manage to present compelling results.

The SDRG method has shown its full potential only years later, thanks to the important contribution by Fisher.[27–29] In his works, the author shows that the SDRG can be employed analytically to obtain a thorough description of the critical behavior of random spin-1/2 chains. In addition, Fisher shows that the SDRG is asymptotically exact for the random spin-1/2 chain, meaning that the perturbative procedure becomes better and better after each iteration. These results have paved the way for a plethora of investigations about random systems using the SDRG method. Nowadays, it is known that the SDRG can be applied to many different problems,[30,31] even though it had been initially designed for random spin chains only.

Given all the examples above that support the importance of inquiring into random systems problems in CMP, we present here a collection of studies on random systems. More specifically, we address two unrelated systems, namely quasi-one-dimensional spin-1/2 chains, and the two-dimensional random Bose-Hubbard model. For each system, we employ a different approach, as outlined in the following. The overall idea is, however, that we start from a strongly-interacting problem and simplify it to a noninteracting one, either exactly or approximately. In addition, both systems exhibit only random-T_c disorder, with the random variables being independent of time (i.e., quenched disorder) — making the random variables time-dependent (i.e., annealed disorder) in general diminishes the effects of disorder.

Chapter 2 contains a reproduction of three works regarding the aforementioned random systems. The first two papers concern the critical properties of random XX spin-1/2 chains. (The XX here means that the spins are coupled only in the xy plane, with the same coupling strength in both directions.) In both papers, we compare the behavior of two variants of the random spin chain model, namely the usual model with an uncorrelated disorder, and the correlated disorder case. In the latter, the random couplings are introduced such that the odd and even sublattices are identical to each other. Our interest in the correlated disorder case relies on previous investigations that have shown that this system exhibits unusual critical behavior, sharing many features with the homogeneous case up to a small disorder threshold.[32,33]

The first paper presented in Chapter 2 covers a topic in which CMP overlaps with quantum information theory: measurements of entanglement and nonlocality. We show in this work that not any amount of disorder in spin chains leads to a violation of a

Bell inequality and, consequently, to nonlocality, contrasting to what has been previously accepted. This observation is, however, only valid for the correlated disorder case.

The measurements performed in the second paper do not change significantly from the first one, as spin-spin correlation functions are related to entanglement and nonlocality measurements. The second work, however, focuses more on validating our current understanding of the random spin-1/2 chain ground state. Most of the results obtained from the SDRG method rely on the picture of the system ground state as a collection of arbitrarily spaced singlets, which has been dubbed as the random-singlet phase. However, recent quantum Monte Carlo results question the SDRG predictions about spin-spin correlation functions,[34] thus suggesting that the random-singlet phase may not be the correct picture. We confront these quantum Monte Carlo results with high-precise measurements of the spin-spin correlation functions for relatively large systems. We also show that much of the nonuniversal properties of the spin-spin correlation functions can be understood via a single parameter scaling theory.

In the third and last work of Chapter 2, we significantly change the scope as we investigate the so-called random Bose-Hubbard model (BHM). This model is known for describing the much sought-after superfluid-Mott insulator phase transition. Moreover, this system can also be realized experimentally, e.g., with ultracold atoms trapped in optical lattices. The importance of the BHM is also noted in the numerous results available in the literature; much of these results, however, concern only the physics of the homogeneous system.

Recently, a new variational mean-field approach has been proposed as an alternative way to study the BHM.[35,36] This new method is particularly compelling because it is also applicable to the random case. Preliminary work on the random BHM employed this mean-field approach to study the localization properties of collective modes in such systems.[37] This study has shown that the apparent lack of well-defined collective modes, according to Monte Carlo measurements in a closely related model, is due to the strong localization of these modes. Our goal in the third paper of Chapter 2 is to extend the results reported in Ref. (37), by providing a more detailed analysis of the localization properties of the collective modes.

Finally, in Chapter 3 we discuss some of the main implications of our findings in the papers reproduced in Chapter 2. We also pinpoint the questions that are still to be answered, as well as indicating what would be interesting to address in future works.

2 COPY OF ARTICLES

Physics Letters A 382 (2018) 2799–2804

Contents lists available at ScienceDirect

Physics Letters A

www.elsevier.com/locate/pla

Violation of the Bell inequality in quantum critical random spin-1/2 chains

João C. Getelina [a,*], Thiago R. de Oliveira [b], José A. Hoyos [a]

[a] Instituto de Física de São Carlos, Universidade de São Paulo, CP 369, 13560-970, São Carlos, SP, Brazil
[b] Instituto de Física, Universidade Federal Fluminense, 24210-346, Niterói, RJ, Brazil

ARTICLE INFO

Article history:
Received 30 April 2018
Received in revised form 1 August 2018
Accepted 3 August 2018
Available online 9 August 2018
Communicated by A. Eisfeld

Keywords:
Disordered systems
Spin chains
Entanglement
Nonlocality

ABSTRACT

We investigate the entanglement and nonlocality properties of two random XX spin-1/2 critical chains, in order to better understand the role of breaking translational invariance to achieve nonlocal states in critical systems. We show that breaking translational invariance is a necessary but not sufficient condition for nonlocality, as the random chains remain in a local ground state up to a small degree of randomness. Furthermore, we demonstrate that the random dimer model does not have the same nonlocality properties of the translationally invariant chain, even though they share the same universality class for a certain range of randomness.

1. Introduction

The use of quantum information tools in condensed matter systems has become widespread, mostly because of their usefulness for a better understanding of the behavior of quantum critical ground states (for a review, see Ref. [1]). Currently, entanglement and nonlocality measurements are under intensive scrutiny since they have shown to be able to signal quantum phase transitions[1] (QPTs) in many-body systems [2–10]. Even though these concepts are frequently associated with each other, it has been shown that they are indeed distinct by the construction of entangled mixed states which do not violate Bell-like inequalities[2] [11]. In addition, finding nonlocal states in many-body systems is of major interest, bearing in mind the many interesting applications of nonlocal states, such as to cryptography [12] and to the generation of random numbers [13].

Although it was observed that nonlocality measures may point out QPTs, it is far from clear what is the relation between nonlocality and QPTs. For instance, a recent study [14] has shown that due to monogamy and translational invariance, any mixed state of a spin pair of the critical XXZ spin-1/2 chain is a local state, i.e., any spin pair does not violate the Bell inequality (even though they can be in an entangled mixed state). This conclusion led us to inquire whether, generically, a critical state is always local.

Therefore, we consider here two different spin-1/2 chains with randomly generated coupling constants. By introducing randomness, we are able to break translational invariance without driving the system out of criticality. In one these random models, the critical state belongs to the so-called infinite-randomness universality class [15]. In this case, when the degree of inhomogeneities is very large, there are spin pairs in nearly Bell-like (singlet) states [16] which become strong candidates to violate the Bell inequality. In the other model, the corresponding universality class is of finite-disorder type. It was shown that the corresponding ground state has many similarities with the one of the translationally invariant case, such as sharing the same set of critical exponets (i.e., belonging to the same universality class) below a certain degree of randomness [17,18]. It is then much less clear whether the Bell inequality is violated or not.

We have shown here that the Bell inequality is violated in both cases, if the degree of randomness is greater than a certain amount (which we have determined). Moreover, for the case in the infinite-randomness universality class, the spin pairs violating the Bell inequality can be widely separated, while for the finite-disorder case only nearest-neighbor spin pairs may be in nonlocal states. The most striking result is that the second model exhibits

* Corresponding author.
E-mail address: getelina@ifsc.usp.br (J.C. Getelina).

[1] This is understood as a consequence of entanglement and nonlocality (as well as discord) inheriting the nonanalytic behavior at the critical point from the usual spin-spin correlation functions.

[2] When we refer to Bell inequalities or Bell-like inequalities we have in mind the original Bell inequality and the CHSH inequality (see Sec. 3).

https://doi.org/10.1016/j.physleta.2018.08.003
0375-9601/

nonlocality even when it belongs to the same universality class of the translationally invariant case (which was shown to be local).

The remainder of this paper is structured as follows: in Sec. 2 we present our random models, emphasizing the differences between them. In Sec. 3 we define and describe how to obtain the entanglement and nonlocality measurements. Sec. 4 presents our numerical results, which are further discussed in Sec. 5 and followed by perspectives of future studies and applications.

2. The random uncorrelated and correlated XX spin-1/2 models

Here, we introduce the two studied models, which are special cases of the disordered XXZ spin-1/2 chain [19,20]. This model is described by the Hamiltonian

$$H = \sum_{i=1}^{L} J_i \left(S_i^x S_{i+1}^x + S_i^y S_{i+1}^y + \Delta_i S_i^z S_{i+1}^z \right), \tag{1}$$

where S_i^α are the usual spin-1/2 operators, $J_i > 0$ are the coupling constants, Δ_i are the anisotropy parameters and L is the chain size which we will assume to be even. In addition, we will consider periodic boundary conditions: $\mathbf{S}_{i+L} = \mathbf{S}_i$.

In the translationally symmetric case ($J_i = J$ and $\Delta_i = \Delta$) the system is critical for $-1 \leq \Delta \leq 1$ and it is described as an exotic Tomonoga-Luttinger spin liquid state [21], which is a highly entangled [1] but local state, i.e., any spin pair does not violate the Bell inequality [3,14].

Conversely, in the uncorrelated random case (J_i and Δ_i being uncorrelated and identically distributed random variables) the system is described as a critical random singlet state for $-1/2 < \Delta_i \leq 1$ [15,22] in which spin pairs can be highly entangled in nearly singlet states [16,23–25], as depicted in Fig. 1. Remarkably, it was shown that this state is universal, in the sense that all of its low-energy critical properties do not depend on (i) the details of the random variables, provided that the width of their distribution is not zero and not unphysically large, and on (ii) the system anisotropy, provided that $-1/2 < \Delta_i \leq 1$.

For this reason, we here restrict our study to the case known as the XX model, in which $\Delta_i = 0$, $\forall i$. Another reason for our choice is due to the existence of a mapping between the XX chain and the tight-biding model of free spinless fermions [26], which allows us to study considerably large chains via the exact diagonalization of the Hamiltonian (1). Finally, it is plausible that our conclusions for the XX model also extend to the XXZ model in the critical random-singlet region $-1/2 < \Delta_i \leq 1$ because, in this region, the ground state of the random XXZ chain depends very weakly on the values of the local anisotropies Δ_i, thus exhibiting the symmetry properties of the SU(2) symmetric Heisenberg model $\Delta_i = 1$ [27].

In our study, we draw the random couplings from a power-law like probability density distribution

$$P(J) = D^{-1} J^{\frac{1}{D}-1}, \tag{2}$$

where $0 < J < 1$. Here, $D \geq 0$ parameterizes the disorder strength, with $D = 0$ recovering the translationally invariant case. The probability distribution (2) is a natural choice as it allows us to assess a wide range of disorder strength by varying the parameter D. Moreover, this probability distribution also coincides with the one of the infinite-randomness fixed point, which governs the critical behavior of the system [15]. Nonetheless, for the sake of completeness, we have also considered the case of box-like distributions, i.e.,

$$P(J) = \begin{cases} 1, & \text{for } J_{\min} < J < 1 \\ 0, & \text{otherwise} \end{cases} \tag{3}$$

In this case, $J_{\min}$ parameterizes the disorder strength, with smaller $J_{\min}$ meaning stronger disorder.

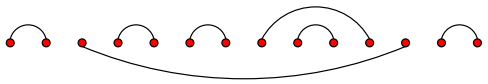

Fig. 1. Representation of the random singlet state where the dots are spins in a regular lattice and the curves connect spin pairs in nearly singlet states.

We now introduce our second model: the random correlated XX spin-1/2 chain. The difference with respect to our first model is that instead of considering an uncorrelated sequence of random couplings $\{J_1, J_2, \ldots, J_L\}$, we consider the special sequence of couplings $\{J_1, J_1, J_2, J_2, \ldots, J_{L/2}, J_{L/2}\}$. Our interest in this special model is because it was recently shown that short-range correlations among the random exchange couplings J_i (e.g., the one we are considering here, $J_{2i} = J_{2i-1}$) can dramatically change the low-energy properties of the XX spin-1/2 chain [17,18,28]. For instance, the ground state of the random correlated model is completely unrelated to the random-singlet state of the uncorrelated one; in fact, it even shares many similarities with the ground state of the translationally invariant case. For $0 \leq D \leq D_c$, the ground-state bipartite (block) entanglement and the low-energy thermodynamics are practically identical to those of the translationally invariant system [18]. Only for $D > D_c \approx 0.3$ these quantities become distinct with, surprisingly, the (block) entanglement entropy increasing with the disorder strength D (and being greater than that of the translationally invariant) [17].

3. Entanglement and violation of Bell inequality

In the strong-disorder limit ($D \gg 1$), it is a good approximation to describe the ground state of (1) (with uncorrelated random couplings) by the random-singlet state (see Fig. 1): a collection of independent singlets. We now would like to test this approximation by measuring how far two spins i and j are from the actual singlet state $|\Psi^-\rangle = (|+-\rangle - |-+\rangle)/\sqrt{2}$. For this reason, we study the so-called fidelity, which is given by

$$F_{ij} = \langle \Psi^- | \rho_{ij} | \Psi^- \rangle, \tag{4}$$

where ρ_{ij} is the ground-state reduce density matrix encoding all the information about the physical state of the two spins i and j. Using the symmetries of the XX spin-1/2 chain Hamiltonian, one can related the fidelity to the ground-state transverse C_{ij}^{xx} and longitudinal C_{ij}^{zz} spin-spin correlation functions [16]:

$$F_{ij} = \frac{1}{4} - 2C_{ij}^{xx} - C_{ij}^{zz}, \tag{5}$$

where $C_{ij}^{\alpha\alpha} = \langle S_i^\alpha S_j^\alpha \rangle = \mathrm{Tr}(\rho_{ij} S_i^\alpha S_j^\alpha)$. More importantly, the fidelity is related to the concurrence $\mathcal{C}_{ij}$ (a *bona fide* entanglement measurement [29–31]) via

$$\mathcal{C}_{ij} = \begin{cases} 0, & \text{if } F_{ij} \leq 1/2, \\ 2F_{ij} - 1, & \text{if } F_{ij} > 1/2. \end{cases} \tag{6}$$

Thus, for this model, the fidelity can be used as a entanglement measurement since it is monotonically related to the concurrence, with

$$F_{ij} > 1/2 \tag{7}$$

meaning that the two spins are entangled.

In addition to the entanglement, we also want to verify if the two-spins physical state is nonlocal by violating the Bell inequality $\mathcal{B}_{ij} \leq 2$ [32,33], where the Bell measurement for our model Hamiltonian is simply [3]

$$\mathcal{B}_{ij} = 8\max\left\{\sqrt{2\left(C_{ij}^{xx}\right)^2}, \sqrt{\left(C_{ij}^{xx}\right)^2 + \left(C_{ij}^{zz}\right)^2}\right\}. \tag{8}$$

Moreover, for the XX spin-1/2 chain, we have verified that in all of our calculations $|C_{ij}^{xx}| \geq |C_{ij}^{zz}|$.[3] Hence, the two-spin state is nonlocal whenever

$$\left|C_{ij}^{xx}\right| > \frac{1}{4\sqrt{2}} \approx 0.1768. \tag{9}$$

Notice furthermore that any spin pair which violates the Bell inequality is also entangled, but the reciprocal is not true.

As mentioned before, the nonviolation of the Bell inequality has been shown in the critical translationally invariant XXZ spin-1/2 chain [3]. This property was later understood using the concept of monogamy in translationally invariant systems [14] which, as a result, forbids that a given spin is in a nonlocal state with two neighbors simultaneously. However, the introduction of disorder breaks translational invariance and, consequently, monogamy plays no longer a role.

Finally, in order to gain further insight on the global structure of the entanglement properties of the ground state, we study the monogamy relation $\sum_{j\neq i} \mathcal{C}_{ij}^2 \leq 1$ (for fixed i) [34–36]. Since we are dealing with random models, it is natural to sum over all sites i and thus, we conveniently rewrite the monogamy relation as

$$M = \frac{2}{L}\sum_{i=1}^{L-1}\sum_{j=i+1}^{L} \mathcal{C}_{ij}^2 \leq 1. \tag{10}$$

Closely related to this quantity is the total number of spin pairs violating the Bell inequality Q_{NL}. As shown in Ref. [14], three spins cannot be simultaneously in pairwise nonlocal states. Thus, Q_{NL} cannot be larger than the total number of spin pairs which is also $L/2$. For this reason, we evaluate the normalized quantity $2Q_{\mathrm{NL}}/L \leq 1$.

4. Numerical results

In this section, we present our numerical study of the entanglement and nonlocality properties of the two random models introduced in Sec. 2. In both cases, the random XX spin-1/2 chains are mapped into free spinless fermions from which we can compute the ground-state transverse and longitudinal spin-spin correlation functions [26]. From these correlation functions, we are then able to compute the fidelity, concurrence, Bell measurement and monogamy, as explained in Sec. 3. Except for the monogamy, due to the lack of translational invariance, these quantities do not acquire a single distance-dependent value. Instead, they are randomly distributed and, for this reason, much more information is gained from their probability density distributions. Therefore, we here compute the corresponding normalized histograms.

We have considered spin chains of sizes $L = 100$ and 200 with periodic boundary conditions and verified that our data are nearly free of finite-size effects. (In most cases, we have also checked this result by comparison with chains of size $L = 400$.) For clarity, we will only show the results for $L = 100$. The data were built considering $N = 10^5$ different disorder configurations for all the sizes studied, yielding an statistical error of a few percent.

4.1. Uncorrelated disorder model

We now present our results for the uncorrelated disorder spin-1/2 chain.

[3] Although this assumption seems obvious, we were not able to prove it rigorously. Further numerical inspections indicates that it is true for all cases in which $-1 < \Delta_i < 1$.

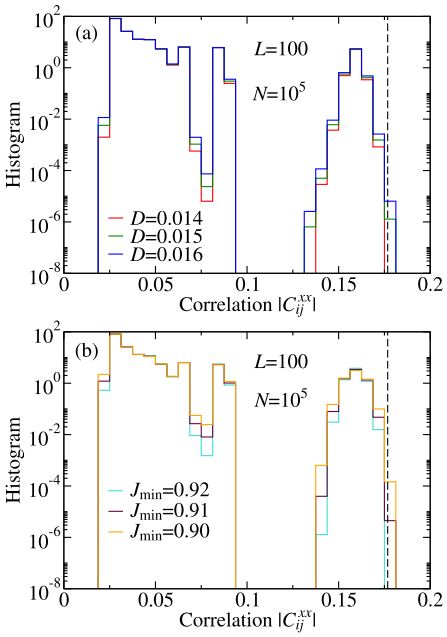

Fig. 2. Normalized histogram of the transverse correlation function C_{ij}^{xx} for all possible spin pairs i and j for the uncorrelated disorder model. In panel (a) the coupling constants are distributed in a power-law fashion [see Eq. (2)] while in panel (b) it is box-like distributed [see Eq. (3)]. The dashed line represents the nonlocality threshold (9).

Our first goal is to investigate the minimum amount of disorder required for the existence of nonlocal states, i.e., spin pairs which violate the Bell inequality. Fig. 2 shows the distribution of all spin pairs transverse correlations C_{ij}^{xx} for the cases in which the couplings are distributed (a) in a power-law (2) and (b) in a box-like fashion. For disorder strength $D < D_{\mathrm{NL}} = 0.015(1)$ (or $J_{\min} > J_{\mathrm{NL}} = 0.91(1)$), with the number in parentheses denoting the statistical error of the last digit, there is no violation of the Bell inequality for any pair, and thus, the state is local as in the translationally invariant case. Conversely, for $D > D_{\mathrm{NL}}$ (or $J_{\min} < J_{\mathrm{NL}}$), we observe spin pairs that do violate the Bell inequality. We then arrive in one of our main results, which is the existence of a nonlocal critical state in disordered systems.

In addition, we would like to highlight one striking feature of the random singlet state (see Fig. 1): the spin pairs in a nonlocal state can be widely separated. In Fig. 3 we show the distributions of fidelities [panel (a)] and transverse correlation functions [panel (b)] for spin pairs widely separated from each other, namely, $|i - j| > L/6$. We verify the existence of entangled pairs and nonlocality for $D > 0.22(1)$ and $D > 0.36(1)$, respectively.

For completeness, we show in Fig. 4 the distribution of the transverse correlations for widely separated spin pairs ($|i - j| > L/6$) for a broader range of disorder strength D. Clearly, the fraction of spin pairs violating the Bell inequality increases with D. This behavior is expected since the random singlet state is known to become a better description of the true ground state in the strong disorder regime [16].

In order to further corroborate this result, we compute the average number of the spin pairs violating the Bell inequality Q_{NL}. In the random singlet state (as sketched in Fig. 1) there are $L/2$ singlet states, and thus, $L/2$ nonlocal spin pairs. Hence, it is expected that $2Q_{\mathrm{NL}}/L \to 1$ in the limit $D \to \infty$, as observed in Fig. 5(a). Likewise, the monogamy relation (10) is expected to saturate in the same limit, which is consistent with our results in Fig. 5(b).

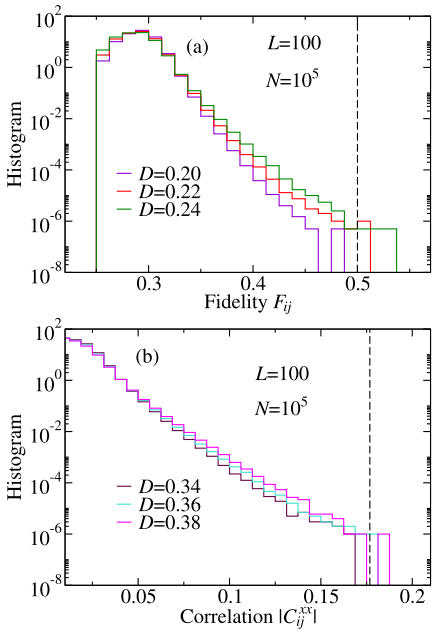

Fig. 3. Normalized histogram of (a) fidelities F_{ij} and (b) transverse correlation C_{ij}^{xx} for the spin pairs $|i-j| > L/6$ for the uncorrelated disorder model. The dashed lines represent the entanglement and nonlocality threshold, Eqs. (7) and (9), respectively.

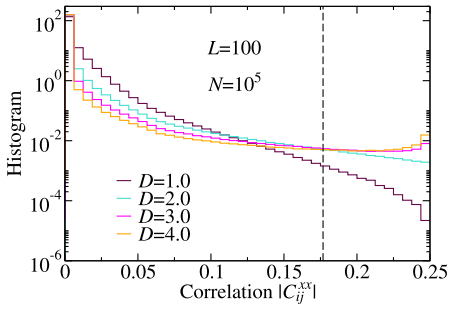

Fig. 4. Same as Fig. 3(b) but for a different set of disorder parameter values D.

4.2. Correlated disorder case

We now present our results for the case in which the couplings constants are correlated random variables appearing in pairs, i.e., the sequence of random coupling constants is $\{J_1, J_1, J_2, J_2, \ldots, J_{L/2}, J_{L/2}\}$, as explained in Sec. 2.

Likewise the random uncorrelated model, we firstly investigate the minimum disorder strength necessary to have nonlocality. As shown in Fig. 6, nonlocality is obtained for $D > D_{\mathrm{NL}}^{*} = 0.037(1)$ and $J < J_{\mathrm{NL}}^{*} = 0.62(1)$ for the cases of power-law [see Eq. (2)] and box-like distributions, respectively. This result is somewhat surprising, since as discussed before, the correlated random case is known to be in the same universality class of the translationally invariant case for $D < D_c \approx 0.3$ [17,18]. However, the translationally invariant case does not have spin pairs in a nonlocal state, which are, in contrast, already observed for the correlated random case with $D_{\mathrm{NL}}^{*} < D < D_c$. Thus, we have a critical model which exhibits nonlocality even though it belongs to same universality class as a system with a local ground state.

We call the attention to the fact that the random correlated and uncorrelated models are fundamentally distinct. In order to see this, we plot in Fig. 7(a) the distribution of fidelities for spin pairs separated by distances ranging from 7 to 13 in the high

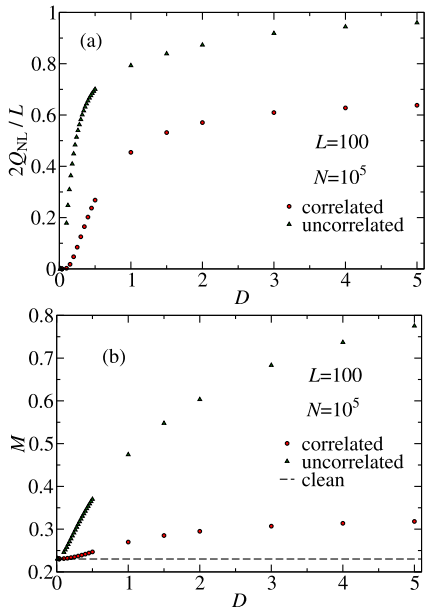

Fig. 5. (a) The average number of spin pairs that violate the Bell inequality Q_{NL} and (b) the monogamy relation for entanglement M as a function of the disorder strength D for both uncorrelated and correlated disordered models. The dashed line is the value for the translationally invariant system (case $D = 0$).

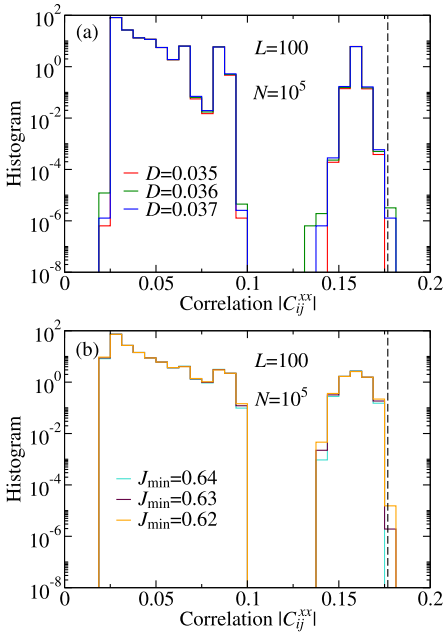

Fig. 6. Normalized histogram of the transverse correlation function C_{ij}^{xx} for all possible spin pairs i and j for the correlated disorder model. In panel (a) the coupling constants are distributed in a power-law fashion [see Eq. (2)] while in panel (b) it is box-like distributed [see Eq. (3)]. The dashed line represents the nonlocality threshold (9).

disordered case $D = 5$. Differently from the random uncorrelated case, only pairs with $|i-j| \leq 9$ are entangled. In Fig. 7(b) we plot, as a function of the disorder strength D, the maximum distance $|i-j|_{\max}$ for entangled spin pairs found among our $N = 10^5$ different chains for all system sizes studied. No entangled spin pair separated by distances greater than 9 was found for any disorder strength.

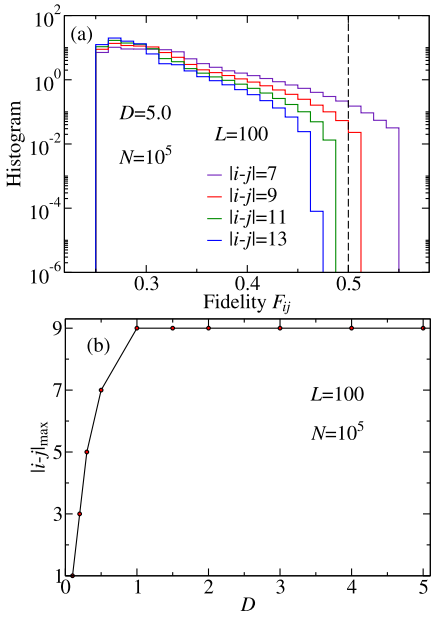

Fig. 7. (a) Normalized histogram of fidelities F_{ij} for the correlated disorder model, considering pairs with separations $|i-j|$ ranging from 7 to 13 and disorder strength $D = 5.0$. The dashed line represents the entanglement threshold (7). (b) The maximum separation for entanglement $|i-j|_{\max}$ as a function of the disorder strength D.

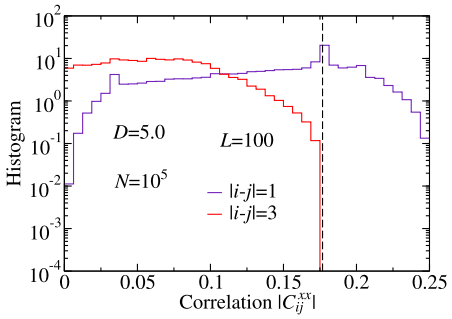

Fig. 8. Normalized histogram of transverse correlation C_{ij}^{xx} for the correlated disorder model, considering only pairs with distance $|i-j| = 1$ and 3 and disorder strength $D = 5.0$. The dashed line represents the nonlocality threshold (9).

In addition, the spin pairs violating the Bell inequality are only the nearest-neighbor ones, as shown in Fig. 8. With these results, there is no doubt about the fundamental difference between the ground states of the correlated and uncorrelated random models.

Finally, we show in Figs. 5(a) and (b) the average number of spin pairs violating the Bell inequality Q_{NL} and the monogamy M [see Eq. (10)] as a function of the disorder strength D, respectively. Although these quantities increase with D, they do not saturate near their corresponding thresholds as in the uncorrelated disorder case.

5. Discussion and conclusion

We have studied the effects of disorder (i.e., spatial inhomogeneities described as random coupling constants) on the pairwise entanglement and nonlocality properties of the ground state of two critical XX spin-1/2 chains. These two chains differ on the nature of the random coupling constants; in one case they are correlated while in the other they are not. We have shown that both random models have spin pairs violating the Bell inequality, which is in contrast with the translationally invariant case, where the interplay with monogamy forbids the violation of Bell inequality. Thus, we have shown that critical random systems can be nonlocal and have determined the minimum amount of disorder necessary. Therefore, it becomes clear that breaking translational invariance is a necessary but not sufficient condition for nonlocality.

We have evaluated the entanglement and nonlocality properties of both random chains for a relatively wide disorder range, considering all possible spin pairs and also fixed distances. As already expected, we have noticed many differences between the uncorrelated and correlated disorder cases. For instance, the former requires less disorder than the latter to have pairs violating the Bell inequality (see Figs. 2 and 6). Moreover, for the uncorrelated case, the spin pairs violating the Bell inequality can be widely separated, while for the correlated case we have shown that only nearest neighbors can be in a nonlocal state (see Fig. 8).

The existence of widely separated nonlocal states for the uncorrelated disorder case can be readily understood as a feature of the random singlet state, which gives a good description of the system ground state in the limit of strong disorder. The random singlet state consists of a collection of $L/2$ arbitrarily spaced singlets (see Fig. 1), where L is the chain length. Thus, as disorder is increased, one could expect the average number of pairs violating the Bell inequality Q_{NL} for the uncorrelated case approaching the maximum value, as it is indeed verified in Fig. 5(a). Furthermore, the monogamy relation (10) exhibits a similar behavior with disorder, as shown in Fig. 5(b), but the saturation takes place only for higher disorder strengths.

However, for the correlated disorder case the system ground state cannot be described by the random singlet state and, thus, the nonlocal states are not widely separated. In fact, for this case we have determined the maximum distances for entangled and nonlocal states, which are $|i-j|_{\max} = 9$ and $|i-j|_{\max} = 1$, respectively. Moreover, the number of pairs violating Bell and the monogamy relation also increase with disorder, but with a saturation value far below the upper bounds. In addition, we would like to call the attention to a rather surprising result: For disorder strength $D_{\mathrm{NL}}^{*} < D < D_{\mathrm{c}} \approx 0.3$, the system has spin pairs in nonlocal states even though it is in the same universality class of the translationally invariant case (i.e., they have the same set of critical exponents), which is known to be local [14]. Thus, critical systems in the same universality class can have different nonlocality properties, which shows that nonlocality is not a universal property.

Finally, nonlocal states were recently found in many-body system of cold-atom system [37,38]. We expect our work to provide a useful reference for future experiments on random spin-1/2 chains.

Acknowledgements

This work was supported by the Brazilian funding agencies CAPES, CNPq, FAPESP, and INCT-IQ.

References

[1] L. Amico, R. Fazio, A. Osterloh, V. Vedral, Rev. Mod. Phys. 80 (2008) 517.
[2] J. Batle, M. Casas, Phys. Rev. A 82 (2010) 062101.
[3] L. Justino, T.R. de Oliveira, Phys. Rev. A 85 (2012) 052128.
[4] D.-L. Deng, C. Wu, J.-L. Chen, S.-J. Gu, S. Yu, C.H. Oh, Phys. Rev. A 86 (2012) 032305.
[5] X. Wang, P. Zanardi, Phys. Lett. A 301 (2002) 1.
[6] Z.-Y. Sun, Y.-Y. Wu, J. Xu, H.-L. Huang, B.-J. Chen, B. Wang, Phys. Rev. A 88 (2013) 054101.
[7] Z.-Y. Sun, S. Liu, H.-L. Huang, D. Zhang, Y.-Y. Wu, J. Xu, B.-F. Zhan, H.-G. Cheng, C.-B. Duan, B. Wang, Phys. Rev. A 90 (2014) 062129.
[8] Z.-Y. Sun, Y.-Y. Wu, J. Xu, H.-L. Huang, B.-F. Zhan, B. Wang, C.-B. Duan, Phys. Rev. A 89 (2014) 022101.
[9] Z.-Y. Sun, Y.-Y. Wu, H.-L. Huang, B. Wang, Solid State Commun. 185 (2014) 30.
[10] H.-L. Huang, Z.-Y. Sun, B. Wang, Eur. Phys. J. B 86 (2013) 279.
[11] R.F. Werner, Phys. Rev. A 40 (1989) 4277.

[12] A.K. Ekert, Phys. Rev. Lett. 67 (1991) 661–663.
[13] S. Pironio, A. Acín, S. Massar, A.B. de la Giroday, D.N. Matsukevich, P. Maunz, S. Olmschenk, D. Hayes, L. Luo, T.A. Manning, C. Monroe, Nature 464 (2010) 1021.
[14] T.R. de Oliveira, A. Saguia, M.S. Sarandy, Europhys. Lett. 100 (2012) 60004.
[15] D.S. Fisher, Phys. Rev. B 50 (1994) 3799.
[16] J.A. Hoyos, G. Rigolin, Phys. Rev. A 74 (2006) 062324.
[17] J.A. Hoyos, N. Laflorencie, A.P. Vieira, T. Vojta, Europhys. Lett. 93 (2011) 30004.
[18] J.C. Getelina, F.C. Alcaraz, J.A. Hoyos, Phys. Rev. B 93 (2016) 045136.
[19] T. Masuda, A. Zheludev, K. Uchinokura, J.-H. Chung, S. Park, Phys. Rev. Lett. 93 (2004) 077206.
[20] A. Macdiarmid, J. Chiang, A. Richter, A. Epstein, Synth. Met. 18 (1987) 285.
[21] T. Giamarchi, Quantum Physics in One Dimension, Clarendon Press, Oxford, 2004.
[22] C.A. Doty, D.S. Fisher, Phys. Rev. B 45 (1992) 2167.
[23] G. Refael, J.E. Moore, Phys. Rev. Lett. 93 (2004) 260602.
[24] N. Laflorencie, Phys. Rev. B 72 (2005) 140408.
[25] J.A. Hoyos, A.P. Vieira, N. Laflorencie, E. Miranda, Phys. Rev. B 76 (2007) 174425.
[26] E. Lieb, T. Schultz, D. Mattis, Ann. Phys. 16 (1961) 407.
[27] V.L. Quito, J.A. Hoyos, E. Miranda, Phys. Rev. Lett. 115 (2015) 167201.
[28] D. Binosi, G. De Chiara, S. Montangero, A. Recati, Phys. Rev. B 76 (2007) 140405.
[29] C.H. Bennett, D.P. DiVincenzo, J.A. Smolin, W.K. Wootters, Phys. Rev. A 54 (1996) 3824.
[30] S. Hill, W.K. Wootters, Phys. Rev. Lett. 78 (1997) 5022.
[31] W.K. Wootters, Phys. Rev. Lett. 80 (1998) 2245.
[32] J.F. Clauser, M.A. Horne, A. Shimony, R.A. Holt, Phys. Rev. Lett. 23 (1969) 880.
[33] R. Horodecki, P. Horodecki, M. Horodecki, Phys. Lett. A 200 (1995) 340.
[34] V. Coffman, J. Kundu, W.K. Wootters, Phys. Rev. A 61 (2000) 052306.
[35] T.J. Osborne, F. Verstraete, Phys. Rev. Lett. 96 (2006) 220503.
[36] T.R. de Oliveira, M.F. Cornelio, F.F. Fanchini, Phys. Rev. A 89 (2014) 034303.
[37] R. Schmied, J.-D. Bancal, B. Allard, M. Fadel, V. Scarani, P. Treutlein, N. Sangouard, Science 352 (2016) 441.
[38] J. Tura, R. Augusiak, A.B. Sainz, T. Vértesi, M. Lewenstein, A. Acín, Science 344 (2014) 1256.

Eur. Phys. J. B (2020) 93: 2
https://doi.org/10.1140/epjb/e2019-100472-7

THE EUROPEAN PHYSICAL JOURNAL B

Regular Article

The correlation functions of certain random antiferromagnetic spin-1/2 critical chains*

João C. Getelina[1,2] and José A. Hoyos[1,a]

[1] Instituto de Física de São Carlos, Universidade de São Paulo, CP 369, 13560-970 São Carlos, SP, Brazil
[2] Department of Physics, Missouri University of Science and Technology, Rolla, MO 65409, USA

Received 30 September 2019 / Received in final form 25 November 2019
Published online 13 January 2020

Abstract. We study the spin-spin correlations in two distinct random critical XX spin-1/2 chain models via exact diagonalization. For the well-known case of uncorrelated random coupling constants, we study the non-universal numerical prefactors and relate them to the corresponding Lyapunov exponent of the underlying single-parameter scaling theory. We have also obtained the functional form of the correct scaling variables important for describing even the strongest finite-size effects. Finally, with respect to the distribution of the correlations, we have numerically determined that they converge to a universal (disorder-independent) non-trivial and narrow distribution when properly rescaled by the spin-spin separation distance in units of the Lyapunov exponent. With respect to the less known case of correlated coupling constants, we have determined the corresponding exponents and shown that both typical and mean correlations functions decay algebraically with the distance. While the exponents of the transverse typical and mean correlations are nearly equal, implying a narrow distribution of transverse correlations, the longitudinal typical and mean correlations critical exponents are quite distinct implying much broader distributions. Further comparisons between these models are given.

1 Introduction

Random quantum spin chains have proved to be a fruitful platform for developing new methodologies and fundamental concepts in condensed matter physics. One of the most successful methods developed so far is the so-called strong-disorder renormalization-group (SDRG) method [1–3], which has been applied to a plethora of random systems (see Refs. [4,5] for reviews). Inherently linked to it is the concept of infinite-randomness fixed points [6,7]. These are critical points in which the statistical fluctuations of local quantities, surprisingly, increase without limits along the renormalization-group flow yielding to an exotic type of activated dynamical scaling. Equally important, due to the unbounded increase of the statistical fluctuations, the SDRG method is believed to exactly capture the universal properties of these fixed points. Finally, it is noteworthy that these fixed points control the phase transitions and critical phases of many quantum, classical and non-equilibrium disordered systems (see Ref. [8] for a review).

In this context, the random antiferromagnetic quantum spin-1/2 chain is a paradigmatic model which for many years has been stimulating theoretical [1,2,7,9–16] and experimental [17–20] studies. For a large range of anisotropies, it is a critical system governed by an infinite-randomness fixed point amenable to many analytical predictions of the SDRG method. A striking one is that the average value spin-spin correlations decays algebraically with the distance $\sim r^{-\eta_\alpha}$ with universal (disorder-independent) isotropic exponent $\eta_x = \eta_z = 2$, while the typical value decays stretched exponentially fast $\sim e^{-\sqrt{r}}$ [7].

Nonetheless, this knowledge is far from satisfactory when compared to the clean chain. Not only the exponents of the leading and subleading terms are know, but also the corresponding numerical prefactors [21–32]. It is the purpose of this work to shorten the knowledge gap between clean and disordered systems by studying non-universal (disorder-dependent) details of the spin-spin correlation functions, such as the numerical prefactors and scaling variables.

Recently, it was discovered that the paradigmatic random antiferromagnetic quantum spin-1/2 chain can also be governed by a line of finite-disorder fixed points when a certain type of correlations are present in the random coupling constants [15,33,34]. This is an exciting result not only because it allows us studying new physical phenomena in a simple and well-known model, but also because the correlations among the disorder variables are the same present in a class of polymers [35–37]. However, unlike the

* Contribution to the Topical Issue "Recent Advances in the Theory of Disordered Systems", edited by Ferenc Iglói and Heiko Rieger.

[a] e-mail: hoyos@ifsc.usp.br

uncorrelated disorder model, much less is known about its average correlation function. Nothing about the typical correlations is known. For this reason, it is also the purpose of this work to study the corresponding critical exponents.

In Section 2, we define the studied models, review further relevant results for our purposes, and provide the methodology of our study. In Sections 3 and 4 we report our results on the correlation functions of the uncorrelated and correlated disordered spin chains, respectively. Finally, we provide further discussions and concluding remarks to Section 5.

2 Models, known results and methods

In this section we define the studied models, review key known results in the literature about the spin-spin correlation functions, and explain our methods.

2.1 Models

The Hamiltonian of the random XXZ spin-1/2 chain is

$$H = \sum_{i=1}^{L} J_i \left(S_i^x S_{i+1}^x + S_i^y S_{i+1}^y + \Delta S_i^z S_{i+1}^z \right), \qquad (1)$$

where S_i^α are spin-1/2 operators, J_i are the random coupling constants, and Δ is the anisotropy parameter. We consider chains of even size L with periodic boundary conditions $S_{i+L}^\alpha = S_i^\alpha$. The coupling constants J_i are realizations of a random variable drawn from the probability distribution

$$P(J) = \begin{cases} \frac{1}{D} J^{\frac{1}{D}-1}, & \text{if } 0 < J < 1 \\ 0, & \text{otherwise.} \end{cases} \qquad (2)$$

Here, the disorder strength is parameterized by $D \geq 0$, with $D = 0$ representing the uniform (clean) system and $D \to \infty$ representing an infinitely disordered system. In addition, we consider the cases of (i) uncorrelated couplings $\overline{J_i J_k} = \overline{J_i} \times \overline{J_k}$ and (ii) perfectly and locally correlated couplings such that the coupling sequence is $\{J_1 J_1 J_2 J_2 \ldots J_{\frac{L}{2}} J_{\frac{L}{2}}\}$, with $\overline{J_i J_k} = \overline{J_i} \times \overline{J_k}$.

Finally, in this work we will consider only the $\Delta = 0$ case.

2.2 Some known results for the case of uncorrelated couplings

For uncorrelated random couplings, the SDRG method predicts that the low-energy critical physics of (1) is governed by an infinite-randomness critical fixed point for $-\frac{1}{2} < \Delta \leq 1$ [7,9]. It is universal in the sense that the corresponding singular behavior does not depend on $P(J)$ provided that $P(J < 0) = 0$ and it is not excessively singular at $J = 0$ [7]. In addition, the method predicts that a good approximation of the corresponding ground state is the random-singlet state (as depicted in Fig. 1) from which much information about the physics can be obtained.

The first one is that spin pairs become locked into SU(2)-symmetric singlet states, and thus, the bare SO(2) symmetry of (1) is enhanced to SU(2). As a consequence, the universal properties of the system become SU(2) isotropic.[1]

Another useful information is related to the distribution of the singlet lengths which decays as $\frac{2}{3} r^{-2}$ [12] for lengths $1 \ll r \ll L$. Since those singlets are strongly correlated, they dominate the (arithmetic average) mean spin-spin correlation function. Thus,

$$\overline{C^{\alpha\alpha}}(r) \equiv \overline{\langle S_i^\alpha S_{i+r}^\alpha \rangle} = \frac{(-1)^r}{12 r^\eta} \times \begin{cases} c_{\mathrm{o},\alpha}, & \text{for } r \text{ odd} \\ c_{\mathrm{e},\alpha}, & \text{for } r \text{ even} \end{cases}, \qquad (3)$$

with universal and isotropic exponent $\eta = 2$, and non-universal and anisotropic multiplicative constants $c_{\mathrm{o,e},\alpha} \geq 0$.[2] Surprisingly, it was conjectured [12] that $c_{\mathrm{o},\alpha} - c_{\mathrm{e},\alpha} = 1$ is universal for α being a symmetry axis, i.e., for $\alpha = z$, and for any α when $\Delta = 1$. (Here, $\langle \cdots \rangle$ and $\overline{\cdots}$ denote the quantum and the disorder averages, respectively.)

The universality of the exponent η was disputed some years ago [41], but there is now a consensus that this is an exact result [10,42–44]. Evidently, numerical confirmations of the constants $c_{\mathrm{e,o},\alpha}$ are much more difficult [12,34].

We note that logarithmic corrections to (3) have been reported in numerical studies for the free-fermion case $\Delta = 0$ [43] in which

$$\overline{C^{xx}} \sim (r^\eta \ln r)^{-1}, \qquad (4)$$

and for the Heisenberg case $\Delta = 1$ [16] in which[3]

$$\overline{C^{\alpha\alpha}} \sim r^{-\eta} \sqrt{\ln r / r_0}. \qquad (5)$$

In contrast, the (geometric average) typical spin-spin correlation function behaves completely different since the spin pairs are weakly coupled in the great majority, as depicted in Figure 1. It was then conjectured [7] that the quantity $r^{-\psi} \overline{\ln \left| \langle S_i^\alpha S_{i+r}^\alpha \rangle \right|}$ converges to a distance-independent distribution. Therefore,

$$C_{\mathrm{typ}}^{\alpha\alpha}(r) \equiv \exp \overline{\ln \left| \langle S_i^\alpha S_{i+r}^\alpha \rangle \right|} \sim \exp\left(-\mathrm{const} \times r^\psi \right), \qquad (6)$$

with universal and isotropic tunneling exponent $\psi = \frac{1}{2}$. This result was confirmed in reference [42] but its dependence with the disorder strength (encoded in the constant prefactor) remains unknown.

[1] This phenomenon of symmetry enhancing is known to be general in random antiferromagnetic SO(N) spin chains exhibiting SU(N) symmetric singular properties [38–40].

[2] For $\Delta = 0$, the longitudinal correlation between spins in the same sublattice vanishes, and thus, $c_{\mathrm{e},z} = 0$ [21].

[3] While the SDRG method have been believed to deliver asymptotic exact results for the XXZ spin chain (1), these numerical results cast some doubts on this belief. As shown latter, our results do not exhibit any logarithmic correction.

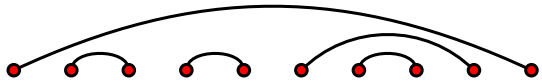

Fig. 1. Schematic of the random-singlet state, which gives the approximate ground state of the Hamiltonian (1) for $-\frac{1}{2} < \Delta \leq 1$, according to the strong-disorder renormalization group method.

2.3 Some known results for the case of correlated couplings

In contrast, for the case of locally correlated couplings (the sequence of couplings being $\{J_1, J_1, J_2, J_2, \ldots J_{\frac{L}{2}}, J_{\frac{L}{2}}\}$) and anisotropy parameter $\Delta = 0$, the physics is quite different [15,33,34].

For weak disorder $D < D_c \approx 0.3$, the critical properties are those of the clean system, i.e., weak disorder is an irrelevant perturbation. Hence, the mean and typical values of the correlation functions are approximately equal, and the corresponding exponents are those of the clean system, i.e., $C^{\alpha\alpha} \approx C^{\alpha\alpha}_{\text{clean}} \sim r^{-\eta_\alpha}$, with $\eta_x = \frac{1}{2}$ and $\eta_z = 2$.

For $D > D_c$, a line of finite-disorder fixed points is tuned and thus the critical exponents vary continuously with the disorder strength [33]. However, in contrast with the infinite-randomness case, we only know that the longitudinal mean correlations decays algebraically with apparently disorder-independent exponent $\eta_z \approx 2$ [34].

We recall that the effects of long-range correlated disorder in closely related systems have been studied in references [45,46]. It was shown that disorder effects are actually enhanced, i.e., the critical theory is of infinite-randomness type accompanied with offcritical enhanced Griffiths singularities. We stress that our correlated disorder has the quite opposite effect [33].

2.4 Methods and further motivations

One of our main goals is to study the non-universal numerical prefactors of the correlation functions. As there is no analytical theory capable of dealing with the clean and random systems on the same footing, we then resort to exact diagonalization of large systems. This is possible only for the $\Delta = 0$ case via the mapping of the Hamiltonian (1) into free spinless fermions [21].

Nonetheless, this is not as simple as it looks. Due to the singularities of strongly disordered systems (namely, large dynamical exponent), we had to use quadruple precision (32 decimal places) in the numerical diagonalization process.

Moreover, regarding the choice of $\Delta = 0$, even though it represents a "non-interacting" system, notice it captures the universal infinite-randomness quantum critical properties (as predicted by the SDRG method) of the entire $-\frac{1}{2} < \Delta < 1$ line, i.e., interactions are RG irrelevant in this range [7]. For the case of correlated couplings, studying the $\Delta = 0$ case is imperative since the finite-disorder character can only be explored for $\Delta = 0$ [34].

Finally, given that the SDRG method is believed to provide exact results concerning the critical singularities of the model (1), it is desirable to investigate large system sizes in order to check the logarithmic corrections mentioned in equations (4) and (5). The motivation for searching them is justified in the early works of homogeneous XXZ spin-1/2 chains [25–27,29–31,47], and also in a recent work of the random XXZ model at $\Delta = -\frac{1}{2}$ [13]. We anticipate that our results are in agreement with (3).

3 Spin–spin correlations for the uncorrelated coupling constants model

We show in this section our results on the (arithmetic average) mean and (geometric average) typical spin-spin correlation functions in the ground state of (1) for $\Delta = 0$ and for uncorrelated disordered coupling constants. We have used quadruple precision (32 decimal places) in order to ensure numerical stability.

3.1 The mean value of the critical correlation function

We start our study with the mean correlation function. All data here presented were averaged over $N = 10^6$ distinct disorder realizations, except for those cases of system size $L = 1\,600$ in which $N = 10^5$.

3.1.1 Longitudinal correlations

In Figure 2, we show $\overline{C^{zz}}$ for fixed system size $L = 800$ and various disorder strengths D in Figure 2a, and fixed $D = 2.0$ and various system sizes L in Figure 2b. The algebraic decay $\overline{C^{zz}} \sim Ar^{-2}$ is identical in both clean and disordered case. The difference is in the numerical prefactor: $A = \pi^{-2}$ in the clean case [21], and is conjectured to be $1/12$ in the disordered case [12]. As we are interested in the long-distance behavior $r \gg \xi_D$ (but not restricted to $r \ll L$), with ξ_D being a clean-disorder crossover length yet to be defined, we then assume that the longitudinal correlation function is

$$\overline{C^{zz}}(r) = -\frac{1}{12}\chi_z(D,r)\left(\ell f_z\left(\frac{r}{L}\right)\right)^{-\eta}, \tag{7}$$

where $\eta = 2$,

$$\ell = \frac{L}{\pi}\sin\left(\frac{\pi r}{L}\right), \tag{8}$$

is the chord length,[4]

$$f_\alpha(x) = 1 + \sum_{n=1}^{\infty} a_{2n,\alpha}\sin^{2n}(\pi x), \tag{9}$$

(with $\alpha = x$ or z) and χ_z is a crossover function which assumes the value $12\pi^{-2}$ in the small separation limit ($r \ll \xi_D$) and converges to 1 otherwise. From Figure 2a, it clearly converges to 1 non-monotonically with respect to D and, from Figure 2b, the convergence happens only after long separations. This non-monotonic behavior can

[4] If the spins were arranged in a circle of perimeter L, then the chord length ℓ is the Euclidean distance between them.

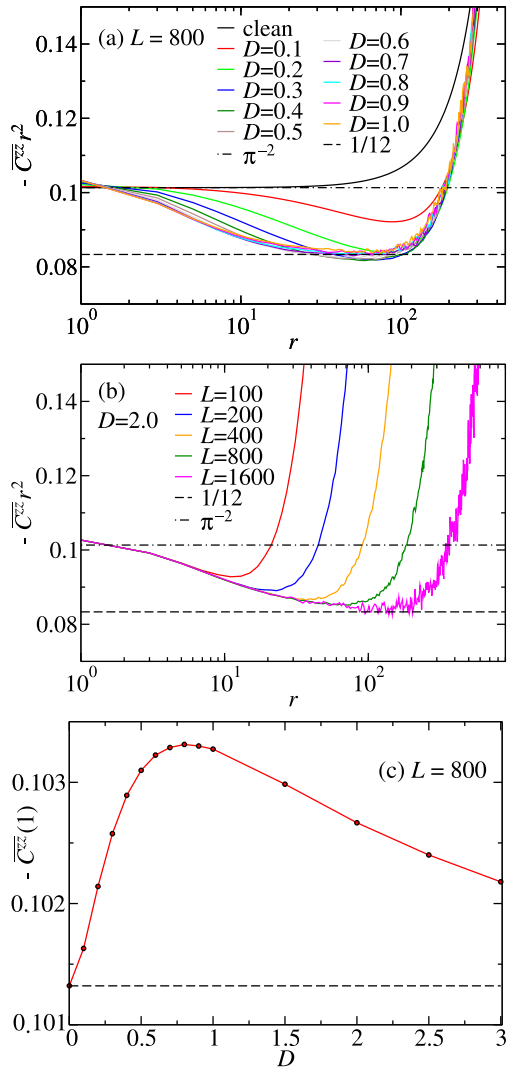

Fig. 2. The mean longitudinal correlation function $\overline{C^{zz}}(r)$ for various chain sizes L and disorder strengths as a function of the separation r in panels (a) and (b), and $\overline{C^{zz}}(r=1)$ for various D and $L = 800$ in panel (c).

be also seen in Figure 2c where the mean correlation for nearest neighbors, $r = 1$, is plotted as a function of D for $L = 800$. Initially it increases (as expected according to the random singlet picture) but then diminishes for larger D. Evidently, this non-monotonic behavior is related to the total spin conservation in the z direction. In other words, χ_z is a non-trivial crossover function and will not be studied here.

In the large separation regime $r \gg \xi_D$, the main dependence of $\overline{C^{zz}}$ on r comes as $\ell f_z\left(\frac{r}{L}\right)$. Simply, it is the most generic function consistent with the periodic boundary conditions: $C(r+L) = C(r)$ and $C(L-r) = C(r)$; with f_z being simply a correction to the chord length ℓ: the true scaling variable in the clean case $C^{zz}_{\text{clean}} = (\pi\ell)^{-2}$.[5]

[5] Corrections to the chord length were reported in the entanglement entropy as well [48].

Throughout this work, we assume that the coefficients $a_{2n,\alpha}$ are disorder-independent. There is no reason why this should be the case. Our assumption, however, is compatible with our numerical data. Nonetheless, due to statistical fluctuations and the lack of knowledge on χ_α, we cannot exclude that $a_{2n,\alpha}$ are indeed disorder dependent.

In order to obtain the correction to the chord length, we appropriately replot our data in Figure 3. In Figure 3a, we consider only the largest and strongest disordered chains in order to minimize the effects of the crossover function χ_z, i.e., we have chosen only systems in which χ_z seems to be very close to 1 for a large range of separations r. All data collapse satisfactorily. Tiny deviations are present which, in principle, are accounted by χ_z. From the collapsed data, we then extract the values of the coefficients $a_{2n,z}$. Best fits using further corrections (up to $a_{8,z}$) do not improve the reduced weighted error sum $\bar{\chi}^2$. Finally, changing the fitting values of $a_{2n,z}$ by 10% does not change appreciably the value of $\bar{\chi}^2$, we then estimate that 10% is the accuracy of our estimates of $a_{2n,z}$.

In Figures 3b and 3c, we plot the square root of the ratio between $-12\overline{C^{zz}}$ and $\left(\ell f_z\left(\frac{r}{L}\right)\right)^{-\eta}$ which should approach 1 provided that f_z is disorder independent. In Figure 3b, disorder strength is fixed while L is increased. Larger the system size L, better the data is described by the scaling variable $\ell f_z\left(\frac{r}{L}\right)$. Deviations for smaller L are due to the crossover function χ_z. In Figure 3c, the system size is fixed while D is changed. Notice the little dependence on D (for large L and the disorder strengths considered). Notice furthermore the non-monotonic behavior of χ_z with D. The convergence to the unity is faster for intermediate disorder $D \approx 1.0$.

3.1.2 Transverse correlations

The study of the mean transverse correlation function $\overline{C^{xx}}(r)$ is much more involving since (i) it is more numerically demanding,[6] (ii) there is no knowledge about its numerical prefactor, and, as shown in reference [10], (iii) the clean-disorder crossover length can be so large that even hinders the clear identification of the correct algebraic decay exponent $\eta = 2$ (see Fig. 4). Moreover and interestingly, as clearly seen in Figure 4b, this numerical prefactor is different from odd and even separations r.[7]

As for the longitudinal correlations (7), the natural choice for the mean transverse correlation function is

$$\overline{C^{xx}}(r) = (-1)^r\, c_{D,r}\chi_x(D,r)\left(\ell f_x\left(\frac{r}{L}\right)\right)^{-\eta}, \qquad (10)$$

where $\eta = 2$, and f_x is analogous to f_z in equation (9). Likewise, the crossover function χ_x is expected to be analogous to χ_z, and thus, is a non-trivial function which should be proportional to $\sim r^{3/2}$ in the $r \ll \xi_D$ regime, and converges to 1 otherwise. Here, $c_{D,r}$ represents the numerical prefactor which, in the large separation limit,

[6] It requires the computation of a large determinant [21] which makes it more prone to numerical round-off errors.

[7] In the clean case [22], the prefactor ≈0.147 09 and is the same for both even and odd separations.

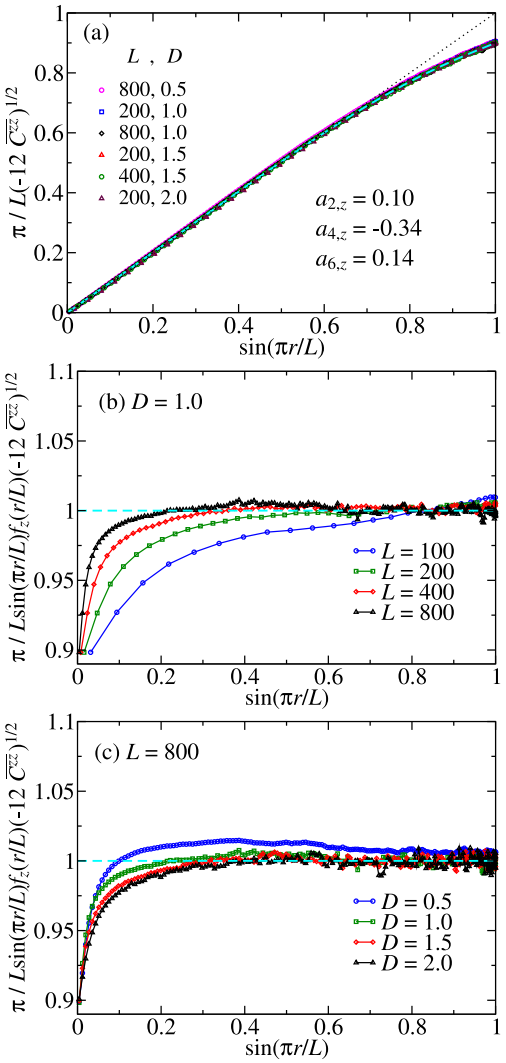

Fig. 3. The mean longitudinal correlation $\overline{C^{zz}}$ as a function of $\sin(\pi r/L)$ re-scaled in many different ways in order to obtain the correction in equation (9) (see text). The dashed line in panel (a) corresponds to our best fit: $a_{2,z} = 0.135$, $a_{4,z} = -0.414$ and $a_{6,z} = 0.179$. The dotted line is simply the identity function.

equals to

$$c_{D,r} = \frac{1}{24}\left(c_{\mathrm{o},D} + c_{\mathrm{e},D} - (-1)^r\left(c_{\mathrm{o},D} - c_{\mathrm{e},D}\right)\right), \qquad (11)$$

with $c_{\mathrm{o(e)},D}$ being the absolute value of the prefactor corresponding to odd (even) separations (multiplied by 12, for comparison with $\overline{C^{zz}}$).

In order to obtain the chord-length correction f_x, it is helpful to have some knowledge of the prefactor $c_{D,r}$. Naively, one could obtain its dependence with D by simply connecting the clean and disordered behaviors, i.e., given that $C^{xx}_{\mathrm{clean}} = A/\sqrt{r}$ and that $\overline{C^{xx}} = c_{D,r}/r^2$, then $C^{xx}_{\mathrm{clean}} = \overline{C^{xx}}$ at, say, a sharp crossover length $r = \xi_D$.

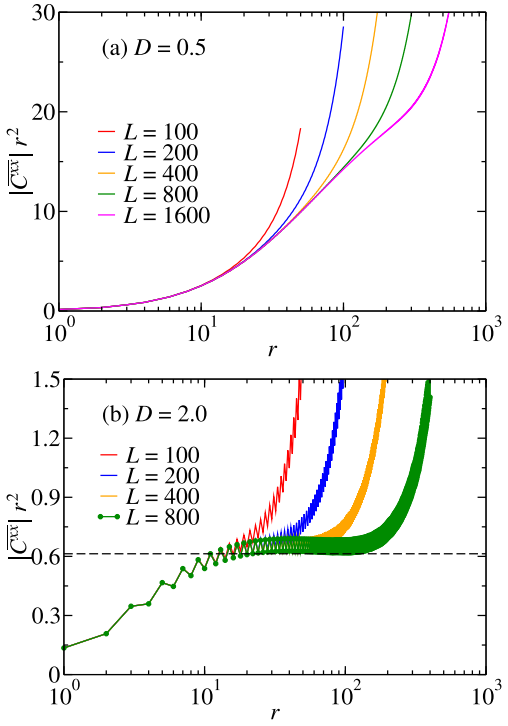

Fig. 4. The mean transverse correlation function $|\overline{C^{xx}}(r)|$ for various chain sizes L and disorder strengths (a) $D = 0.5$ and (b) $D = 2.0$.

Hence, $c_{D,r} \sim \xi_D^{3/2}$ and thus, we need knowledge on the crossover length.

Using field-theory methods (accurate at the weak-disorder limit $D \ll 1$), it was shown that $\xi_D \sim 1/\mathrm{var}\,(J) = D^{-2}\,(1+D)^2\,(1+2D)$. However, while this relation is accurate for small D, it was numerically found that $\xi_D \sim D^{-(2.0\pm0.2)}$ is much more satisfactory for any D [10]. Later, it was shown that a single-parameter theory holds at the band center of particle-hole symmetric tight-binding chains [49] [which maps to the Hamiltonian (1)]. The wavefunction is stretched-exponentially localized with the inverse of the Lyapunov exponent (or localization length) being[8]

$$\gamma_D^{-1} = \frac{\pi}{8\mathrm{Var}\,(\ln J)} = \frac{\pi}{8D^2}. \qquad (12)$$

With those arguments in mind, we now try to rescale the $\overline{C^{xx}}$ [shown in the inset (i) of Fig. 5a] appropriately. Given that (i) $c_{D,r} \sim \gamma_D^{-3/2}$ (naive crossover), that (ii) the natural length scale is γ_D^{-1} and that (iii) the chord length ℓ is weakly corrected, we then rescale the chord length in units of γ_D^{-1} and, therefore, $\overline{C^{xx}}$ must scale as $\sim \sqrt{\gamma_D}$. Somewhat surprisingly, with this naive rescaling [see inset (ii) of Fig. 5a] we almost achieve a perfect data collapse. In order to improve the data collapse, we fit the data in the

[8] Comparing the definition of the Lyapunov exponent (12) with the values of the crossover length numerically provided in reference [10], we simply find that $\xi_D \approx 51\gamma_D^{-1} \approx 20D^{-2}$.

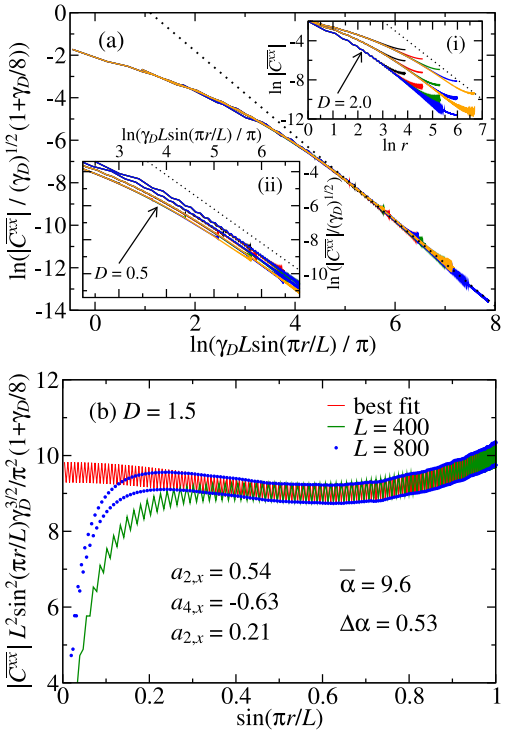

Fig. 5. (a) The mean transverse correlation function $\overline{C^{xx}}$ as a function of the spin separation r for various disorder strengths $D = 0.5$, $D = 1.0$, $D = 1.5$ and $D = 2.0$ and system sizes $L = 100$ (black), 200 (red), 400 (green), 800 (blue) and 1600 (orange, and only for $D = 0.5$ and 1.0). For clarity, the data for $D = 1.5$ is not shown in inset (i). The dotted lines are $y \sim x^{-2}$ for comparison. (b) The data is rescaled in order to highlight the correction to the chord length scaling (see text). In addition, the numerical prefactors in (14) can be extracted via a fitting and are $\bar{\alpha} = 9.6(2)$, $\Delta\alpha_{D=0.5} = 0.018(3)$, $\Delta\alpha_{D=1.0} = 0.18(1)$, $\Delta\alpha_{D=1.5} = 0.53(1)$, and $\Delta\alpha_{D=2.0} = 1.06(2)$.

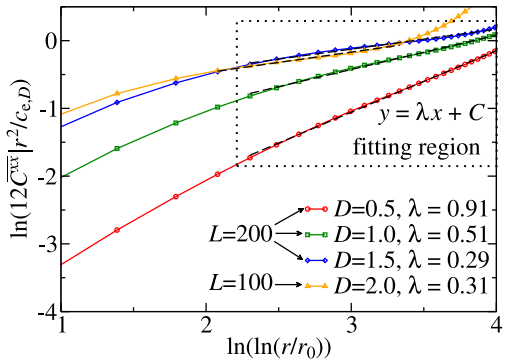

Fig. 6. Mean transverse correlation function $\overline{C^{xx}}(r)$ plotted according to equation (15) for even separations r, considering various disorder strengths D and chain sizes L. The upturn for $L = 100$ is due to the periodic boundary condition. For comparison, the data is fitted to the function $y = \lambda x + \text{const}$ (dashed lines) within the region compatible with that of reference [14].

inset (ii) to a power-law function $A\,(\gamma_D \ell)^{-2}$, and find that $A \propto 1 + 0.125\gamma_D$ in the long distance regime $\gamma_D \ell \gg 1$. We then correct our naive scaling to

$$\overline{C^{xx}} \sim \left(1 + \frac{1}{8}\gamma_D\right)\sqrt{\gamma_D} \tag{13}$$

and plot the resulting data in the main panel of Figure 5a. The collapse is remarkable even for small separations, suggesting a crossover function $\chi_x\,(D, r) \approx \chi_x\,(\gamma_D r)$ for $\gamma_D r \gtrsim 1$. In addition, we find useful to recast the prefactor (11) as

$$c_{D,r} = \left(1 + \frac{1}{8}\gamma_D\right)\gamma_D^{-3/2}\left(\bar{\alpha} - \frac{1}{2}\,(-1)^r\,\Delta\alpha_D\right), \tag{14}$$

where $\bar{\alpha}$ is disorder independent.

In Figure 5b, we plot $Y = \overline{C^{xx}}\,(\gamma_D \ell)^2 \,/\, \left(1 + \frac{1}{8}\gamma_D\right)\sqrt{\gamma_D}$ as a function of $X = \sin(\pi r/L)$ in order to obtain the values $a_{2n,x}$, $\bar{\alpha}$ and $\Delta\alpha_D$. This is achieved via, according to (10), fitting $Y = \chi_x\left(\bar{\alpha} - \frac{1}{2}\,(-1)^r\,\Delta\alpha_D\right)/f_x(X)$ to our data. For clarity, we have shown only the data for $L = 400$ and 800 and $D = 1.5$.[9] Clearly, the crossover function χ_x is converged to 1 for $X \geq 0.4$ (our fitting region) and $L = 800$. The best fit is shown as a solid red line. Notice that this plot is similar to those in Figures 3b and 3c.

Finally, it is interesting to observe the prefactor difference $\Delta c_D = c_{o,D} - c_{e,D}$ and mean value $\bar{c}_D = \frac{1}{2}\,(c_{o,D} + c_{e,D})$. Using the relations (11) and (14), together with the values of $\Delta\alpha_D$ and $\bar{\alpha}$ listed in the caption of Figure 5, we find that $(\Delta c_D, \bar{c}_D) = (0.46, 244)$, $(0.70, 37)$, $(0.80, 14)$, and $(0.89, 8)$ for $D = 0.5$, 1.0, 1.5, and 2.0, respectively. Notice it is not much different from 1 for all values of D. As conjectured in reference [12], this difference should be equal 1 for correlations along a symmetry axis. The total magnetization in the x direction is not conserved. However, perhaps due to the the emergent symmetry SO(2)→SU(2) character of the random singlet state, violations of this difference are small when compared to the values of the coefficients themselves.

3.1.3 Mimicking logarithmic corrections

Having characterized the long-distance ($\gamma_D r \gg 1$) behavior of the transverse mean correlation function equation (10), we now call attention to their strong finite-size effects when characterizing the random-singlet state in numerical studies via the use of small systems. Interestingly, as can be seen in Figure 6, the data is compatible with a logarithmic correction to the SDRG prediction of the leading term, i.e., based on small system sizes, one could conclude that

$$\overline{C^{xx}}(r) r^2 \sim \ln^{\lambda}\left(\frac{r}{r_0}\right). \tag{15}$$

[9] We report that the corresponding curves for $D = 0.5$, 1.0 and 2.0 are quite consistent with the collapse in Figure 5a. The only difference being on the value of $\Delta\alpha_D$. For $D = 0.5$, the crossover function χ_x is evidently larger yielding a smaller fitting region $X \geq 0.8$.

Corrections to the SDRG prediction were reported in the literature over the years, ranging from non-universal critical exponents [41] to logarithmic corrections [14,43]. Here, we have plotted and fitted our data in the same range compatible with those of reference [14] for the Heisenberg random spin chain. The values of the corresponding effective exponent λ are within the range found in that work.

We emphasize that our data show no evidence of logarithmic corrections in the long distance and long chain regime. We also stress that we do not have shown the absence of the logarithmic corrections reported in reference [14] (which study the isotropic $\Delta = 1$ case), we have only showed that the combination of crossover and finite-size effects [as in Eq. (10)] can be interpreted as logarithmic corrections in the case of the XX random spin-1/2 chain. The main culprit being the crossover function χ_x.

3.1.4 Random-singlet correlations

Finally, and just for completeness, we end our study on the mean correlations by focusing only on the main culprits for their behavior: the rare singlet pairs of the random-singlet state (depicted in Fig. 1). Once they are identified (by means of the SDRG decimation procedure [7]), we compute their mean correlations as a function of the separation r as shown in Figure 7. The naive expectation based on the clean-disordered crossover is the following. For short distances $\gamma_D r \ll 1$ (smaller than the crossover length), the correlation decays just as in the clean case. For larger distances, on the other hand, the SDRG singlets become a good approximation and thus, their correlations are expected to saturate monotonically and stretched-exponentially fast to a finite value. This expectation is only partially fulfilled as a non-monotonous saturation is observed. In addition, the saturation is much slower than one would expect. (Actually, one could argue that saturation is barely achieved only for the largest and strongest disordered chains.)

Finally, we would like to call attention for the importance of using quadruple precision and having extra care with the numerical instabilities. Using double precision for $L = 800$ and $D = 2.0$ yields to data different from those in Figure 7. Surprisingly, the observed data (not shown here) exhibits a drop in the correlations (due to the inability of capturing the longest and weakest coupled spin pairs) compatible with a logarithmic correction of type (15) with negative exponent of order 1, compatible with that reported in reference [43] [see Eq. (4)]. Since these rare singlets dominate the mean correlations, this means that a spurious logarithmic correction can obtained.

3.2 Typical correlation function and probability distributions

We now turn our attention to the typical value of the spin-spin correlations [as defined in Eq. (6)]. In this study, we report that our data were averaged over $N = 10^5$ distinct disorder realizations.

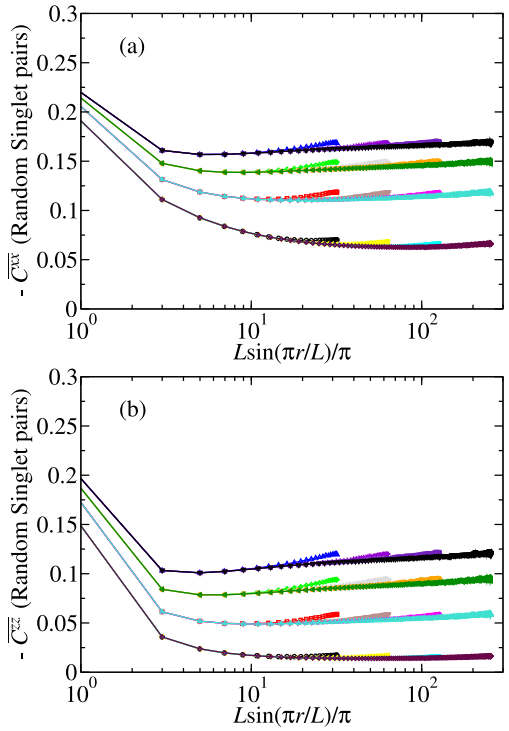

Fig. 7. The mean (a) transverse and (b) longitudinal correlation functions as a function of the chord length $\ell = \frac{L}{\pi}\sin\left(\frac{\pi r}{L}\right)$ considering only the rare singlets of the random-singlet state obtained via the strong-disorder renormalization-group decimation procedure. The disorder strengths are $D = 0.5$ (bottommost data sets), 1.0, 1.5 and 2.0 (topmost data sets), and the system sizes are $L = 100$ (leftmost data sets), 200, 400 and 800 (rightmost data sets).

We start by assuming that, in the long-distance regime $\gamma_D r \gg 1$, the typical correlations can be well approximated by

$$C^{\alpha\alpha}_{\rm typ} = (-1)^r\, c_{\alpha,D}\chi_\alpha\,(D,r)\, e^{-A_\alpha\sqrt{\gamma_D \ell f_\alpha(r/L)}}, \qquad (16)$$

where $c_{\alpha,D}$ is a disorder-dependent prefactor, χ_α represents the crossover function (which $\chi_\alpha \to 1$ for $\gamma_D r \gg 1$), A_α is a disorder-independent constant, ℓ is the chord length (8), γ_D is the Lyapunov exponent (12), and the correction to the chord length f_α is analogous to those for the average correlations (9). Notice that (16) recovers the SDRG prediction of a stretched exponential decay $\ln\left|C^{\alpha\alpha}_{\rm typ}\right| \sim -r^{\psi_\alpha}$ with universal (disorder-independent) and isotropic exponent $\psi_\alpha = \psi = \frac{1}{2}$. Equation (16) assumes that disorder enters in the exponential only via the Lyapunov exponent γ_D. While its presence is natural since the stretched exponential form requires a length scale, and thus the corresponding Lyapunov exponent of the underlying single-parameter scaling theory [49], it is not clear why A_α and f_α should be disorder independent. Nonetheless, as we show below, this hypothesis is compatible with our data. Finally, we mention that, unlike

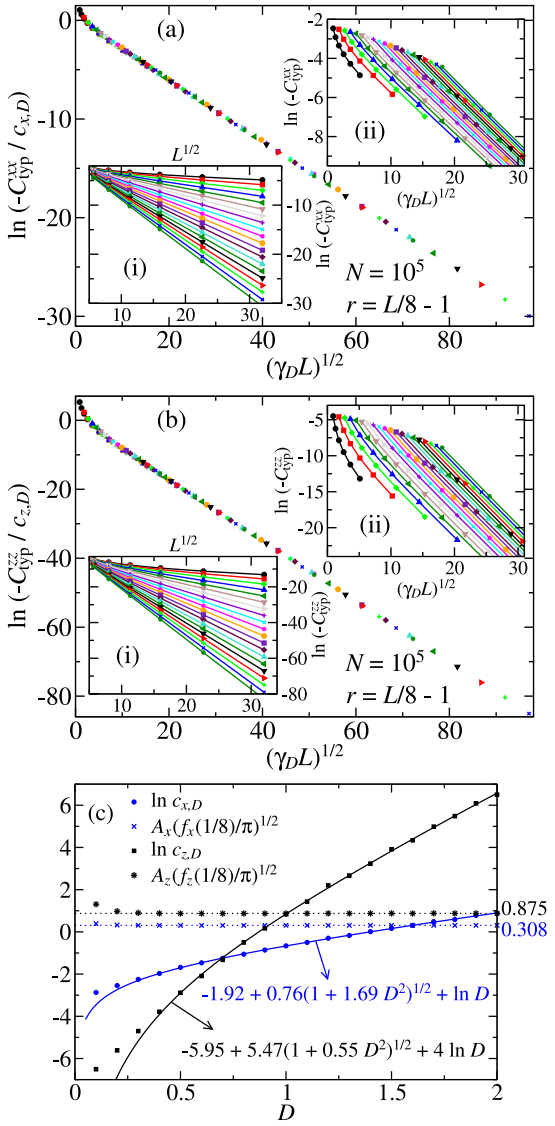

Fig. 8. Uncorrelated disorder model: the typical value of the (a) transverse and (b) longitudinal spin-spin correlations as a function of the system size L [inset (i)] and $\gamma_D L$ [close up in inset (ii)], for various disorder strengths D and separation $r = L/8 - 1$. System sizes are $L = 2^n$, with n ranging from 5 to 10. Disorder strength varies from $D = 0.1$ to 2.0 [topmost and bottommost curves in inset (i), respectively] in equal steps of 0.1. The lines are guide to the eyes. In panel (c), $c_{\alpha,D}$ and A_α are plotted against D. They are the best fits (16) to the data in insets (ii) (restricted to $\left|C^{xx}_{\rm typ}\right| < 2.5 \times 10^{-2}$ and $\left|C^{zz}_{\rm typ}\right| < 2.0 \times 10^{-4}$). The solid lines are the best fits to equation (17) restricted to $D \geq 0.4$ and are used to obtain the data collapse in the main plots of panels (a) and (b).

the mean correlations, the numerical prefactor $c_{x,D}$ is the same for both even and odd separations r.

In Figures 8a and 8b we plot respectively the transverse and longitudinal typical correlations for $r = L/8 - 1$ and various chain sizes L and disorder strengths D. The insets (i) of those figures bring the raw data from which the SDRG prediction $\ln\left|C^{\alpha\alpha}_{\rm typ}\right| \sim -\sqrt{r}$ is confirmed.

We then replot the correlations as a function of $(\gamma_D L)^\psi$ as shown in the insets (ii) of those figures. Apparently, the constant A_α is disorder-independent. Moreover, the values of L used seem to be sufficiently large (at least for $D \geq 0.4$) such that $\chi_{\alpha,D} \approx 1$. Therefore, it is safe to obtain the values of $c_{\alpha,D}$ and A_α by simply fitting equation (16) to our data.[10] The fitting values of $c_{\alpha,D}$ and $A_\alpha\sqrt{f_\alpha\,(1/8)}$ are plotted in Figure 8c. For $D \leq 0.3$, these are effective values [not in the asymptotic regime $\gamma_D r \gg 1$, as can be seen in insets (ii)]. The fitting values are consistent with A_α and f_α being disorder independent.

In order to proceed, as in the analysis of the mean correlation $\overline{C^{xx}}$, we need the relation between the numerical prefactor $c_{\alpha,D}$ and the disorder strength D. Clearly, one needs a theory capable of capturing both the clean and the disorder critical behaviors. Here, however, we will simply try to connect the clean behavior $C^{\alpha\alpha}_{\rm clean} \sim c_{1,\alpha} r^{-\eta_\alpha}$ (with $\eta_x = 1/2$ and $\eta_z = 2$) to the strong-disorder one $C^{\alpha\alpha}_{\rm typ} \sim c_{\alpha,D} e^{-c_{2,\alpha}\sqrt{\gamma_D r}}$. Assuming a sharp crossover at $r = r^*_\alpha = c_{3,\alpha}\gamma_D^{-1}$, continuity requires that $\ln c_{\alpha,D} = p_\alpha + 2\phi_\alpha \ln D$. However, this poorly fits the data in Figure 8c. We have tried several modifications of this scenario in order to improve the fit. They include adding one or two polynomials $\propto D^n$ and power-laws $\propto D^{-n}$, and also changing the prefactor of the logarithmic term. The worst modifications are those in which the logarithmic term is dropped out, implying that $c_{\alpha,D} \propto D^{2\phi_\alpha}$ is very robust. The most successful modification is such that we admit a sharp crossover happening at $r^*_\alpha = c_{3,\alpha}\gamma_D^{-1} + c_{4,\alpha}$. The exponential in the typical correlation then acquires a dependence on D yielding to

$$\ln c_{\alpha,D} = o_\alpha + p_\alpha\sqrt{1 + q_\alpha D^2} + 2\phi_\alpha \ln D, \qquad (17)$$

with o_α, p_α and q_α being fitting parameters. The fitting values are shown in Figure 8c for which only the data for $D \geq 0.4$ were used. The reason is that for smaller values of D, the slope A_α is not fully saturated (due to the effects of the crossover function χ_α). We have checked that changing any of the fitting parameters values by 5% does not change the quality of the fit, i.e., the reduced weighted error sum $\bar{\chi}^2$ remains the same within the statistical error. This means that 5% is a reasonable estimate for the accuracy of our fit.

We now put equation (17) to test by assuming that it holds for all disorder strengths. In the main panels of Figures 8a and 8b, we plot $C^{\alpha\alpha}_{\rm typ}/c_{\alpha,D}$ as a function of $\sqrt{\gamma_D L}$ (recall $r/L \approx 1/8$ is fixed). Remarkably, and somewhat surprisingly, we obtain good data collapse even for the least disordered system studied $D = 0.1$. For small $\sqrt{\gamma_D L}$, $C^{\alpha\alpha}_{\rm typ}/c_{\alpha,D}$ deviates from the pure stretched exponential, which is attributed to the crossover term

[10] We consider only the data such that $\left|C^{xx}_{\rm typ}\right| < 2.5 \times 10^{-2}$ and $\left|C^{zz}_{\rm typ}\right| < 2.0 \times 10^{-4}$. This is simply to ensure some meaning to the fitting function (16) when disorder is weak ($D < 0.6$). As we explain latter on, this has no influence in our results.

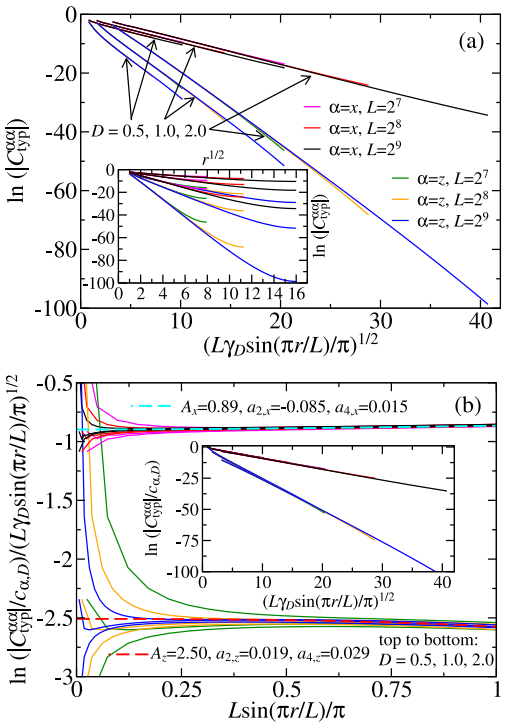

Fig. 9. The transverse and longitudinal typical value of the correlation function $C^{\alpha\alpha}_{\rm typ}(r)$ for chain sizes $L = 2^n$, with $n =$ 7, 8, and 9, and disorder strengths $D = 0.5$, 1.0, and $D = 2.0$. The corresponding legends are given in panel (a). The same data were plotted in different ways in the main panels and insets (see text). The dashed lines in panel (b) are the best fits according to equation (16).

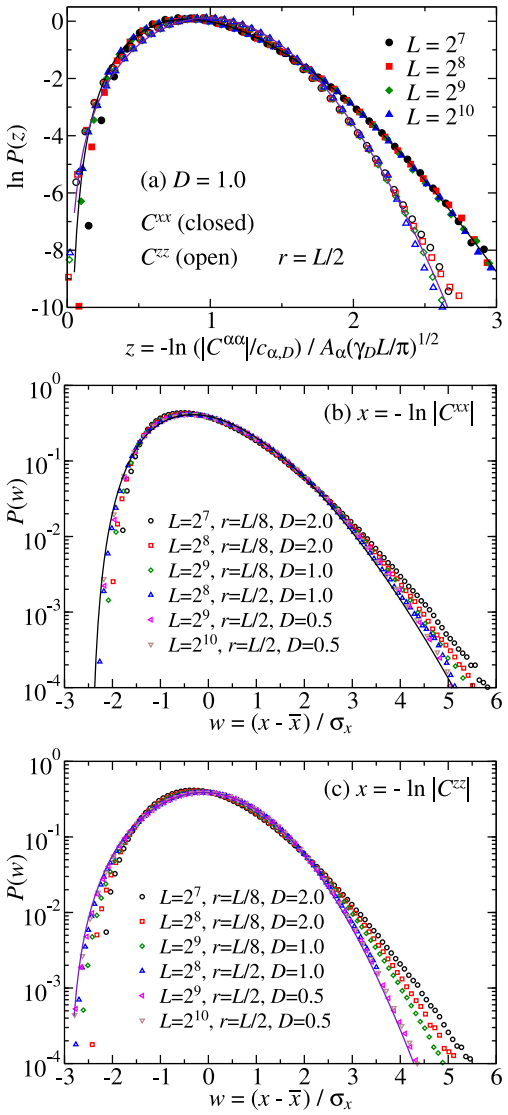

Fig. 10. Rescaled distribution of the correlation function $C^{\alpha\alpha}(r)$, for (a) fixed distance $r = L/2$ and disorder strength $D = 1.0$, and (b) and (c) distances $r = L/8$ and $L/2$ and various disorder strengths D for various system sizes L. The lines are best fits of equation (18) (see text for details).

$\chi_{\alpha,D}(r)$. The fact that the data collapse for all disorder strengths means that, to a good approximation, disorder enters in $\chi_{\alpha,D}$ through the combination $\gamma_D r$, i.e., $\chi_{\alpha,D}(r) = \chi_\alpha(\gamma_D r)$. Once more, this data collapse also supports that f_α is a disorder-independent function.

We are now in the position to study the chord-length-correction function f_α in equation (16). In Figure 9, we plot $C^{\alpha\alpha}_{\rm typ}$ as a function of suitable combinations of r, L and γ_D. For clarity, we show only a few data such as $L = 2^n$, with $n = 7$, 8, and 9, and $D = 0.5$, 1.0, and 2.0. As can be seen in the main panel of Figure 9a, the chord length $\ell = \frac{L}{\pi}\sin(\pi r/L)$ is nearly enough for accounting all the finite-size effects. The combination $\gamma_D \ell$ [see the inset of Fig. 9b] nearly collapses all the data. The role played by the crossover function $\chi_{\alpha,D}$ and the chord-length-correction function $f_{\alpha,D}$ are shown in the main panel of Figure 9b. We note that all curves converge to a single one in the large-L limit, in agreement with the hypothesis (16). The dashed lines are the best fits restricted to the region $\ell = \frac{L}{\pi}\sin\left(\frac{\pi r}{L}\right) > 0.5$ and considering only the large system size $L = 512$. The fitting values of A_α and $a_{2n,\alpha}$ are reported in Figure 9b. (Adding higher order terms do not improve our fit.) Notice the small correction to the chord length $a_{2,4,\alpha} \ll 1$, much smaller than those for the mean correlations. Interestingly, the crossover function $\chi_{\alpha,D}$ is non-monotonic with respect to D. Notice that $\chi_{\alpha,D}$ tends to 1 from above for weak disorder $D \lessapprox 1.0$, and from below otherwise. Finally, we verified (not shown) that $|\chi_{x,D} - 1| / |\chi_{z,D} - 1|$ is nearly a constant for large $\gamma_D r$.

We now turn our attention to the correlation function distribution. In the pioneering work by Fisher, it was conjectured that $\ln|C^{\alpha\alpha}|/\sqrt{r}$ converges to a non-trivial distribution for large separation r. This conjecture was confirmed in references [42,50] by numerically computing the distribution of $\ln|C^{\alpha\alpha}|/\sqrt{r}$ for a fixed disorder strength D. We confirm this conjecture by studying the distribution of $z = -\ln(|C^{\alpha\alpha}|/c_{\alpha,D})/A_\alpha\sqrt{\gamma_D L/\pi}$ for fixed separation $r = L/2$ and disorder strength $D = 1.0$, for various system sizes L. As shown in Figure 10a the

distribution $P_\alpha(z)$ converges to a non-trivial one for large L. According to equation (16), the first moment of P_x and P_z converges to the unity in the $\gamma_D r \gg 1$ regime. We first notice that P_x and P_z are not equal. Also, both distributions are narrow. We have tried many different fitting functions. Since they are narrow, we tried Weibull and Gaussian distributions but with poor success. The most satisfactory one is

$$P_\alpha(z) = C_\alpha \exp\left(-\left|\frac{z}{\delta_\alpha} - \zeta_\alpha\right|^{\gamma_\alpha} + b_\alpha\left(\frac{\delta_\alpha}{z}\right)^{\gamma'_\alpha}\right), \quad (18)$$

where C_α is a normalization constant, and δ_α, ζ_α, b_α, γ_α and γ'_α are fitting parameters with obvious interpretations. The first term in the exponential dictates the large-distance behavior $\gamma_D r \gg 1$ which, naively, we expect to be near a Gaussian. Then, γ_α is the corresponding exponent for the tail, δ_α would represent the width and ζ_α the rescaled offset. The second term dictates the low-distance behavior $\gamma_D r \ll 1$ with corresponding exponent γ'_α.[11] Notice that this term represents a sharp cutoff for $z < 0$. We have tried to offset this term via $z - z_0$ and found that $|z_0| \lessapprox 0.02$. Surprisingly, our choice of z makes the $P_\alpha(z < 0) = 0$. Our fits extrapolated to $L \to \infty$ are shown as solid lines in Figure 10a and are numerically equal to $\zeta_x = 0.65(5)$, $\zeta_z = 1.1(2)$, $\delta_x = 0.64(3)$, $\delta_z = 0.62(2)$, $\gamma_x = 1.71(3)$, $\gamma_z = 2.11(5)$, $b_x = 4.6(3)$, $b_z = 8.7(5)$, $\gamma'_x = 0.41(3)$, and $\gamma'_z = 0.19(2)$.

We now step forward and study how P_α depends on D. In Figures 10b and 10c we plot the distribution of $-\ln|C^{\alpha\alpha}|$ (shifted by its average and divided by its standard deviation) for various disorder strengths D, system sizes L, and separations $r = L/8$ and $L/2$. For comparison, we replot the corresponding fits of Figure 10a in Figures 10b and 10c, also shifted by the corresponding mean values (which are both equal to one) and divided by the corresponding standard deviation (0.38 and 0.35, respectively for $\alpha = x$ and $\alpha = z$). For separations $r = L/2$, all distributions are clearly universal, i.e., disorder independent. For shorter separations $r = L/8$, the distributions differ from the universal one. Given the systematic tendency towards the universal distribution for larger and larger system sizes L, we then attribute this discrepancy to the fact that the limit of large separation has not been achieved for those cases. We therefore conclude that, in the large separation limit, the distribution of $\ln|C^{\alpha\alpha}|/\sqrt{\gamma_D r}$ converges to a non-trivial, narrow and universal (disorder-independent) distribution.

4 Spin-spin correlations for the correlated coupling constants model

In this section we report our results on the average and typical correlation functions for the case of correlated disorder in the model (1), which is defined by a set of coupling constants $\{J_1, J_1, J_2, J_2, \ldots, J_{L/2}, J_{L/2}\}$ (see Sect. 2).

[11] We also have tried polynomials $P_\alpha \propto z^{\lambda'_\alpha}$ and verified satisfactory fits with $\lambda'_x \approx 5 \pm 1$ and $\lambda'_z \approx 2.6 \pm 0.6$.

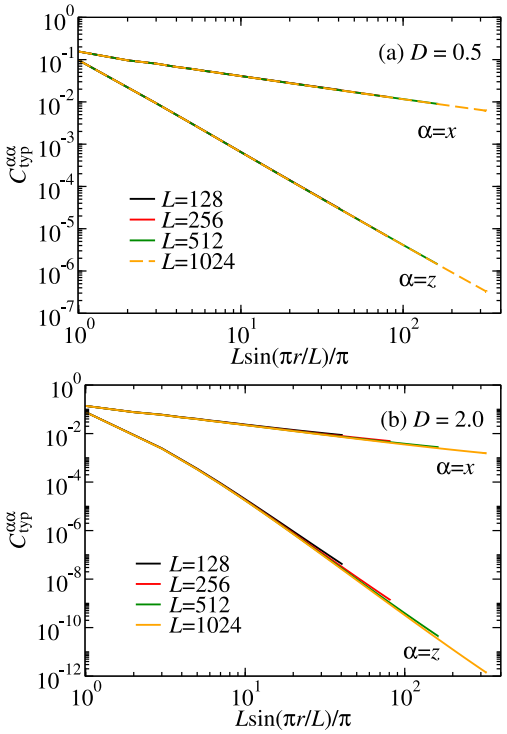

Fig. 11. The typical correlation functions as a function of the chord length (8) for the case of correlated disorder. The data were averaged over $N = 10^5$ disorder realizations.

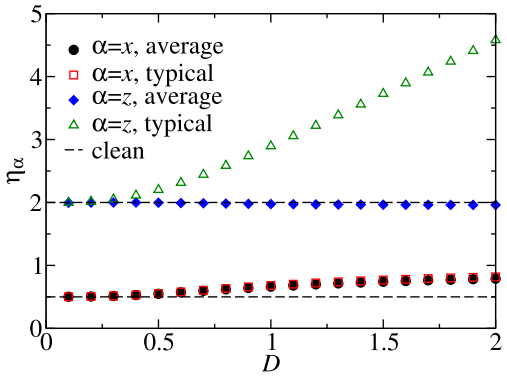

Fig. 12. The average and typical correlation function critical exponents $\eta_{x,z}$ as a function of the disorder strength D for the correlated disorder model. The dashed lines correspond to the homogeneous (clean) system values.

Unlike the uncorrelated disorder model, there is no analytical theory predicting the critical exponents. Here, our purpose is to determine them for the average and typical correlation functions.

In Figure 11, we plot the typical correlations for various chain lengths L and disorder strengths $D = 0.5$ and 1.0. Clearly, the chord length (8) is almost a perfect scaling variable.[12]

[12] Likewise, the chord length was verified to be nearly the correct scaling variable for the Rényi entanglement entropy for any disorder strength D [34].

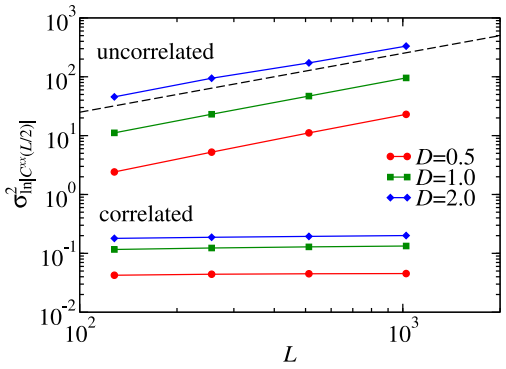

Fig. 13. The variance $\sigma_x^2 = \overline{x^2} - \overline{x}^2$ of the transverse correlation $x = \ln|C^{xx}(L/2)|$ as the chain size L is varied for different disorder strengths D for both the uncorrelated and correlated disorder models. The dashed line is the infinite-randomness prediction that $\sigma_x^2 \sim L$.

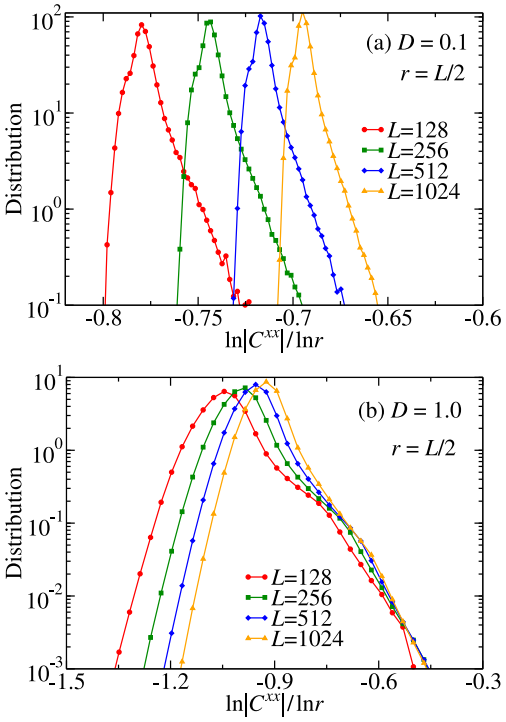

Fig. 14. Correlated disorder model: The distribution of the transverse correlation function $C^{xx}(r)$ for disorder strengths (a) $D = 0.1$ and (b) $D = 1.0$ and $r = L/2$. The data was obtained from $N = 10^3$ disorder realizations for panel (a) and $N = 10^5$ for panel (b).

Clearly, the typical correlations decay algebraically, which is very distinct from their uncorrelated disorder counterpart. Evidently (not shown here), the average correlations also decays algebraically with the spin separation r. Simple fits restricted to the long-distance tail provide the corresponding exponents which are shown in Figure 12.

For disorder strengths below the threshold $D_c \approx 0.3$, the exponent agrees with those of the clean system $\eta_z = 4\eta_x = 2$, as expected. Tuning the line of finite-disorder fixed points by increasing D beyond D_c, the exponents vary continuously and in a non-trivial fashion.

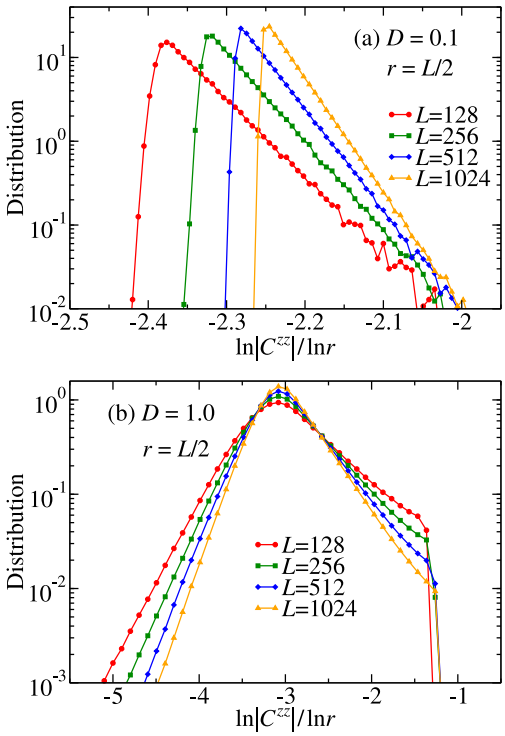

Fig. 15. Same as Figure 14, but for the longitudinal component of the correlation function.

With respect to the transverse correlation, both typical and average exponents are equal within our statistical error, and increase monotonically but is bounded to 1. This suggests that the distribution of $\ln|C^{xx}|$ has finite and small width for any distance r and system size L as can be verified in Figures 13 and 14.

In contrast, the typical and average longitudinal correlations behave quite differently from each other. The average critical exponent remains equal to the clean one for all disorder strengths studied. The typical one increases linearly for $D > D_c$ apparently without bounds. This implies that the width of the distribution of $\ln|C^{zz}| / \ln r$ increases with D, as verified in Figure 15, but is fixed for L and r (as we have verified but it is not shown here).

We end this section by calling attention to the striking difference between transverse and longitudinal correlations. Certainly, the ground state is far from the random singlet state of the uncorrelated disorder model. As pointed out in reference [34], the entanglement properties of the correlated disorder model shares many similarities with the clean ground state. The fact that typical and average longitudinal correlations are quite different points towards less similarities.

5 Conclusions

In this work we have studied the spin-spin correlation functions for the quantum critical spin-1/2 XX chain in

the case of uncorrelated and correlated coupling constants (see Sect. 2). In the former case, the chain is governed by a universal (disorder independent) infinite-randomness fixed point, while in the latter, it is governed by the clean fixed point for weak disorder ($D < D_c$) and by a line of finite-randomness fixed points tuned by the disorder strength ($D > D_c$).

For uncorrelated disorder, we have proposed and numerically verified that the correlations in equations (7), (10), (16) are good approximations in the regime $\gamma_D r \gg 1$ (not restricted to the thermodynamic limit $r \ll L$) for periodic boundary conditions. We have shown that the chord length (8) is not the true scaling variable, exhibiting small corrections for the mean correlations and even smaller for the typical ones. We have parameterized and quantified these corrections through the function f_α in equation (9). In principle, these corrections should be non-universal, i.e., disorder dependent. While this may be indeed the case, we could fit our data using the hypothesis that f_α is universal. Naturally, deciding whether f_α is universal or not requires better statistics and larger systems which are out of our current reach.

In addition, we have studied the corresponding non-universal numerical prefactors and linked them to the corresponding Lyapunov exponent (12) which, ultimately, link them to the disorder strength. Surprisingly, we have determined an accurate scaling as quantified in equations (14) and (17) for the mean transverse correlations and the typical longitudinal and transverse correlations, respectively. In general, these prefactors and their scaling with a crossover length depend on the dimensions of the related relevant and irrelevant operators. It is not the scope of the present work to find those operators and their dimensions. We leave this as an open question and hope that our findings serve as future motivation.

We have also studied the distribution of correlations. We have confirmed (not for the first time) the conjecture that the quantity $\ln|C^{\alpha\alpha}|/\sqrt{r}$ converges to a non-trivial distribution in the large-separation regime. In addition, based on the knowledge built from the typical correlation and its relation with the Lyapunov exponent, we have numerically determined that, in the large separation limit, the distribution of $\ln|C^{\alpha\alpha}|/\sqrt{\gamma_D r}$ converges to a non-trivial α-dependent, narrow and universal (disorder-independent) distribution quantified in equation (18).

It is desirable to generalize our results to other anisotropies $\Delta \neq 0$. It is not entirely clear whether a single-parameter scaling will be possible for all $-\frac{1}{2} < \Delta \leq 1$. Assuming that the SDRG method is indeed asymptotically exact in this range of anisotropies, it is then plausible that our results generalize (since $\Delta \to 0$ under the SDRG flow) at the simple cost of correcting the Lyapunov exponent. Based on the field-theory methods of reference [9,25], it is plausible that equation (12) generalizes to $\gamma_D \sim D^{\frac{2}{3-2K}}$, with the Luttinger parameter $K = 1 - \pi^{-1}\arccos(\Delta)$. Evidently, the values of non-universal quantities such as $a_{2n,\alpha}$ in (9) may depend on Δ.

Last but not least, we have shown the importance of the finite-size effect and numerical instabilities when characterizing the random-singlet state. They are so strong that can mimic logarithmic corrections to the correct scaling (see Fig. 6).

Conversely, for the correlated disorder model we have shown that the typical correlation functions decay as a power law (see Fig. 11), just like the mean correlations. The corresponding exponents were determined (see Fig. 12) and vary continuously for $D > D_c \approx 0.3$. While the exponents for the mean and typical transverse correlations remain nearly equal (implying a narrow distribution of correlations), the behavior is strikingly different for the longitudinal correlations, a consequence of the fact that the distribution of longitudinal correlations are much broader. In addition, we have determined the chord length is not the correct scaling variable (but it is a very good approximation to it). The fact that the transverse and longitudinal correlations behave so differently implies that the random-singlet state is far from being a good approximation of the true ground state even when $D \to \infty$. The infinite-randomness low-energy physics of the uncorrelated disorder model is not adiabatically connected to the strong but finite-randomness behavior of the correlated disorder model.

We would like to thank Anders Sandvik and Róbert Juhász for useful discussions, and Nicolas Laflorencie for bringing reference [14] to our attention. This study was financed in part by the Coordenação de Aperfeiçoamento de Pessoal de Nível Superior - Brasil (CAPES) - Finance Code 001, and also by the Brazilian funding agencies CNPq and FAPESP.

Author contribution statement

All authors contributed equally to this work.

References

1. S.K. Ma, C. Dasgupta, C.H. Hu, Phys. Rev. Lett. **43**, 1434 (1979)
2. C. Dasgupta, S.K. Ma, Phys. Rev. B **22**, 1305 (1980)
3. R.N. Bhatt, P.A. Lee, Phys. Rev. Lett. **48**, 344 (1982)
4. F. Iglói, C. Monthus, Phys. Rep. **412**, 277 (2005)
5. F. Iglói, C. Monthus, Eur. Phys. J. B **91**, 290 (2018)
6. D.S. Fisher, Phys. Rev. Lett. **69**, 534 (1992)
7. D.S. Fisher, Phys. Rev. B **50**, 3799 (1994)
8. T. Vojta, J. Phys. A: Math. Gen. **39**, R143 (2006)
9. C.A. Doty, D.S. Fisher, Phys. Rev. B **45**, 2167 (1992)
10. N. Laflorencie, H. Rieger, A. Sandvik, P. Henelius, Phys. Rev. B **70**, 054430 (2004)
11. J.A. Hoyos, G. Rigolin, Phys. Rev. A **74**, 062324 (2006)
12. J.A. Hoyos, A.P. Vieira, N. Laflorencie, E. Miranda, Phys. Rev. B **76**, 174425 (2007)
13. Z. Ristivojevic, A. Petković, T. Giamarchi, Nucl. Phys. B **864**, 317 (2012)
14. Y.R. Shu, D.X. Yao, C.W. Ke, Y.C. Lin, A.W. Sandvik, Phys. Rev. B **94**, 1 (2016)
15. J.C. Getelina, T.R. de Oliveira, J.A. Hoyos, Phys. Lett. A **382**, 2799 (2018)
16. Y.-R. Shu, M. Dupont, D.-X. Yao, S. Capponi, A.W. Sandvik, Phys. Rev. B **97**, 104424 (2018)
17. G. Theodorou, Phys. Rev. B **16**, 2264 (1977)

18. T. Masuda, A. Zheludev, K. Uchinokura, J.-H. Chung, S. Park, Phys. Rev. Lett. **93**, 077206 (2004)
19. T. Shiroka, F. Casola, W. Lorenz, K. Prša, A. Zheludev, H.-R. Ott, J. Mesot, Phys. Rev. B **88**, 054422 (2013)
20. T. Shiroka, F. Eggenschwiler, H.-R. Ott, J. Mesot, Phys. Rev. B **99**, 035116 (2019)
21. E. Lieb, T. Schultz, D. Mattis, Ann. Phys. **16**, 407 (1961)
22. B.M. McCoy, Phys. Rev. **173**, 531 (1968)
23. A. Luther, I. Peschel, Phys. Rev. B **12**, 3908 (1975)
24. F.D.M. Haldane, Phys. Rev. Lett. **45**, 1358 (1980)
25. T. Giamarchi, H.J. Schulz, Phys. Rev. B **39**, 4620 (1989)
26. R.R.P. Singh, M.E. Fisher, R. Shankar, Phys. Rev. B **39**, 2562 (1989)
27. K.A. Hallberg, P. Horsch, G. Martínez, Phys. Rev. B **52**, R719 (1995)
28. S. Lukyanov, A. Zamolodchikov, Nucl. Phys. B **493**, 571 (1997)
29. I. Affleck, J. Phys. A: Math. General **31**, 4573 (1998)
30. S. Lukyanov, Nucl. Phys. B **522**, 533 (1998)
31. T. Hikihara, A. Furusaki, Phys. Rev. B **58**, R583 (1998)
32. S. Lukyanov, Phys. Rev. B **59**, 11163 (1999)
33. J.A. Hoyos, N. Laflorencie, A.P. Vieira, T. Vojta, Europhys. Lett. **93**, 30004 (2011)
34. J.C. Getelina, F.C. Alcaraz, J.A. Hoyos, Phys. Rev. B **93**, 045136 (2016)
35. A. Macdiarmid, J. Chiang, A. Richter, A. Epstein, Synth. Met. **18**, 285 (1987)
36. D.H. Dunlap, H.-L. Wu, P.W. Phillips, Phys. Rev. Lett. **65**, 88 (1990)
37. H.-L. Wu, P. Phillips, Phys. Rev. Lett. **66**, 1366 (1991)
38. V.L. Quito, J.A. Hoyos, E. Miranda, Phys. Rev. Lett. **115**, 167201 (2015)
39. V.L. Quito, P.L.S. Lopes, J.A. Hoyos, E. Miranda (2017), arXiv:1711.04781 [cond-mat.str-el]
40. V.L. Quito, P.L.S. Lopes, J.A. Hoyos, E. Miranda, Phys. Rev. B **100**, 224407 (2019)
41. K. Hamacher, J. Stolze, W. Wenzel, Phys. Rev. Lett. **89**, 127202 (2002)
42. P. Henelius, S.M. Girvin, Phys. Rev. B **57**, 11457 (1998)
43. F. Iglói, R. Juhász, H. Rieger, Phys. Rev. B **61**, 552 (2000)
44. J.C. Xavier, J.A. Hoyos, E. Miranda, Phys. Rev. B **98**, 195115 (2018)
45. H. Rieger, F. Iglói, Phys. Rev. Lett. **83**, 3741 (1999)
46. A.K. Ibrahim, H. Barghathi, T. Vojta, Phys. Rev. E **90**, 042132 (2014)
47. I. Affleck, D. Gepner, H.J. Schulz, T. Ziman, J. Phys. A **22**, 511 (1989)
48. M. Fagotti, P. Calabrese, J.E. Moore, Phys. Rev. B **83**, 1 (2011)
49. H. Javan Mard, J.A. Hoyos, E. Miranda, V. Dobrosavljević, Phys. Rev. B **90**, 125141 (2014)
50. A. Young, H. Rieger, Phys. Rev. B **53**, 8486 (1996)

Inhomogeneous mean-field approach to collective excitations in disordered interacting bosons

Martin Puschmann[a,b], João C. Getelina[a,c], José A. Hoyos[c], Thomas Vojta[a]

[a] *Department of Physics, Missouri University of Science and Technology, Rolla, Missouri, 65409, USA*
[b] *Institute of Theoretical Physics, University of Regensburg, D-93040, Regensburg, Germany*
[c] *Instituto de Física de São Carlos, Universidade de São Paulo, C.P. 369, São Carlos, São Paulo, 13560-970, Brazil*

Abstract

We develop an inhomogeneous quantum mean-field theory for disordered particle-hole symmetric Bose-Hubbard models in two dimensions. Collective excitations are described by fluctuations about the mean-field ground state. In quadratic (Gaussian) approximation, the Goldstone (phase) and Higgs (amplitude) modes completely decouple. Each is described by a disordered Bogoliubov Hamiltonian which can be solved by an inhomogeneous multi-mode Bogoliubov transformation. We find that the Higgs modes are noncritical and strictly localized everywhere in the phase diagram. In contrast, the lowest-energy Goldstone mode delocalizes in the superfluid phase. We discuss these findings from the perspective of conventional Anderson localization theory. We also compare the effects of different types of disorder such as site dilution and random interactions; we relate our results to recent quantum Monte Carlo simulations, and we discuss the limits and generality of our approach.

Keywords: quantum phase transition, disorder, collective excitation, superfluid, localization

1. Introduction

Systems of disordered interacting bosons find diverse experimental applications such as helium absorbed in porous media [1, 2], thin superconducting films [3, 4], Josephson junction arrays [5, 6], ultracold gases in optical lattices [7–9], and certain disordered magnetic materials [10–14]. Their zero-temperature phase transitions between superfluid and insulating quantum ground states are prototypical disordered quantum phase transitions.

The influence of impurities, defects, and other types of quenched disorder on quantum phase transitions has been analyzed extensively since the 1990's. The resulting body of work has established that quantum phase transitions are generally more strongly affected by quenched disorder than their classical counterparts. Unconventional phenomena such as infinite-randomness criticality [15, 16], smeared phase transitions [17, 18], and quantum Griffiths singularities [19, 20] appear in a variety of systems. They can be classified [21–23] based on the symmetries of the order parameter and the defects, on the order parameter dynamics, and on the importance of rare fluctuations (for reviews see, e.g., Refs. [24–26]).

The majority of the past theoretical work on disordered quantum phase transitions was focused on the behavior of thermodynamic quantities across the transition. The character and dynamics of excitations has been explored less, despite the fact that they govern a variety of

experiments ranging from inelastic neutron scattering in magnetic materials to various electrical and thermal transport measurements.

In the present paper, we therefore address the behavior of excitations in the vicinity of the superfluid-insulator quantum phase transition of disordered interacting bosons. To this end, we develop a quantum mean-field approach to a two-dimensional particle-hole symmetric disordered Bose-Hubbard Hamiltonian. It generalizes the theories of Refs. [27, 28] to the disordered case and is also related to the bond-operator method for disordered magnets [29]. Our theory captures the spatially inhomogeneous character of the local order parameter in a disordered system. Excitations are obtained from an expansion about the mean-field ground state. Of particular interest are the collective excitations that emerge because the superfluid phase spontaneously breaks a continuous $U(1)$ symmetry. These include a phase (Goldstone) mode that is related to oscillations of the order parameter direction and an amplitude (Higgs) mode that is related to oscillations of the order parameter magnitude (see, e.g., Refs. [30, 31]).

More specifically, the Hamiltonian arising from expanding the Bose-Hubbard model to quadratic (Gaussian) order in the deviations from the mean-field ground contains two completely decoupled sectors, representing the Goldstone and Higgs excitations, respectively. Each sector takes the form of a disordered Bogoliubov Hamiltonian and can be solved by an inhomogeneous multi-mode Bogoliubov transformation, giving us direct access to the excitation energies and wave functions.

Our main results can be summarized as follows. The thermodynamic properties of the superfluid-insulator transition are completely conventional. The mean-field ground state in the superfluid phase features a spatially inhomogeneous local order parameter. The relative spatial variations of the order parameter are small deep inside the superfluid phase but they grow as the transition is approached, reflecting the Griffiths region close to the transition. Goldstone and Higgs excitations show qualitatively different behaviors. The lowest Goldstone excitation is extended over the entire system in the superfluid phase whereas the lowest Higgs excitation is localized. In the insulating (Mott) phase, where the two modes are degenerate because the $U(1)$ symmetry is not broken, both modes are localized. Therefore, the incipient Goldstone mode undergoes a striking delocalization transition upon entering the superfluid. The Higgs mode, in contrast, is always localized and remains uncritical across the superfluid-insulator transition. At higher excitation energies, both modes are localized. These qualitative features are independent of the disorder strength and type (provided the disorder respects the particle-hole symmetry).

The rest of the paper is organized as follows. Section 2 defines the model. The inhomogeneous quantum mean-field theory is developed in Sec. 3. The effective Hamiltonians for the Goldstone and Higgs excitations are derived in Sec. 4, and their diagonalization is discussed in Sec. 5. Section 6 introduces the specific quantities and data analysis techniques we employ to study the excitations. For comparison purposes, Sec. 7 summarizes the results for a clean square lattice Bose-Hubbard model. Simulations for both the Goldstone and the Higgs mode are discussed in Sec. 8. We conclude in Sec. 9. A short account of part of this work has already been published in Ref. [32].

2. Bose-Hubbard model

The Bose-Hubbard model (BHM) describes interacting bosons on a lattice. Its Hamiltonian reads

$$H = -\frac{1}{2}\sum_{ij} J_{ij}(a_i^\dagger a_j + \text{h.c.}) + \frac{1}{2}\sum_i U_i(n_i - \bar{n})^2 \tag{1}$$

where $a_i^\dagger$ and a_i are the boson creation and annihilation operator on lattice site i, and $n_i = a_i^\dagger a_i$ is the boson number operator. U_i is a repulsive on-site interaction, and J_{ij} denotes the hopping amplitude between sites i and j. Later, we will focus on the square lattice with nearest-neighbor hopping only, but the theory can be developed without these restrictions. $\bar{n}$ is the filling (or background "charge"). A nonzero chemical potential can be absorbed in a shift of $\bar{n}$. We are interested in the case of large integer $\bar{n}$ for which the Bose-Hubbard model is particle-hole symmetric.

In the clean case, consisting of an undiluted lattice with uniform $U_i \equiv U$ and translationally invariant $J_{ij} = f(\mathbf{r}_{ij})$ (where f decays sufficiently rapidly with the distance $\mathbf{r}_{ij}$ between sites i and j), the qualitative behavior of the model is readily understood. If the interactions dominate over the hopping terms, $J_{ij} \ll U$, the ground state is a gapped, incompressible Mott insulator. In the opposite limit, $J_{ij} \gg U$, the ground state is a superfluid. These two phases are separated by a continuous quantum phase transition in the $(2 + 1)$ dimensional XY universality class.

In the presence of quenched disorder, the superfluid and Mott insulator phases are always separated by an insulating "glass" phase in which rare large regions of local superfluid order (superfluid "puddles") coexist with the insulating bulk [33–36]. This glass phase thus constitutes the quantum Griffiths phase of the superfluid-Mott insulator quantum phase transition. The nature of the glassy intermediate phase depends on the symmetry properties of the disorder. For generic disorder that locally breaks the particle-hole symmetry (realized, e.g., via a random potential for the bosons), it is the so-called Bose glass, a compressible gapless insulator. In the present paper, we focus on disorder that does not break the particle-hole symmetry. In this case, the intermediate phase between superfluid and Mott insulator is not a Bose glass but rather the incompressible gapless Mott glass [37, 38].

We employ two different types of the (particle-hole symmetry preserving) disorder. The first disorder type is site dilution, i.e., we randomly remove a nonzero fraction p of lattice sites while the U_i and J_{ij} of the remaining sites stay translationally invariant. This can be formally written as $U_i = \epsilon_i U$, $J_{ij} = \epsilon_i \epsilon_j f(\mathbf{r}_{ij})$ where the ϵ_i are independent random variables that take the values 0 (vacancy) with probability p and 1 (occupied site) with probability $1 - p$.

Within the second disorder type, the lattice is undiluted but the values of the onsite interactions U_i are independent random variables drawn from a uniform probability density of average U and relative width r,

$$P(U_i) = \begin{cases} 1/(rU) & \text{for} \quad (1 - r/2)U < U_i < (1 + r/2)U \\ 0 & \text{otherwise} \end{cases} \tag{2}$$

whereas the J_{ij} remain translationally invariant. The values of r are restricted to $0 \leq r < 2$ to avoid finding sites where the onsite interaction is zero or even attractive, $U_i < 0$. The strength of this "random-U" disorder can be tuned to zero continuously whereas the defects created by site dilution always have a finite strength locally.

3. Inhomogeneous mean-field theory

Our approach follows Ref. [27, 28] and generalizes the theory to the disordered case. It is also related to the bond-operator method for disordered magnets [29]. In the Mott-insulating phase, the local boson numbers n_i fluctuate only weakly about their preferred value $\bar{n}$. The problem is thus well approximated by truncating the local Hilbert space associated with site i to the space spanned by the boson number eigenstates $|\bar{n} - 1\rangle_i$, $|\bar{n}\rangle_i$, and $|\bar{n} + 1\rangle_i$. This truncation qualitatively captures the essential physics even in the superfluid phase. The truncated local Hilbert space at

site i can be constructed employing three commuting $t_{i,\alpha}$ bosons ($\alpha = -1, 0, 1$) forming the states $|\bar{n}+\alpha\rangle_i = t^\dagger_{i,\alpha}|\text{vac}\rangle$ out of the fictitious vacuum $|\text{vac}\rangle$. They fulfill the constraint $\sum_\alpha t^\dagger_{i,\alpha} t_{i,\alpha} = 1$. The original $a^\dagger_i$ boson creation operators of the Bose-Hubbard model (1) can be represented as $a^\dagger_i = \sqrt{\bar{n}}\, t^\dagger_{i,0} t_{i,-1} + \sqrt{\bar{n}+1}\, t^\dagger_{i,1} t_{i,0}$.

In the limit of large filling, $\bar{n} \gg 1$, the Bose-Hubbard model takes the simple pseudo-spin-one form

$$H_S = -\frac{1}{4}\sum_{ij} \tilde{J}_{ij}(S^+_i S^-_j + \text{h.c.}) + \frac{1}{2}\sum_i U_i (S^z_i)^2 \,, \tag{3}$$

with $\tilde{J}_{ij} = \bar{n} J_{ij}$. The spin operators are given by

$$S^+_i = \sqrt{2}\left(t^\dagger_{i,1} t_{i,0} + t^\dagger_{i,0} t_{i,-1}\right) = (S^-_i)^\dagger \,, \tag{4}$$

$$S^z_i = t^\dagger_{i,1} t_{i,1} - t^\dagger_{i,-1} t_{i,-1} \,, \tag{5}$$

and the eigenstates of the S^z_i operator, $|+\rangle_i$, $|0\rangle_i$, and $|-\rangle_i$ correspond to the original boson number eigenstates $|\bar{n}+1\rangle_i$, $|\bar{n}\rangle_i$, and $|\bar{n}-1\rangle_i$, respectively.

The inhomogeneous mean-field theory is based on a product ansatz for the ground state wave function

$$|\Phi_0\rangle = \prod_j |\phi_0\rangle_j = \prod_j \left[\cos(\theta_j/2)|0\rangle_j + \sin(\theta_j/2)\left(\mathrm{e}^{i\eta_j}|+\rangle_j + \mathrm{e}^{-i\eta_j}|-\rangle_j\right)/\sqrt{2}\right] \tag{6}$$

where θ_j and η_j are local variational parameters ($0 \le \theta_j \le \pi/2$, $0 \le \eta_j < 2\pi$). For $\theta_j = 0$, the wave function describes the Mott-insulating phase because the local boson number is fixed at $n_i = \bar{n}$, without any fluctuations. For $\theta_j > 0$, the wave function features a nonzero local superfluid order parameter $\langle a^\dagger_j\rangle = \sqrt{\bar{n}}\,\psi_j$ with $\psi_j = \langle S^+_j\rangle = \mathrm{e}^{-i\eta_j}\sin(\theta_j)$. Thus, the mixing angle θ_j parameterizes the local order parameter amplitude and η_j its phase.

Evaluating the expectation value of H_S in the product state (6) yields the variational ground state energy

$$E_0 = \langle\Phi_0|H_s|\Phi_0\rangle = \frac{1}{2}\sum_i U_i \sin^2(\theta_i/2) - \frac{1}{2}\sum_{ij} \tilde{J}_{ij}\sin(\theta_i)\sin(\theta_j)\cos(\eta_i - \eta_j) \,. \tag{7}$$

It is minimized by mixing angles fulfilling the coupled mean-field equations

$$4\cos(\theta_i)\sum_j \tilde{J}_{ij}\sin(\theta_j) = U_i \sin(\theta_i) \tag{8}$$

while the phases are uniform, $\eta_i \equiv \eta = \text{const}$. In the following, we set these phases to zero without loss of generality. The trivial Mott-insulating state, $\sin(\theta_i) = 0$, is always a solution of the mean-field equations (8). For sufficiently large $\tilde{J}_{ij}$ or small U_i, a nontrivial superfluid solution of (8) may appear.

In the presence of disorder, the system of equations (8) usually needs to be solved numerically. In the clean case, in contrast, the system (8) reduces to a single equation which can be solved analytically. An example will be presented in Sec. 7.

4. Fluctuation Hamiltonians

Having obtained the mean-field ground state, we now consider excitations on top of it. The goal is to derive effective Hamiltonians for these excitations. As a first step, we introduce a new set of local boson operators via the unitary transformation

$$\begin{pmatrix} b^\dagger_{0,j} \\ b^\dagger_{G,j} \\ b^\dagger_{H,j} \end{pmatrix} = \begin{pmatrix} \frac{1}{\sqrt{2}}\sin(\theta_j/2) & \cos(\theta_j/2) & \frac{1}{\sqrt{2}}\sin(\theta_j/2) \\ \frac{i}{\sqrt{2}} & 0 & -\frac{i}{\sqrt{2}} \\ \frac{1}{\sqrt{2}}\cos(\theta_j/2) & -\sin(\theta_j/2) & \frac{1}{\sqrt{2}}\cos(\theta_j/2) \end{pmatrix} \begin{pmatrix} t^\dagger_{+,j} \\ t^\dagger_{0,j} \\ t^\dagger_{-,j} \end{pmatrix}, \tag{9}$$

such that $b^\dagger_{0,j}$ creates the local mean-field ground state out of the fictitious vacuum. $b^\dagger_{G,j}$ and $b^\dagger_{H,j}$ create states orthogonal to $b^\dagger_{0,j}|\text{vac}\rangle$ and describe, respectively, a change in the local order parameter phase η_j and a change in the local order parameter amplitude $\sin(\theta_j)$. These operators fulfill the constraint

$$b^\dagger_{0,j} b_{0,j} + b^\dagger_{G,j} b_{G,j} + b^\dagger_{H,j} b_{H,j} = 1\ . \tag{10}$$

To express the Bose-Hubbard Hamiltonian in terms b bosons, we first rewrite the spin-one operators

$$(S^z_j)^2 = \sin^2(\theta_j/2) n_{0,j} + n_{G,j} + \cos^2(\theta_j/2) n_{H,j} + \sin(\theta_j/2)\cos(\theta_j/2)(b^\dagger_{0,j} b_{H,j} + b^\dagger_{H,j} b_{0,j}), \tag{11}$$

$$\begin{aligned} S^+_j &= \sin(\theta_j)(n_{0,j} - n_{H,j}) + \cos(\theta_j)(b^\dagger_{0,j} b_{H,j} + b^\dagger_{H,j} b_{0,j}) \\ &\quad - i\cos(\theta_j/2)(b^\dagger_{0,j} b_{G,j} + b^\dagger_{G,j} b_{0,j}) + i\sin(\theta_j/2)(b^\dagger_{G,j} b_{H,j} + b^\dagger_{H,j} b_{G,j}). \end{aligned} \tag{12}$$

We eliminate ("fully condense") by means of the constraint (10) the operators $b^\dagger_{0,j}$ and $b_{0,j}$ that correspond to the mean-field ground state. This is analogous to a Holstein-Primakoff formalism with $n_{0,j} \gg n_{G,j}$ and $n_{0,j} \gg n_{H,j}$. Expanding to quadratic order in $b_{G,j}$ and $b_{H,j}$, the spin-one operators can be written as

$$(S^z_j)^2 = \sin^2(\theta_j/2) + \cos^2(\theta_j/2) n_{G,j} + \cos(\theta_j) n_{H,j} + \sin(\theta_j/2)\cos(\theta_j/2)(b_{H,j} + b^\dagger_{H,j})\ , \tag{13}$$

$$S^+_j = \sin(\theta_j)(1 - n_{G,j} - 2n_{H,j}) + \cos(\theta_j)(b_{H,j} + b^\dagger_{H,j}) - i\cos(\theta_j/2)(b_{G,j} + b^\dagger_{G,j})\ . \tag{14}$$

Inserting these representations into the pseudo-spin Hamiltonian (3), and using the mean-field equations (8) to cancel out terms linear in $b_{G,j}$ and $b_{H,j}$, the Hamiltonian becomes, to quadratic order in $b_{G,j}$ and $b_{H,j}$, the sum of the mean-field ground state energy and two fluctuation contributions, $H = E_0 + \mathcal{H}_G + \mathcal{H}_H$. The fluctuation Hamiltonians read

$$\mathcal{H}_G = -\frac{1}{2}\sum_{ij} \tilde{J}_{ij}\cos(\theta_i/2)\cos(\theta_j/2)(b_{G,i} + b^\dagger_{G,i})(b_{G,j} + b^\dagger_{G,j}) + \sum_i \varpi_{G,i} n_{G,i}\ , \tag{15}$$

$$\mathcal{H}_H = -\frac{1}{2}\sum_{ij} \tilde{J}_{ij}\cos(\theta_i)\cos(\theta_j)(b_{H,i} + b^\dagger_{H,i})(b_{H,j} + b^\dagger_{H,j}) + \sum_i \varpi_{H,i} n_{H,i}. \tag{16}$$

The Goldstone and Higgs modes thus completely decouple to quadratic order in $b_{G,j}$ and $b_{H,j}$. $\mathcal{H}_G$ and $\mathcal{H}_H$ each take the form of a disordered Bogoliubov Hamiltonian describing a set of coupled harmonic oscillators with the local frequencies $\varpi_{G,i} = (U_i/2)\cos^2(\theta_i/2) + \zeta_i$ and $\varpi_{H,i} = (U_i/2)\cos(\theta_i) + 2\zeta_i$ where $\zeta_i = \sin(\theta_i)\sum_j \tilde{J}_{ij}\sin(\theta_j)$.

In the Mott-insulating phase, the local mixing angles θ_i all vanish. Thus $\mathcal{H}_G$ and $\mathcal{H}_H$ are identical, in agreement with the fact that the two excitation modes are degenerate if the $U(1)$ order parameter symmetry is not broken.

5. Bogoliubov transformation

Due to the presence of anomalous $b^\dagger b^\dagger$ and bb terms, the fluctuation Hamiltonians $\mathcal{H}_G$ and $\mathcal{H}_H$ have to be solved by means of a multi-modal Bogoliubov transformation ($\alpha = G, H$)

$$b_{\alpha j} = \sum_n (u_{\alpha jn} d_{\alpha n} + v^*_{\alpha jn} d^\dagger_{\alpha n}) \tag{17}$$

where the d (Bogoliubov) bosons correspond to the excitation eigenstates of our system.

The transformation coefficients u and v can be found efficiently by interpreting each of the fluctuation Hamiltonians as a system of coupled harmonic oscillators and switching to a first-quantization framework. The local oscillator energies in eqs. (15) and (16) can be written as $\varpi_{\alpha,i}(n_{\alpha,i} + 1/2) = p^2_{\alpha,i}/2 + \varpi_{\alpha,i} x^2_{\alpha,i}/2$ where $p_{\alpha,i}$ and $x_{\alpha,i}$ represent the momentum and position operators of the fictitious oscillator at the site i. (The mass can be set to unity without loss of generality.) The terms $(b_{\alpha,i} + b^\dagger_{\alpha,i})$ that appear in the intersite couplings in eqs. (15) and (16) can be expressed as $(b_{\alpha,i} + b^\dagger_{\alpha,i}) = \sqrt{2\varpi_{\alpha,i}}\, x$. In first quantization, the fluctuation Hamiltonians $\mathcal{H}_G$ and $\mathcal{H}_H$ thus take the form

$$\mathcal{H}_\alpha = \sum_i \frac{p^2_{\alpha,i}}{2} + \sum_{ij} \frac{x_{\alpha,i} X_{\alpha,ij} x_{\alpha,j}}{2} \,. \tag{18}$$

The coupling matrices are given by

$$X_{G,ij} = \varpi^2_{G,i}\delta_{ij} - 2\cos(\theta_i/2)\cos(\theta_j/2)\tilde{J}_{ij}\sqrt{\varpi_{G,i}\varpi_{G,j}} \tag{19}$$

$$X_{H,ij} = \varpi^2_{H,i}\delta_{ij} - 2\cos(\theta_i)\cos(\theta_j)\tilde{J}_{ij}\sqrt{\varpi_{H,i}\varpi_{H,j}} \tag{20}$$

for the Goldstone and Higgs modes, respectively. The Hamiltonians (18) are now easily solved by diagonalizing the coupling matrices $\mathbf{X}_\alpha$ which are real symmetric $N \times N$ matrices in a system of N lattice sites,

$$\sum_k X_{\alpha,jk} \mathcal{V}_{\alpha,kn} = \nu^2_{\alpha,n} \mathcal{V}_{\alpha,jn} \tag{21}$$

where $\nu_{\alpha,n}$ is the n-th nonnegative excitation eigenfrequency (energy), and the n-th column of the matrix $\mathcal{V}_{\alpha,jn}$ contains the n-th eigenvector. Going back to second quantization in the eigenbasis of $\mathbf{X}_\alpha$ yields

$$\mathcal{H}_G = \sum_n \nu_{G,n} d^\dagger_{G,n} d_{G,n} \,, \qquad \mathcal{H}_H = \sum_n \nu_{H,n} d^\dagger_{H,n} d_{H,n} \tag{22}$$

with the d bosons given by

$$\begin{aligned} d_{\alpha,n} &= \sqrt{\frac{\nu_{\alpha,n}}{2}}\left(\tilde{x}_{\alpha,n} + \frac{i}{\nu_{\alpha,n}}\tilde{p}_{\alpha,n}\right) = \sqrt{\frac{\nu_{\alpha,n}}{2}} \sum_j \mathcal{V}_{\alpha,jn}\left(x_{\alpha,j} + \frac{i}{\nu_{\alpha,n}} p_{\alpha,j}\right) \\ &= \frac{1}{2}\sum_j \mathcal{V}_{\alpha,jn}\left[\left(\sqrt{\frac{\nu_{\alpha,n}}{\varpi_{\alpha,j}}} - \sqrt{\frac{\varpi_{\alpha,j}}{\nu_{\alpha,n}}}\right) b^\dagger_{\alpha,j} + \left(\sqrt{\frac{\nu_{\alpha,n}}{\varpi_{\alpha,j}}} + \sqrt{\frac{\varpi_{\alpha,j}}{\nu_{\alpha,n}}}\right) b_{\alpha,j}\right] . \end{aligned} \tag{23}$$

Here, $\tilde{x}_{\alpha,n}$ and $\tilde{p}_{\alpha,n}$ are the position and momentum operators in the eigenbasis of $\mathbf{X}_\alpha$. Using the definitions $R_{\alpha,jn} = \mathcal{V}_{\alpha,jn}\sqrt{\nu_{\alpha,n}/\varpi_{\alpha,j}}$ and $L_{\alpha,jn} = \mathcal{V}_{\alpha,jn}\sqrt{\varpi_{\alpha,j}/\nu_{\alpha,n}}$, the multi-modal Bogoliubov transformation can be written in the compact form

$$\begin{pmatrix} \mathbf{d}_\alpha \\ \mathbf{d}^\dagger_\alpha \end{pmatrix} = \frac{1}{2}\begin{pmatrix} \mathbf{R}^{\mathrm{T}}_\alpha + \mathbf{L}^{\mathrm{T}}_\alpha & \mathbf{R}^{\mathrm{T}}_\alpha - \mathbf{L}^{\mathrm{T}}_\alpha \\ \mathbf{R}^{\mathrm{T}}_\alpha - \mathbf{L}^{\mathrm{T}}_\alpha & \mathbf{R}^{\mathrm{T}}_\alpha + \mathbf{L}^{\mathrm{T}}_\alpha \end{pmatrix}\begin{pmatrix} \mathbf{b}_\alpha \\ \mathbf{b}^\dagger_\alpha \end{pmatrix} , \qquad \begin{pmatrix} \mathbf{b}_\alpha \\ \mathbf{b}^\dagger_\alpha \end{pmatrix} = \frac{1}{2}\begin{pmatrix} \mathbf{L}_\alpha + \mathbf{R}_\alpha & \mathbf{L}_\alpha - \mathbf{R}_\alpha \\ \mathbf{L}_\alpha - \mathbf{R}_\alpha & \mathbf{L}_\alpha + \mathbf{R}_\alpha \end{pmatrix}\begin{pmatrix} \mathbf{d}_\alpha \\ \mathbf{d}^\dagger_\alpha \end{pmatrix} , \tag{24}$$

implying that the transformation coefficients u and v in eq. (17) are given by $u_{\alpha,jn} = (L_{\alpha,jn} + R_{\alpha,jn})/2$ and $v_{\alpha,jn} = (L_{\alpha,jn} - R_{\alpha,jn})/2$.

The ground states $|GS\rangle$ of the fluctuation Hamiltonians $\mathcal{H}_G$ and $\mathcal{H}_H$ are defined by the absence of d bosons, i.e., they correspond to d vacuums. Expressing the b operators in terms of the d operators shows that the ground states are *not* b vacuums. Instead, the b number operator has the ground state expectation value

$$\langle GS|b^\dagger_{\alpha,j}b_{\alpha,j}|GS\rangle = \frac{1}{4}\sum_n (L_{\alpha,jn} - R_{\alpha,jn})^2 \,. \tag{25}$$

6. Observables and data analysis

In order to study the character and dynamics of the excitations, we analyze the eigenfunctions $\mathcal{V}_{\alpha,jk}$, and we compute a number of additional observables.

6.1. Dynamic susceptibilities

We are interested in the longitudinal and transversal order parameter susceptibilities as well as in the scalar susceptibility (the susceptibility of the order parameter magnitude). In terms of the pseudo-spin-1 operators introduced in eqs. (4) and (5), the longitudinal local order parameter component is given by $S^x_j = (S^+_j + S^-_j)/2$ (because we have fixed the phase η_j of the order parameter at zero in the mean-field solution). The transversal component is given by $S^y_j = (S^+_j - S^-_j)/(2i)$, and the (squared) order parameter amplitude is associated with $(S^x_j)^2 + (S^y_j)^2 = 2 - (S^z_j)^2$. For each of these operators, we define the retarded Green function. The longitudinal susceptibility reads

$$G^{\parallel}_{jk} = -i\Theta(t)\langle GS|\,[S^x_j(t), S^x_k(0)]\,|GS\rangle \,. \tag{26}$$

The transversal and scalar susceptibilities, $G^{\perp}_{jk}$ and G^{S}_{jk}, are defined analogously. Expanding the operators to quadratic order in the b bosons, the longitudinal, transversal and scalar susceptibilities

$$G^{\parallel}_{jk}(t) = \cos(\theta_i)\cos(\theta_j)\,G^H_{jk}(t) \,, \tag{27}$$

$$G^{\perp}_{jk}(t) = \cos(\theta_i/2)\cos(\theta_j/2)\,G^G_{jk}(t) \,, \tag{28}$$

$$G^{\mathrm{S}}_{jk}(t) = \frac{1}{4}\sin(\theta_i)\sin(\theta_j)\,G^H_{jk}(t) \tag{29}$$

can be decomposed into functions of the local order parameters (mixing angles θ_j) and the Green functions of the elementary excitations in the Higgs and Goldstone channels which are defined as

$$G^G_{jk}(t) = -i\Theta(t)\langle GS|\,[b_{G,j}(t) + b^\dagger_{G,j}(t), b_{G,k}(0) + b^\dagger_{G,k}(0)]\,|GS\rangle \,, \tag{30}$$

$$G^H_{jk}(t) = -i\Theta(t)\langle GS|\,[b_{H,j}(t) + b^\dagger_{H,j}(t), b_{H,k}(0) + b^\dagger_{H,k}(0)]\,|GS\rangle \,. \tag{31}$$

To evaluate the ground state expectation values, we transform the b bosons to the Bogoliubov d bosons by means of eq. (23), yielding $b_{\alpha,j}+b^\dagger_{\alpha,j} = \sum_n L_{\alpha,jn}(d_{\alpha,n}+d^\dagger_{\alpha,n})$. After Fourier-transforming

$G^G_{jk}(t)$ and $G^H_{jk}(t)$ w.r.t. time, the spectral functions $A^G_{jk}(\omega)$ and $A^H_{jk}(\omega)$ are obtained as

$$A^\alpha_{jk}(\omega) = -\frac{1}{\pi}\mathrm{Im}G^\alpha_{jk}(\omega) = \sum_n L_{\alpha,jn}L_{\alpha,kn}[\delta(\omega-\nu_{\alpha,n})-\delta(\omega+\nu_{\alpha,n})] \quad (32)$$

$$= \sum_n \frac{\sqrt{\varpi_{\alpha,j}\varpi_{\alpha,k}}}{\nu_{\alpha,n}}\mathcal{V}_{\alpha,jn}\mathcal{V}_{\alpha,kn}[\delta(\omega-\nu_{\alpha,n})-\delta(\omega+\nu_{\alpha,n})]\,. \quad (33)$$

In the presence of disorder, the spectral functions $A^\alpha_{jk}(\omega)$ are not translationally invariant in space. Translational invariance is restored after an ensemble average over disorder configurations. We can then perform a spatial Fourier transformation to wave vector $\mathbf{q}$,

$$A^\alpha_{\mathbf{q}}(\omega) = \frac{1}{N}\sum_{j,k} e^{i(\mathbf{r}_j-\mathbf{r}_k)\cdot\mathbf{q}}\langle A^\alpha_{jk}(\omega)\rangle \quad (34)$$

where $\mathbf{r}_j$ is the position vector of site j, and $\langle\ldots\rangle$ denotes the disorder average.

Let us briefly discuss some qualitative features of the longitudinal, transversal, and scalar susceptibilities. In the Mott-insulating phase, the Goldstone and Higgs Green functions $G^G_{jk}(t)$ and $G^H_{jk}(t)$ are identical because the corresponding fluctuation Hamiltonians agree with each other, as discussed at the end of Sec. 4. As the local mixing angles θ_i all vanish in the Mott insulator, eqs. (27) and (28) imply that the longitudinal and transversal susceptibilities coincide, $G^\parallel_{jk}(t) = G^\perp_{jk}(t)$, in agreement with the fact that the order parameter symmetry is not broken in the insulator phase. In contrast, the scalar susceptibility $G^S_{jk}(t)$ vanishes in the Mott insulating phase. (This is an artefact of the Gaussian approximation, as was already noted in Ref. [28] for the clean case.) In the superfluid phase, these susceptibilities all differ from each other.

6.2. Localization properties: multifractal analysis

Because the Goldstone and Higgs excitations are the eigenstates of the spatially disordered fluctuation Hamiltonians $\mathcal{H}_G$ and $\mathcal{H}_H$, they are expected to feature nontrivial localization properties. We analyze these properties by means of two methods, (i) a multifractal analysis of the eigenstates and (ii) the scaling of the Lyapunov exponent in a quasi-one-dimensional geometry found via the recursive Green function method.

Within the multifractal analysis [39–42], we partition the system defined on a square lattice of L^2 sites into square boxes of linear size l. For each eigenstate n of the fluctuation Hamiltonians $\mathcal{H}_\alpha$ (with $\alpha = G, H$), we define a measure $\mu_j(n,l,L)$ characterizing the probability of the eigenstate in a box of size l with lower left corner at site j. It reads

$$\mu_j(n,l,L) = \sum_{k\in\mathrm{box}} |\mathcal{V}_{\alpha,kn}|^2 = \sum_{k\in\mathrm{box}} (|u_{\alpha,kn}|^2 - |v_{\alpha,kn}|^2) \quad (35)$$

where the sum runs over all lattice sites k in the box. We then construct the q-th moment of these box probabilities,

$$P_q(n,l,L) = \frac{1}{l^2}\sum_j \mu_j^q(n,l,L)\,. \quad (36)$$

The sum runs over all sites j, i.e., it considers all possible (overlapping) boxes of size l. The prefactor $1/l^2$ guaranties the proper normalization of the probability, $P_1(n,l,L) = 1$. Note that $P_2(n,1,L)$ corresponds to the inverse participation number of state n.

For multifractal wave functions[1], P_q is expected to feature power law dependencies on l and L. The multifractal exponent τ_q of state n can be defined as

$$\tau_q(n) = \lim_{L/l\to\infty} \tau_q(n,l,L) = \lim_{L/l\to\infty} \frac{\ln P_q(n,l,L)}{\ln(l/L)} \,. \tag{37}$$

In our numerical analysis, we consider averages over the disorder distribution and/or over several states for a given disorder realization. They are obtained by averaging the moments $P_q(n,l,L)$

$$\tau_q = \lim_{L/l\to\infty} \tau_q(l,L) = \lim_{L/l\to\infty} \frac{\ln\langle P_q(n,l,L)\rangle}{\ln(l/L)} \tag{38}$$

where $\langle \ldots \rangle$ denotes the appropriate average.

6.3. Localization properties: recursive Green function approach

In addition to the multifractal analysis, we calculate the smallest positive Lyapunov exponent γ, characterizing the exponential decay of an eigenstate in a quasi-one-dimensional geometry by means of the recursive Green function approach [43–45].

We consider a system defined on a quasi-one-dimensional strip of size $N \times L$ sites with $N \gg L$. (Geometrically, it can be considered a being stack of N layers, each containing L sites.) If the Hamiltonian contains nearest-neighbor interactions only, the coupling matrices $\mathbf{X}_G$ and $\mathbf{X}_H$ defined in eqs. (19) and (20) take a block-tridiagonal form

$$\mathbf{X} = \begin{pmatrix} \mathbf{X}_1 & \mathbf{T}_1 & & & \\ \mathbf{T}_1^T & \mathbf{X}_2 & \mathbf{T}_2 & & \\ & \mathbf{T}_2^T & \mathbf{X}_3 & \ddots & \\ & & \ddots & \ddots & \mathbf{T}_{N-1} \\ & & & \mathbf{T}_{N-1}^T & \mathbf{X}_N \end{pmatrix} . \tag{39}$$

The diagonal block $\mathbf{X}_i$ contains the onsite terms as well couplings within the ith layer, while the upper diagonal block $\mathbf{T}_i$ contains the interlayer couplings between the layers i and $i+1$.

We consider the Green function $\mathbf{g}(\omega^2) = \lim_{\eta\to 0}\left[(\omega^2 + i\eta)\mathbf{I} - \mathbf{X}\right]^{-1}$ associated with $\mathbf{X}$ at energy ω. Here, $\mathbf{I}$ is the identity matrix and η shifts the energy into the complex plane to avoid singularities. We use the tridiagonal form (39) to calculate the Green function and related physical quantities in a recursive manner. We start with a single layer, and each further iteration step adds a new layer to the stack. Denoting the Green functions between layers j and k after N iterations as $\mathbf{g}^N_{j,k}$, the recursion can be written as

$$\mathbf{g}^{N+1}_{1,N+1} = \mathbf{g}^N_{1,N} \cdot \mathbf{T}_N \cdot \mathbf{g}^{N+1}_{N+1,N+1} \,, \tag{40}$$

$$\mathbf{g}^{N+1}_{N+1,N+1} = \left[(\omega^2 + i\eta)\mathbf{I} - \mathbf{X}_{N+1} - \mathbf{T}_N^T \cdot \mathbf{g}^N_{N,N} \cdot \mathbf{T}_N\right]^{-1} \,. \tag{41}$$

The iteration is initialized by $\mathbf{g}^1_{11} = \left[(\omega^2 + i\eta)\mathbf{I} - \mathbf{X}_1\right]^{-1}$. In this formalism, the smallest positive Lyapunov exponent (inverse localization length) reads

$$\gamma(\omega^2, L) = \lim_{N\to\infty} \frac{1}{2N} \ln |\mathbf{g}^N_{1N}|^2 \,. \tag{42}$$

[1] Multifractality is usually a property of critical states only, but the scaling behavior of the associated observables can be used to identify the localization characteristics of all eigenstates in the thermodynamic limit.

Localization properties are conveniently extracted from the finite-size scaling behavior of the dimensionless Lyapunov exponent $\Gamma = \gamma L$.

The matrix elements in $\mathbf{g}^N_{1,N}$ usually decay quickly with increasing N. To sustain numerical stability during the iteration, we extract the leading order of magnitude of the elements after each $\kappa = 100$ iterations. Mathematically, this means that we rewrite the logarithm in eq. (42) as

$$\ln |\mathbf{g}^N_{1,N}|^2 = \ln |\mathbf{g}^\kappa_{1,\kappa}|^2 + \sum_{b=2}^{N/\kappa} \ln \frac{|\mathbf{g}^{b\kappa}_{1,b\kappa}|^2}{|\mathbf{g}^{(b-1)\kappa}_{1,(b-1)\kappa}|^2} \,. \tag{43}$$

7. Collective excitations in the clean Bose-Hubbard model

In this section, we apply our approach to the clean Bose-Hubbard model with nearest-neighbor interactions,

$$H = -J \sum_{\langle ij \rangle} (a_i^\dagger a_j + \text{h.c.}) + \frac{U}{2} \sum_i (n_i - \bar{n})^2 \,, \tag{44}$$

defined on a Bravais lattice of N sites with coordination number (number of nearest neighbors) z. In the first sum, $\langle ij \rangle$ denotes pairs of nearest-neighbor sites. The results reproduce earlier work in the literature [27, 28]; they are summarized here to simplify the comparison of the clean and disordered cases. The Hamiltonian (44) is a special case of the general Bose-Hubbard model (1) with $U_i \equiv U$ and $J_{ij} \equiv J$ if sites i and j are nearest neighbors (but zero otherwise). After truncation of the local Hilbert spaces, the corresponding pseudo-spin-1 Hamiltonian reads

$$H_S = -\frac{\tilde{J}}{2} \sum_{\langle ij \rangle} (S_i^+ S_j^- + \text{h.c.}) + \frac{U}{2} \sum_i (S_i^z)^2 \,, \tag{45}$$

where $\tilde{J} = \bar{n} J$.

In a Bravais lattice, all sites are equivalent. This implies that the variational parameters in the product ansatz (6) for the ground state wave function do not depend on the lattice site, $\theta_i \equiv \theta$, $\eta_i \equiv \eta$. The variational ground state energy simplifies to

$$E_0 = \langle \Phi_0 | H_s | \Phi_0 \rangle = \frac{1}{2} NU \sin^2(\theta/2) - \frac{1}{2} Nz\tilde{J} \sin^2(\theta) \tag{46}$$

where N is the number of sites. It is minimized by a mixing angle θ that fulfills the mean-field equation $4z\tilde{J}\cos(\theta)\sin(\theta) = U\sin(\theta)$. A superfluid solution $\cos(\theta) = U/U_{c0}$ appears for interactions U below the critical value $U_{c0} = 4z\tilde{J}$. Its local order parameter $\psi_j = \langle S_j^+ \rangle = \mathrm{e}^{-i\eta} \sin(\theta)$ is uniform in space; it has magnitude $\sin(\theta) = \sqrt{1 - (U/U_{c0})^2}$ and arbitrary phase η (which we set to zero, as before).

We now turn to excitations on top of the mean-field ground state. In the clean case, the fluctuation Hamiltonians (15) and (16) take the form

$$\mathcal{H}_G = -\tilde{J}\cos^2(\theta/2) \sum_{\langle ij \rangle} (b_{G,i} + b_{G,i}^\dagger)(b_{G,j} + b_{G,j}^\dagger) + \varpi_G \sum_i n_{G,i} \,, \tag{47}$$

$$\mathcal{H}_H = -\tilde{J}\cos^2(\theta) \sum_{\langle ij \rangle} (b_{H,i} + b_{H,i}^\dagger)(b_{H,j} + b_{H,j}^\dagger) + \varpi_H \sum_i n_{H,i} \tag{48}$$

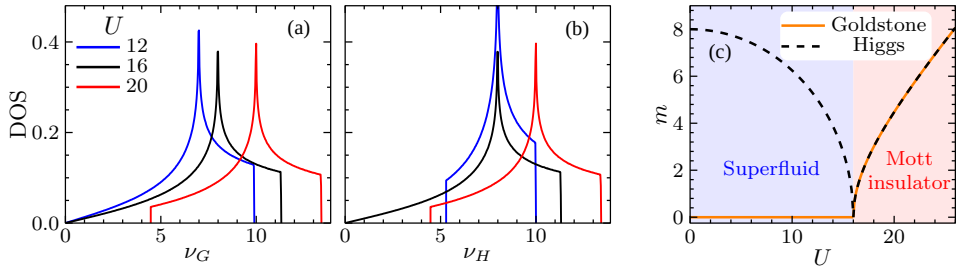

Figure 1: Eigenfrequency spectra (densities of states) of the collective Goldstone (a) and Higgs (b) modes for the clean square lattice Bose-Hubbard model for three values of U: superfluid ($U = 12$), critical point ($U = 16$), Mott phase ($U = 20$). ($\tilde{J}$ is set to unity.) (c) The masses (energy gaps) m_G and m_H of the Goldstone and Higgs collective modes.

with $\varpi_G = (U/2)\cos^2(\theta/2)+z\tilde{J}\sin^2(\theta)$ and $\varpi_H = (U/2)\cos(\theta)+2z\tilde{J}\sin^2(\theta)$. These Hamiltonians are translationally invariant. After a spatial Fourier transformation, they can be written as

$$\mathcal{H}_\alpha = \frac{1}{2}\sum_{\mathbf{q}} \left(b^\dagger_{\alpha,\mathbf{q}}, b_{\alpha,-\mathbf{q}}\right) \begin{pmatrix} C_{\alpha,\mathbf{q}} & D_{\alpha,\mathbf{q}} \\ D_{\alpha,\mathbf{q}} & C_{\alpha,\mathbf{q}} \end{pmatrix} \begin{pmatrix} b_{\alpha,\mathbf{q}} \\ b^\dagger_{\alpha,-\mathbf{q}} \end{pmatrix} + \text{const} \tag{49}$$

where $\mathbf{q}$ is the wave vector. The coefficients read

$$C_{G,\mathbf{q}} = \varpi_G - D_{G,\mathbf{q}}\,, \qquad D_{G,\mathbf{q}} = \epsilon(\mathbf{q})\cos^2(\theta/2)\,, \tag{50}$$

$$C_{H,\mathbf{q}} = \varpi_H - D_{H,\mathbf{q}}\,, \qquad D_{H,\mathbf{q}} = \epsilon(\mathbf{q})\cos^2(\theta)\,. \tag{51}$$

Here $\epsilon(\mathbf{q}) = \sum_j \tilde{J}_{ij} e^{i\mathbf{q}\cdot\mathbf{r}_{ij}}$ is the dispersion of the lattice. For a square lattice with nearest-neighbor interactions, it is given by $\epsilon(\mathbf{q}) = 2\tilde{J}\cos(q_x) + 2\tilde{J}\cos(q_y)$.

The Hamiltonians (49) can be solved by applying a (unimodal) Bogoliubov transformation to each $(\mathbf{q}, -\mathbf{q})$ pair. This yields

$$\mathcal{H}_\alpha = \sum_{\mathbf{q}} \nu_{\alpha,\mathbf{q}} d^\dagger_{\alpha,\mathbf{q}} d_{\alpha,\mathbf{q}} \tag{52}$$

with the excitation eigenenergies given by

$$\nu^2_{G,\mathbf{q}} = [\varpi_G - \epsilon(\mathbf{q})\cos^2(\theta/2)]^2 - [\epsilon(\mathbf{q})\cos^2(\theta/2)]^2\,, \tag{53}$$

$$\nu^2_{H,\mathbf{q}} = [\varpi_H - \epsilon(\mathbf{q})\cos^2(\theta)]^2 - [\epsilon(\mathbf{q})\cos^2(\theta)]^2\,. \tag{54}$$

The same result can also be obtained by using the first-quantization framework of Sec. 5, i.e., by transforming the fluctuation Hamiltonians (47) and (48) to position and momentum representation and diagonalizing the resulting coupling matrix via Fourier transformation. Figures 1(a) and 1(b) shows the resulting densities of states of the collective excitations.

The mass (or energy gap) m_α of the Goldstone and Higgs modes is given by the lowest excitation energy for a given set of parameters, i.e., $m_\alpha = \nu_{\alpha,\mathbf{q}=0}$. Using $\epsilon(\mathbf{q} = 0) = z\tilde{J}$, we therefore obtain $m^2_G = m^2_H = (U/4)(U - U_{c0})$ in the Mott insulating phase ($U > U_{c0}$). In the superfluid phase ($U < U_{c0}$), the gap of Goldstone mode vanishes, $m^2_G = 0$, whereas the gap of the Higgs mode reads $m^2_H = (1/4)(U^2_{c0} - U^2)$. Thus the Higgs mode is gapless at the critical point $U = U_{c0}$ only. The dependence of the masses on U is illustrated in Fig. 1(c).

8. Simulations and results

8.1. Overview

We now turn to the properties of the disordered Bose-Hubbard model for which the mean-field theory developed in Sec. 3 needs to be solved by means of computer simulations. Specifically, we focus on a square-lattice Bose-Hubbard model with nearest neighbor hopping. The quantum phase transition between superfluid and Mott insulator is tuned by varying the Hubbard interaction U whereas the scaled hopping amplitude is set to unity, $\tilde{J} = 1$, fixing the energy scale. As described in Sec. 2, we consider two types of (particle-hole-symmetry preserving) disorder, site dilution and random Hubbard interactions U_i.

In the case of site dilution, we employ dilution values (vacancy probabilities) $p = 0$, 1/8, 1/5, 1/4, and 1/3. For comparison, the site percolation threshold for the square lattice is $p_c = 0.407253$ [46]. For dilutions $p > p_c$, the lattice consists of disconnected finite-size clusters only that do not support long-range superfluid order. For dilutions $p < p_c$, an "infinite" cluster that spans the entire sample coexists with disconnected finite-size clusters. Since we are interested in long-range ordered states, we only consider the infinite cluster and neglect the finite clusters. In the case of random-U disorder, the lattice is undiluted but the local Hubbard interactions U_i are drawn from the distribution (2). We consider disorder strengths $r = 0.5$, 1.0 and 1.5.

Most calculations are performed on lattices of $L\times L$ sites with linear sizes up to $L = 256$. For a few calculations of excitations at higher energies, we employ linear sizes as large as $L = 1536$. In addition, we analyze strips of up to 128×10^6 sites within the recursive Green function approach of Sec. 6.3. All results are averaged over a large number of disorder realizations.

The first step in our approach is the numerical solution of the mean-field equations (8) which constitute a large system of coupled nonlinear equations. We implement two different numerical algorithms to solve these equations efficiently and accurately, a simple iterative method and a gradient descent method. In Appendix A, we describe these methods in more detail and discuss their accuracy and numerical stability.

8.2. Mean-field ground state

We now discuss the results of our computer simulations, starting with the properties of the mean-field ground state. To characterize the superfluid order, we compute the average and typical order parameters for a given sample (disorder realization), defined as the arithmetic and geometric means, respectively, of the local order parameters $\psi_j = \sin(\theta_j)$,

$$\Psi_{\rm av} = \frac{1}{N}\sum_j \psi_j \quad , \qquad \Psi_{\rm typ} = \exp\left(\frac{1}{N}\sum_j \ln(\psi_j)\right) . \tag{55}$$

Figure 2 presents the dependence of these quantities, averaged over a large number of disorder realizations,[2] on the Hubbard interaction for several strengths of both disorder types. In the clean case (included in Fig. 2(a) as dilution $p = 0$ and in Fig. 2(b) as $r = 0$), the average and typical order parameter coincide because all local order parameters ψ_j are identical. They follow the typical mean-field behavior $\Psi_{\rm av} = \Psi_{\rm typ} = \sqrt{1-(U/U_{c0})^2}$ for $U < U_{c0} = 16$ and $\Psi_{\rm av} = \Psi_{\rm typ} = 0$ for $U > U_{c0}$, as derived in Sec. 7.

[2] We have employed an arithmetic average over the disorder configurations; using a geometric average gives essentially the same results. This indicates that $\Psi_{\rm av}$ and $\Psi_{\rm typ}$ are already self-averaging for the system sizes considered.

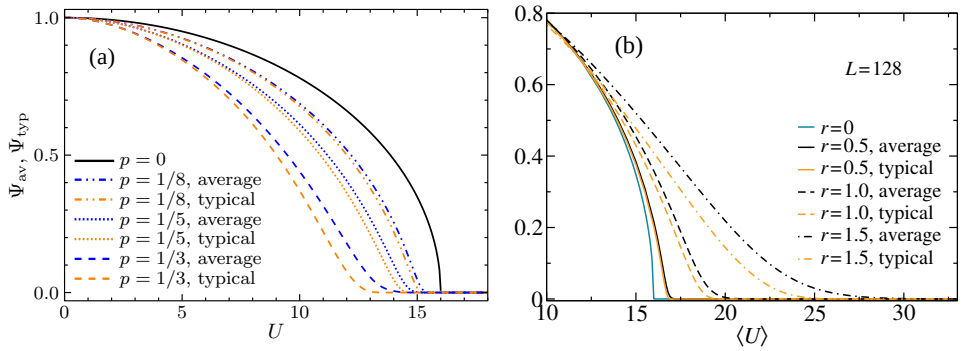

Figure 2: Average and typical order parameters Ψ_{av} and Ψ_{typ} vs. Hubbard interaction U. (a) Site-diluted systems of dilutions $p = 0, 1/8, 1/5$, and $1/3$. (b) Random-U disorder with disorder strength $r = 0.5, 1$, and 1.5. The data are based on (arithmetic) averages of Ψ_{av} and Ψ_{typ} over 1000 disorder realizations for square lattices of linear size $L = 128$. The statistical errors are below the line thickness.

Figure 2(a) demonstrates that the superfluid order is suppressed with increasing dilution, as expected, because the missing neighbors lead to an overall reduction of the coupling strength. Close to the onset of superfluidity, the typical order parameter is significantly smaller than the average one, indicating that rare superfluid islands (puddles) coexist with insulating regions. These rare puddles are also responsible for the pronounced tails of the order parameter curves towards large U. In an infinite system, impurity-free regions of arbitrary size exist with exponentially small (in their size) but nonzero probability. As the largest of these regions develop superfluid order for U values right below the clean critical point $U_{c0} = 16$, the exponential tails of the order parameter curves stretch all the way to the clean critical point in the thermodynamic limit. It must be emphasized that these tails are artifacts of the mean-field theory which is unable to describe fluctuations of the superfluid order. In reality, the superfluid order on isolated rare regions is not static and thus does not contribute to the order parameter. The rare regions instead fluctuate, as expected in a quantum Griffiths phase [24, 25]. Indeed, quantum Monte Carlo simulations do not show exponential tails in the order parameter curves but sharp power-law singularities associated with a conventional critical point at $U_c(p) < U_{c0}$ [47, 48]. Effectively, the mean-field approximation (incorrectly) replaces the quantum Griffiths phase by the tail of a smeared quantum phase transition [17, 49]. This also implies that the exact location of the quantum phase transition cannot be determined within the mean-field theory. Deeper inside the ordered phase where superfluidity is not restricted to rare puddles but becomes more homogeneous, the mean-field description becomes qualitatively correct.

Figure 2(b) shows the order parameter curves for the case of random-U disorder. Interestingly, the onset of superfluidity shifts to larger (average) Hubbard interaction $\langle U \rangle$ with increasing disorder strength. This is caused by spatial regions in which the majority of the local Hubbard interactions U_i are below the average $\langle U \rangle$. These regions are locally in the superfluid phase before $\langle U \rangle$ reaches the clean critical value U_{c0}. Analogous to the case of dilution disorder, the order parameter curves develop spurious exponential tails towards large U. In the thermodynamic limit, these tails terminate at $U_{c0}/(1 - r/2)$.

To further elucidate the inhomogeneous mean-field ground state, the first row of Fig. 3 presents heat maps of the local order parameter ψ_j for a single disorder realization of a sys-

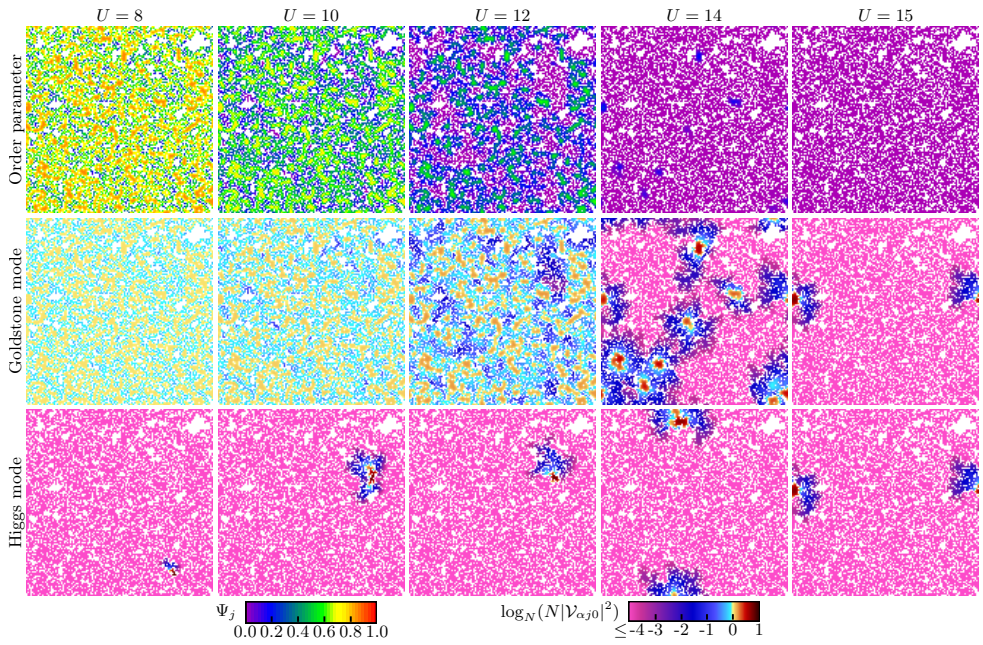

Figure 3: Local order parameters ψ_j, and eigenstate wavefunctions $\mathcal{V}_{Gj0}$ and $\mathcal{V}_{Hj0}$ of the lowest Goldstone and Higgs excitations of a single disorder realization (diluted lattice with $L = 128$, $p = 1/3$, and different U). White sites represent vacancies or sites of disconnected finite-size clusters that have been neglected.

tem with dilution $p = 1/3$. The figure illustrates that the superfluid order consists of puddles embedded in an insulating bulk for U values close to the quantum phase transition (i.e., in the tail of the superfluid phase). In contrast, the order parameter is only moderately inhomogeneous at lower U, deeper in the superfluid phase. An analogous plot of the local order parameter for the case of random-U disorder is shown in Fig. B.14 in Appendix B.

8.3. Excitation spectrum

We now turn to the excitations on top of the mean-field ground state, starting with a discussion of the excitation spectrum, i.e., the eigenvalues of the fluctuation Hamiltonians $\mathcal{H}_G$ and $\mathcal{H}_H$ given in eqs. (15) and (16), respectively. Figures 4(a) and 4(b) present the densities of state for the Goldstone and Higgs excitations for the case of dilution disorder with $p = 1/3$ for several values of U. The qualitative behavior is analogous to the clean case shown in Fig. 1. In the superfluid phase, the Higgs mode has a nonzero energy gap (mass) m_H whereas the energy gap m_G of the Goldstone mode vanishes identically in agreement with Goldstone's theorem. In the Mott-insulating phase, the two excitation sectors are degenerate and gapped. The U-dependence of both energy gaps is further illustrated in Fig. 4(c). As expected, the Higgs mode softens close to the superfluid-Mott insulator transition, i.e., its mass approaches zero. In contrast to the clean case shown in Fig. 1, the (average) Higgs mass does not appear to reach exactly the value zero at the transition point. This can be attributed to finite-size effects, as each finite-size sample (disorder realization) has a slightly different critical U for which a superfluid solution first appears. Averaging the masses thus smears the gap. This effect is exacerbated by the artifacts of

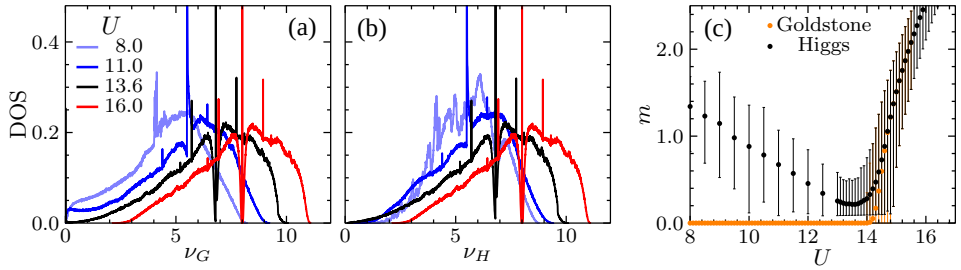

Figure 4: Eigenfrequency spectra (density of states) of the Goldstone (a) and Higgs (b) modes for dilution $p = 1/3$ and four interaction values, $U = 8$ (superfluid phase), 11 and 13.6 (close to the quantum phase transition), and 16 (Mott-insulating phase). The data are averages over 384 disorder realizations of square lattices of linear size $L = 128$. (c) Masses (energy gaps) m_G and m_H of the Goldstone and Higgs modes. The dots show the average over 1000 realizations, the bars show the spread of observed values.

the mean-field solution discussed in Sec. 8.2. The mean-field solution allows static superfluid order to appear on isolated rare regions, greatly increasing the variations of the critical U between (finite-size) disorder configurations, and shifting their values towards the clean $U_{c0} = 16$.

At higher energies, the densities of state of both modes show sharp features. They are caused by the discrete nature of the dilution disorder, i.e., they stem from small finite-size clusters of sites which support excitations of fixed energies.

Systems with random-U disorder feature analogous behavior, as can be seen in Fig. 5. Note that their densities of state do not show the sharp features at higher energies present for dilution disorder because the random-U distribution is continuous.

8.4. Localization properties of lowest Goldstone and Higgs excitations

After having discussed the energy spectrum of the excitations, we now consider the eigenstates. The present section focuses on the lowest-energy excitations in both the Goldstone and Higgs channels. Figure 3 visualizes examples of their eigenstates for a diluted lattice with $p = 1/3$ and several U. Examples of the lowest-energy Goldstone and Higgs eigenstates in a system with random-U disorder are shown in the appendix in Fig. B.14. Clearly, the eigenstates feature nontrivial spatial localization behavior that depends on the channel and varies with U.

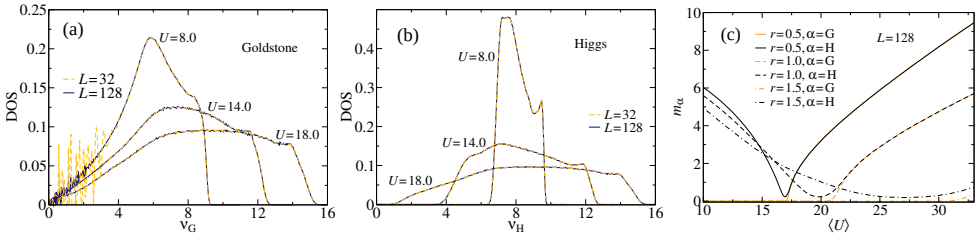

Figure 5: Eigenfrequency spectra (density of states) of the Goldstone (a) and Higgs (b) modes for three values of U: $U = 8$, and $U = 14$ in the superfluid phase as well as $U = 18$ close to the quantum phase transition. (Square lattices of linear sizes $L = 32$ and 128, random-U disorder with $r = 1.0$.) (c) Masses (energy gaps) m_G and m_H of the Goldstone and Higgs modes for several disorder strengths r. All data are averages over 1000 disorder realizations.

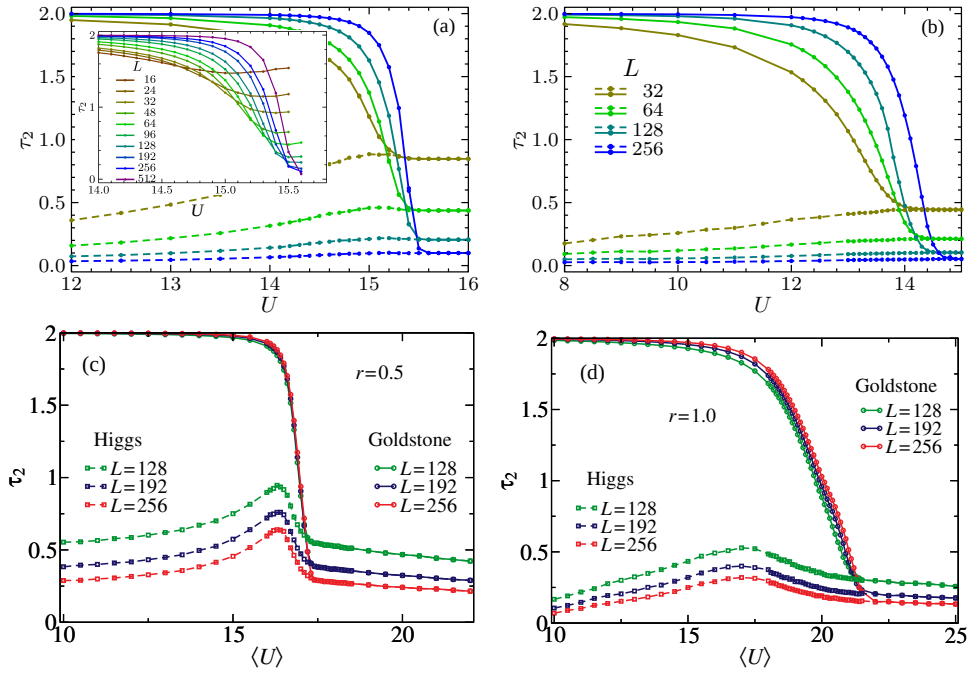

Figure 6: Generalized dimension τ_2 of the lowest-energy Goldstone (solid lines) and Higgs (dashed lines) excitations vs. interaction U for several system sizes L. (a) dilution $p = 1/8$, (b) dilution $p = 1/3$, (c) random-U disorder of strengths $r = 0.5$, and (d) random-U disorder of strengths $r = 1.0$. The box size l is chosen according to $L/l = 8$. The data are averages over 1000 disorder realizations. Statistical errors are smaller than the symbol size. The inset of panel (a) shows a magnification of the transition region, using the analytic expression (57) for the lowest Goldstone excitation.

To analyze the localization properties quantitatively, we compute the generalized dimension τ_2 of the lowest Goldstone and Higgs excitations, as defined in eq. (38). The dependence of τ_2 on the Hubbard interaction U is shown in Fig. 6 for both types of disorder and several disorder strengths. All cases feature the same qualitative behavior. In the Mott-insulating phase (large U), both excitations are degenerate. The τ_2 values rapidly decrease towards zero with increasing system size, indicating strong localization.

As the system enters the superfluid phase with decreasing U, the two excitation branches evolve in qualitatively different ways. The lowest Higgs excitation stays localized for all U. For strong disorder, the degree of localization even seems to increase in the superfluid phase as τ_2 further decreases. The lowest Goldstone excitation, in contrast, undergoes a striking delocalization transition upon entering the superfluid phase. Its τ_2 value rapidly increases with decreasing U. Importantly, the system-size dependence of τ_2 also changes sign, it now increases with increasing L towards the value $\tau_2 = 2$ characteristic of an extended state.

The delocalization transition of the lowest Goldstone excitation as a function of U is also observed in the dimensionless Lyapunov exponent Γ_G calculated from quasi-one-dimensional (strip) samples, as described in Sec. 6.3. Figure 7 presents the U-dependence of the dimensionless Lyapunov exponents for diluted lattices with $p = 1/8$ and $1/3$. For both dilutions, Γ_G rapidly increases with increasing L in the Mott-insulating phase, indicating strong localization. In the

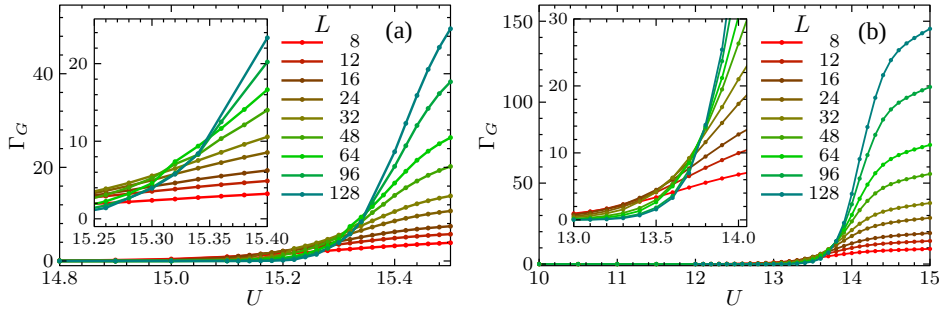

Figure 7: Dimensionless Lyapunov exponent of the lowest-energy Goldstone excitation vs. interaction U for several strip width L. (a) dilution $p = 1/8$. (b) dilution $p = 1/3$. The data are averages over 12 strips of size $L \times 10^6$ sites. Statistical errors are smaller than the symbol size. The insets show magnifications of the crossing regions.

superfluid phase Γ_G is small and decreases with increasing L, as expected for spatially extended states.

Our numerical results for the generalized dimension τ_2 and the dimensionless Lyapunov exponent Γ demonstrate that the location of the delocalization transition of the lowest Goldstone excitation as a function of U is closely tied to that of the (thermodynamic) quantum phase transition between Mott insulator and superfluid. It would be desirable to establish whether or not these two transitions actually coincide, i.e., occur at the same value of U. Unfortunately, the numerical determination of the delocalization transition point suffers from the same mean-field artifacts already discussed in Secs. 8.2 and 8.3: As mean-field theory produces a spurious tail of the ordered phase, the seeming transition point moves to larger U with increasing system size, reaching the clean critical value U_{c0} in the thermodynamic limit in the case of dilution disorder.[3] This effect can actually be observed in our numerical data. The insets of Figs. 6(a), 7(a), and 7(b) show that the crossing points of the τ_2 and Γ_G curves with consecutive system sizes L move towards larger U and towards the localized limit with increasing L.

Even though the artifacts of mean-field theory prevent us from accurately determining the delocalization transition point, we can show analytically that the lowest Goldstone excitation is extended over the entire sample if the system features superfluid long-range order. This can be demonstrated as follows. According to Goldstone's theorem, the lowest eigenstate of the Goldstone Hamiltonian $\mathcal{H}_G$ must have zero energy, $\nu_{G,0} = 0$, in the superfluid phase because the superfluid ground state spontaneously breaks the $U(1)$ order-parameter symmetry. (We have verified this numerically for all samples.) For this state, the corresponding eigenvalue problem (21) simplifies to a system of linear equations,

$$\sum_k X_{G,jk} \mathcal{V}_{G,k0} = \nu_{G,0}^2 \mathcal{V}_{G,j0} = 0 \,. \tag{56}$$

A non-trivial solution of this system is given by

$$\mathcal{V}_{G,j0} = \Upsilon \frac{\sin(\theta_j/2)}{\sqrt{\varpi_{G,j}}} \tag{57}$$

[3] For random-U disorder, the tail is expected to stretch to $U_{c0}/(1 - r/2)$.

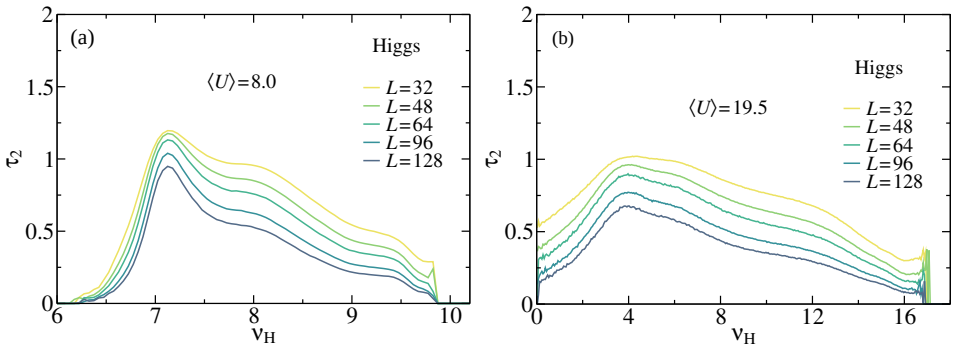

Figure 8: Generalized dimension τ_2 vs. excitation energy ν_H of the Higgs excitations for two different values of $\langle U\rangle$ and several system sizes L. (Random-U disorder of strength $r = 1.0$.) The data are averages over 1000 disorder realizations. Statistical errors are similar to the line widths.

as can be easily checked by inserting it back into the system (56). Here, Υ is a normalization constant. Thus, the lowest Goldstone eigenstate depends on the order parameter $\sin(\theta_j)$ and local interactions (via $\varpi_{G,j}$) only. The denominator of the solution (57) is bounded from both below and above. (For dilution disorder, $\varpi_{G,j} \geq U/4$ and $\varpi_{G,j} \leq U/2 + 4\tilde{J}$.) Consequently, the localization character of $\mathcal{V}_{G,j0}$ is governed by that of the order parameter.

A long-range ordered superfluid state features a nonzero macroscopic order parameter $\Psi_{\rm av}$ in the thermodynamic limit. This implies either a more-or-less homogeneous superfluid or at least a nonzero density of superfluid puddles. According to Eq. (57), this means that the wave function of the lowest Goldstone excitation is nonzero on a finite fraction of the lattice sites, i.e., it is extended. In the Mott-insulating phase, the local order parameters $\psi_j = \sin(\theta_j)$ vanishes on all lattice sites. Thus, the state (57) is not normalizable, indicating the absence of a zero-energy mode.

8.5. Localization properties of higher Goldstone and Higgs excitations

We now turn to higher excitations in both the Goldstone and the Higgs channels. In the Mott-insulating phase their behavior is easily understood. As all local order parameters ψ_j vanish in the Mott insulating phase, the disorder in the fluctuation Hamiltonians $\mathcal{H}_G$ and $\mathcal{H}_H$ or, equivalently, the disorder in the coupling matrices $\mathbf{X}_G$ and $\mathbf{X}_H$ is produced by the values of U_i and $\tilde{J}_{ij}$ only. The disorder is thus uncorrelated in space guaranteeing that all excitations in the Mott-insulating phase are localized in two space dimensions.

The situation in the superfluid phase is more complicated because the coefficients of $\mathcal{H}_G$ and $\mathcal{H}_H$ (or the matrix elements $X_{G,jk}$ and $X_{H,jk}$) depend on the local mixing angles θ_j. These angles are correlated because they fulfill the mean-field equations (8). Close to the superfluid-Mott insulator transition, the correlations become long-ranged. For correlated disorder, both extended and localized states are possible even in two space dimensions.

We first analyze the Higgs excitations in the superfluid phase. Figure 8 presents the generalized dimension τ_2 as a function of excitation energy ν_H for a system with random-U disorder of strength $r = 1$. For both interaction strengths shown, viz., $\langle U\rangle = 8$ (deep in the superfluid phase) and $\langle U\rangle = 19.5$ (close to the superfluid-Mott insulator transition), τ_2 decreases with increasing system size at all energies ν_H. This implies that the Higgs excitations are localized for all ener-

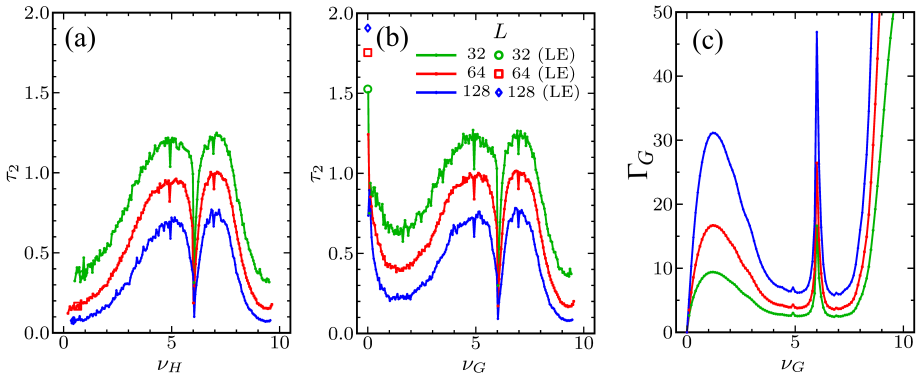

Figure 9: Generalized dimension τ_2 of Higgs (a) and Goldstone (b) excitations vs. excitation energy ν for $U = 12$, dilution $p = 1/3$ and several system sizes L with $L/l = 8$. The solid lines represent averages of τ_2 over small energy windows (width 0.1) and 100 to 400 disorder configurations, depending on L. The values of τ_2 of the lowest-energy excitation (averaged over all disorder configurations) are shown as open symbols. (c) Dimensionless Lyapunov exponent Γ_G of the Goldstone excitations vs. excitation energy ν_G, calculated using the iterative Green's function method on strips of $L \times 10^6$ sites (the data are averages over 12 strips)

gies. We have obtained the same result for the other studied strengths, $r = 0.5$ and 1.5, of the random-U disorder as wells as for dilution disorder, as illustrated in Fig. 9(a).

The Goldstone excitations in the superfluid phase display a more complex behavior. Figure 9(b) presents the generalized dimension τ_2 of the Goldstone excitation as a function of excitation energy ν_G for a diluted system with $p = 1/3$ at $U = 12$, slightly inside the superfluid phase. The figure shows that τ_2 for the lowest Goldstone excitation increases with system size. This indicates an extended state in agreement with the results discussed in Sec. 8.4. For all other excitation energies, τ_2 decreases with system size, implying that all Goldstone excitations except the lowest one are localized. The same information can also be gained from Fig. 9(c) which shows the dimensionless Lyapunov exponent Γ (calculated via the recursive Green function approach) as a function of energy ν_G. Γ increases with increasing strip width for all nonzero energies, indicating that the Goldstone mode is localized. However, Γ decreases rapidly as the energy ν_G approaches zero, and for $\nu_G = 0$, the Lyapunov exponent vanishes for all strip widths, indicating an extended state.

We observe analogous behavior for other dilution values as well as for random-U disorder, as illustrated in Fig. 10. If the disorder is weak and/or the system is deep in the superfluid phase [as in Fig. 10(a)], the data seem to suggest – at the first glance – an entire range of energies with extended states because the τ_2 vs. ν_G curves for different system sizes display a crossing at a nonzero energy. Below the crossing τ_2 increases with size. However, a more careful analysis shows that the crossing energy ν_G^* between the τ_2 curves for two consecutive sizes shifts towards $\nu_G = 0$ with increasing size, as illustrated in the inset of Fig. 10(a). In all such cases we have found no indication of the crossing points converging to a nonzero energy. We thus conclude that all Goldstone modes with nonzero excitation energy are localized in the thermodynamic limit, even if the system is weakly disordered and/or deep inside the superfluid phase.

It is interesting to compare Figs. 9(a) and (b). The Higgs and Goldstone modes show almost identical τ_2 for larger excitation energies, $\nu \gtrsim 3$, reflecting the fact that the two modes are still almost degenerate close to the quantum phase transition. Analogously, the Higgs mode shown

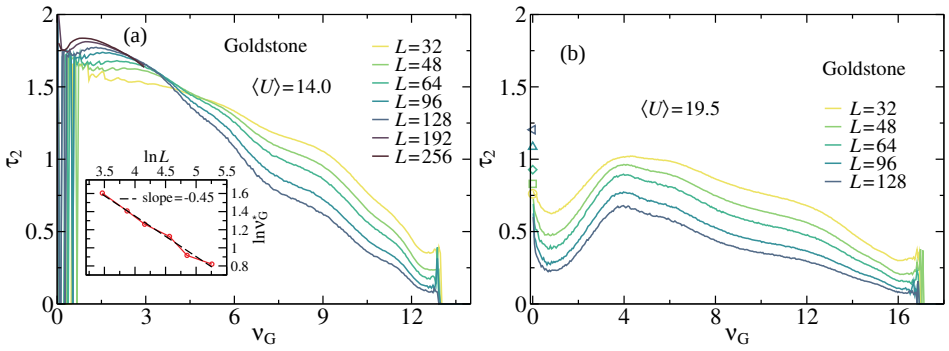

Figure 10: Generalized dimension τ_2 vs. excitation energy ν_G of the Goldstone excitations for several linear system sizes L and two different values of U. (Random-U disorder of strengths $r = 1.0$.) The data are averages over 1000 disorder realizations. Statistical errors are comparable to the line widths. Inset: Crossing energy ν_G^* vs. linear system size L.

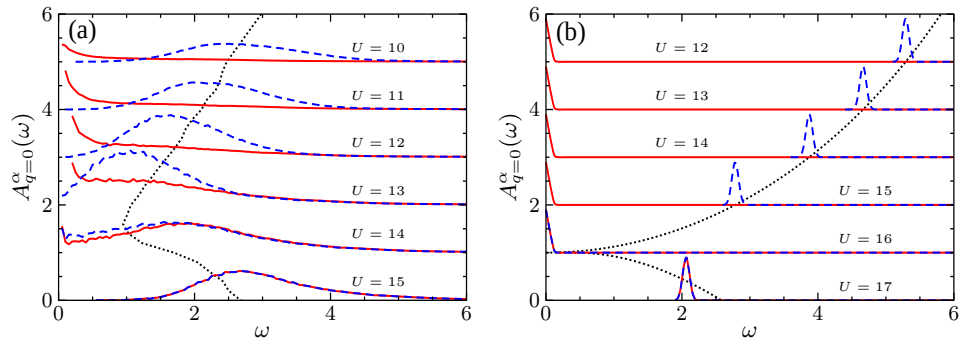

Figure 11: Spectral functions $A^G_{\mathbf{q}=0}(\omega)$ and $A^H_{\mathbf{q}=0}(\omega)$ of the Goldstone (solid lines) Higgs (dashed lines) excitations, respectively, for several interaction strengths U. The curves are shifted upwards with increasing U. Dotted lines mark the position of the Higgs peak in A^H. (a) Dilution $p = 1/3$ ($L = 128$, 240 disorder realizations, statistical errors are comparable to the line widths). (b) Clean case, $p = 0$; here the peaks in the figure represent δ functions.

in Fig. 8(b) and the Goldstone mode shown in Fig. 10(b) for the case of random-U disorder feature the same τ_2 for energies $\nu \gtrsim 4$. Also note that the sharp features at energies around $\nu = 6$ observed in all panels of Fig. 9 are the result of the discrete character of the site dilution disorder. They are absent for random-U disorder (where the local interactions are drawn from a continuous distribution).

8.6. Dynamic susceptibilities

We now analyze the spectral functions A^G and A^H associated with the Goldstone and Higgs Green functions (30) and (31), respectively. Figure 11 presents these spectral functions, computed from the mean-field eigenenergies and eigenstates using (34), at zero wave vector for several interactions U, contrasting the clean case with dilution $p = 1/3$. The spectral functions of the diluted system are very broad, even though the (single-particle) eigenstates of $\mathcal{H}_G$ and $\mathcal{H}_H$ are noninteracting within the Gaussian approximation and thus have no intrinsic width. This

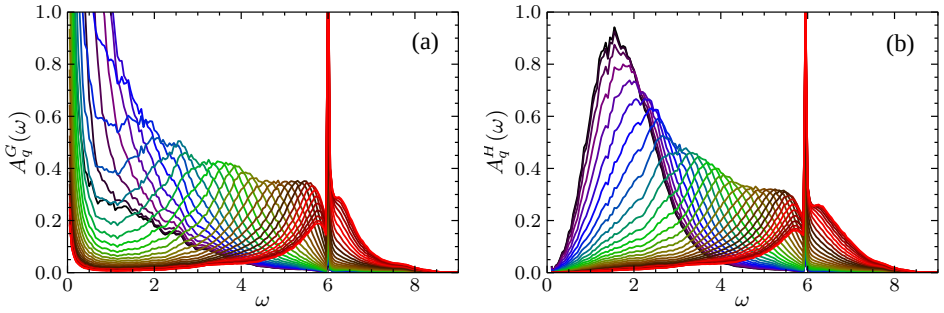

Figure 12: Spectral functions $A^G_{\mathbf{q}}(\omega)$ and $A^H_{\mathbf{q}}(\omega)$ vs. ω for a diluted system with $p = 1/3$ and $U = 12$ ($L = 128$, 240 disorder realizations, statistical errors are comparable to the line widths). The wavevector q_x varies from $q_x = 0$ (black) to $q_x = \pi$ (red) in 32 steps while q_y is fixed at zero.

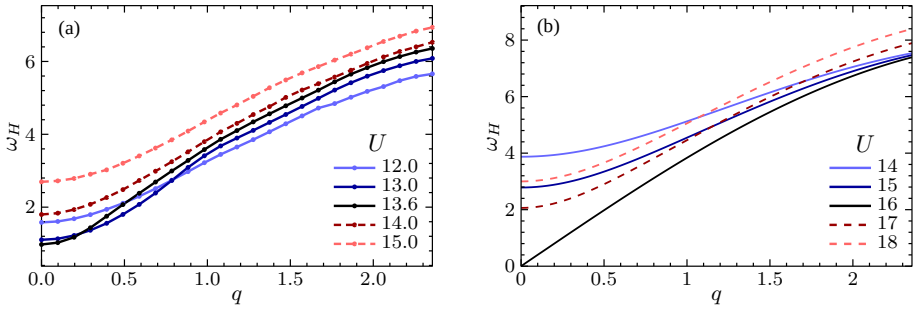

Figure 13: (a) Peak position ω_H of the Higgs spectral function $A^H_{\mathbf{q}}(\omega)$ shown in Fig. 12 vs. wave vector q (along the coordinate directions). (b) ω_H vs. q for the clean case.

broadening stems from the fact that many localized eigenstates contribute to the zero-wave-vector spectral function, i.e., it is caused by disorder-induced localization effects. We also observe that the peak energy ω_H of the Higgs spectral function does not soften at the superfluid-Mott insulator transition, mirroring the Monte Carlo results of Ref. [32]. (Note that the peak energy ω_H differs from the energy gap m_H that marks the lowest excitation energy.) In contrast, the clean spectral functions show the expected δ peaks at energies corresponding to the Higgs and Goldstone masses.

We also investigate the q-dependence of the Goldstone and Higgs spectral functions. Figure 12 presents $A^G_{\mathbf{q}}(\omega)$ and $A^H_{\mathbf{q}}(\omega)$ for a diluted system ($p = 1/3$) slightly inside the superfluid phase. The Higgs spectral function $A^H_{\mathbf{q}}(\omega)$ further broadens with increasing q, and the peak energy ω_H increases. The resulting dispersion relation $\omega_H(q)$ is presented in Fig. 13 and compared to that of the clean system. In the clean case, the data show the behavior expected for a $z = 1$ quantum critical point. The low-energy dispersion is linear, $\omega_H \sim |\mathbf{q}|$, at criticality $U = U_{c0} = 16$. Away from criticality, it crosses over to the quadratic form $\omega_H(q) = \omega_H(0) + c\mathbf{q}^2$. In contrast, the dispersion of the diluted system does not change much with the distance from criticality, and features always a quadratic q-dependence for small q. The Goldstone spectral function $A^G_{\mathbf{q}}(\omega)$

also develops a finite-energy peak for larger q. However, even at the largest q, $A^G_{\mathbf{q}}(\omega)$ retains a zero-energy peak, albeit of reduced amplitude. This suggests that the lowest (zero-energy) Goldstone excitation has nonzero Fourier components in the entire Brillouin zone.

9. Conclusions

In summary, we have developed a quantum mean-field theory for a model of disordered and interacting bosons. It describes the quantum ground state as an inhomogeneous product wave function. The mean-field theory needs to be solved numerically, but it is able to capture the spatial inhomogeneities of the superfluid order parameter. Collective excitations are then obtained from an expansion of the Hamiltonian in the fluctuations about the mean-field ground state up to quadratic order. Extensive numerical calculations have demonstrated that all excitations are spatially localized in the Mott-insulating phase (where the two modes are degenerate because the $U(1)$ order parameter symmetry is not broken) for arbitrary excitation energy. The Higgs mode is still localized for all energies in the superfluid phase. In contrast, the lowest (zero-energy) Goldstone excitation delocalizes in the superfluid phase whereas all higher-energy Goldstone excitations are localized. This implies that there is no mobility edge for the excitations at a nonzero energy. In this concluding section we put our results into a broader perspective, and we discuss open questions.

Let us comment on the validity of the mean-field approach. Based on a comparison with recent Monte Carlo simulations [47, 48, 50], the qualitative thermodynamic properties of the model are well described by the mean-field solution outside of the immediate vicinity of the superfluid-Mott insulator quantum phase transition. The mean-field ground state in the superfluid phase features a spatially inhomogeneous local order parameter. The relative spatial variations of the order parameter are small deep inside the phase but they grow as the quantum phase transition is approached. Unfortunately (but not unexpectedly), the mean-field approach fails to correctly describe the Mott glass, i.e., the quantum Griffiths phase of the superfluid-Mott insulator transition in which isolated superfluid puddles coexist with an insulating bulk. As the mean-field theory cannot account for order parameter fluctuations, it assigns a static superfluid order parameter to these puddles (rare regions), effectively replacing the quantum Griffiths phase with the tail of a smeared quantum phase transition. If it were correct, such an exotic smeared quantum phase transition would be an exciting finding. Here it is a mean-field artifact as the superfluid-insulator quantum phase transition in our model has been shown to be conventional by the above-mentioned Monte Carlo simulations, in agreement with the general classification of disordered quantum phase transitions [22–24].

One important consequence of this shortcoming of mean-field theory is that we are unable to locate the exact position of the delocalization transition of the lowest Goldstone excitation as a function of U and its relation to the location of the (thermodynamic) superfluid-Mott insulator quantum phase transition. For the same reasons we also cannot study the localization properties of excitations associated with fluctuating rare regions in the Griffiths (Mott glass) phase.

The quadratic (Gaussian) approximation of the fluctuation Hamiltonians $\mathcal{H}_G$ and $\mathcal{H}_H$ does not take anharmonic (mode-coupling) effects into account. They could be included by keeping higher-order terms in the expansion of the Hamiltonian. Exploring their effects and the interplay between the anharmonicities and the disorder remains a task for the future. Despite these limitations, the predictions of the mean-field approach for the Goldstone and Higgs excitations (outside of the Griffiths phase) agree well with the results of recent, numerically exact Monte Carlo simulations of the excitations [32], giving us confidence in their qualitative validity.

Let us now consider our results from the point of view of localization physics. The collective mode eigenvalue problems (21) are governed by real symmetric disordered coupling matrices. Based on the properties of single-particle (Anderson) localization in the orthogonal symmetry class, the generic expectation in a two-dimensional system therefore is that all states are localized, at least if the disorder is uncorrelated [51]. As pointed out at the beginning of Sec. 8.5, the disorder in the fluctuation Hamiltonians in the Mott insulating phase is indeed uncorrelated because it depends on the uncorrelated random variables U_i and $\tilde{J}_{jk}$ only. Thus, the localization of all excitations in the Mott insulating phase is a direct consequence of well-known single-particle localization physics. In the superfluid phase, in contrast, the disorder in the fluctuation Hamiltonians is correlated because it depends on the local order parameters ψ_j which are the solutions of the coupled mean-field equations (8). Interestingly, these correlations seem to have the opposite effects for the Goldstone and Higgs Hamiltonians. The Higgs excitations remain localized in the superfluid phase, and the degree of localization often increases, whereas the lowest Goldstone excitation completely delocalizes into an extended state. Understanding in detail what properties of the correlations are responsible for these opposite results remains a task for future work, as it has proven to be a formidable task in Hubbard chains [52].

The Goldstone mode actually features two separate localization transitions, (i) the transition of the lowest excitation as function of U, from localized in the Mott phase to extended in the superfluid phase, and (ii) the transition at fixed U (in the superfluid phase) from extended at zero energy to localized at nonzero excitation energies. The critical behaviors of these transitions and their relation are important open problems. Do the transitions meet at a multicritical point located at zero energy and some critical U which may or may not coincide with the thermodynamic critical point?

Within the quadratic (Gaussian) approximation, the fluctuation Hamiltonians describe noninteracting quasi particles. It is interesting to ask whether concepts of many-body localization become important for the collective excitations once anharmonic terms beyond the quadratic approximation are included. Specifically, will mode coupling effects have delocalizing tendencies for higher excitations in the middle of the energy band where the density of states is large and anharmonic terms should be able to couple a large number of states?

In this paper, we have focused on the two-dimensional Bose-Hubbard Hamiltonian. However, the mean-field approach can be applied to three-dimensional systems as well. The thermodynamic critical behavior of the superfluid-Mott glass quantum phase transition in three dimensions has recently been shown to be conventional and similar to the two-dimensional transition [53]. It will be interesting to study the collective excitations in this case. Some work along these lines is already in progress. In addition, the mean-field approach can be generalized to other problems such as the generic superfluid-Bose glass transition.

In conclusion, our results show that disordered quantum phase transitions can feature unconventional collective excitations even if their thermodynamic critical behavior is entirely conventional. This raises the question of whether or not one can classify the excitation dynamics of disordered quantum phase transitions along similar lines as their thermodynamics [22–24]. Is the lowest Goldstone mode always delocalized? Under what conditions does a mobility edge appear? Is it related to many-body localization? What role is played by the space dimensionality? These questions will be addressed in future work.

Acknowledgements

This work was supported by the NSF under Grant Nos. DMR-1506152, DMR-1828489, PHY-1607611, and OAC-1919789, by Conselho Nacional de Desenvolvimento Científico e Tecnológico (CNPq) under Grant No. 312352/2018-2, and by FAPESP under Grant Nos. 2015/23849-7 and 2016/10826-1. T.V. and J.A.H. acknowledge the hospitality of the Aspen Center for Physics, and T.V. thanks the Kavli Institute for Theoretical Physics where part of the work was performed.

Appendix A. Numerical solution of the mean-field equations

The first step in our approach is the numerical solution of the mean-field equations (8) which constitute a large system of coupled nonlinear equations. We implement two different numerical algorithms to solve these equations efficiently and accurately, a simple iteration and a gradient descent method.

The first method consists of rewriting the mean-field equations (8) in the form

$$\sin(\theta_i) = (4/U_i)\sqrt{1-\sin^2(\theta_i)}\sum_j \tilde{J}_{ij}\sin(\theta_j)\,. \tag{A.1}$$

It then starts from a guess for the local order parameters $\psi_i = \sin(\theta_i)$, for example random numbers between 0 and 1. Inserting these values on the r.h.s. of (A.1) produces new values on the l.h.s. of the equation. This step is iterated until the difference between the old and new values falls below an accuracy threshold. As our model does not contain competing interactions, the mean-field ground state is unique (up to the overall phase which we have fixed at zero). The iterative method reliably converges to the ground state even though the convergence becomes very slow close to the superfluid-Mott insulator transition.

The gradient descent method numerically minimizes the mean-field ground state energy (7),

$$E_0 = -\frac{1}{2}\sum_{ij}\tilde{J}_{ij}\sin(\theta_i)\sin(\theta_j) + \frac{1}{2}\sum_i U_i\sin^2(\theta_i/2), \tag{A.2}$$

with respect to local order parameters $\sin(\theta_i)$. In each step of the method, we obtain an improved set of order parameters by finding the local energy minimum along the gradient direction $-\partial E_0/\partial\sin(\theta_i)$. This approach converges when no energy reduction can be achieved within a prescribed accuracy.

Interestingly, the simple iterative solution of (A.1) turns out to be more accurate, in particular in situations where the local order parameters are close to zero. The gradient method loses the ability to discriminate between states that are close in energy, mainly due to the numerical errors in the transformation between $\sin(\theta_i)$ and $\cos(\theta_i)$ and the computation of energy differences. The strongest impact of the numerical inaccuracies occurs in the Griffith region, where superfluid puddles in a insulating matrix lead to differences of several orders of magnitudes in the local order parameter. In the Griffiths region, the energy difference between the lowest and second-lowest Goldstone excitations can become extremely small, and the numerical inaccuracies can cause them to switch places. If that happens, the seeming (but incorrect) lowest Goldstone excitation disagrees with the analytical expression (57). As the two lowest Goldstone excitations can have very different localization properties, such switches introduce sizable errors in the results. Using

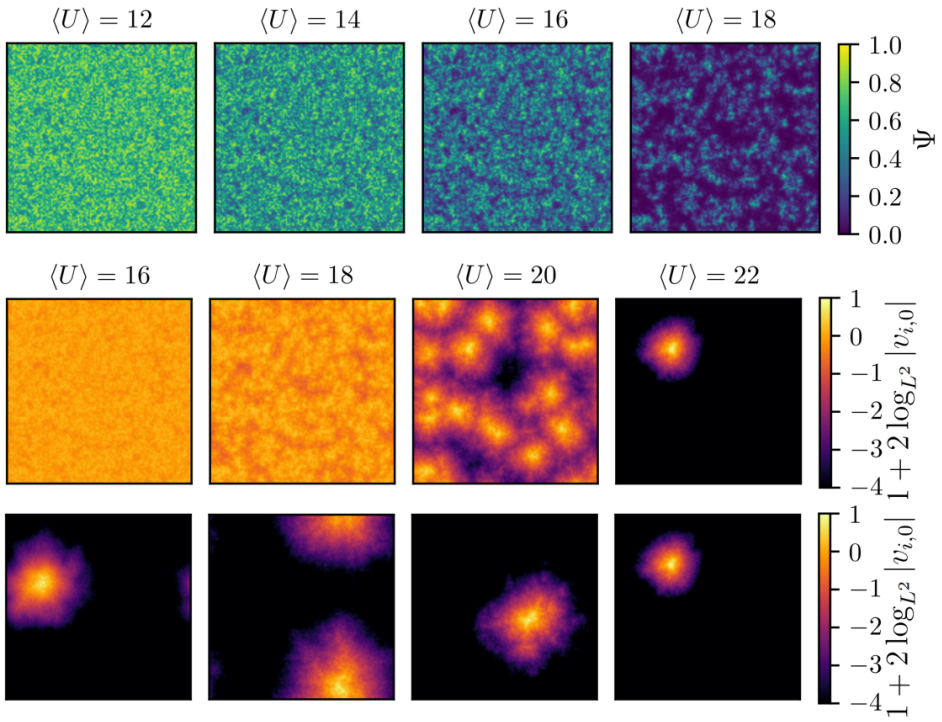

Figure B.14: Local order parameters ψ_j (top row), and eigenstate wavefunctions $\mathcal{V}_{G,j0}$ and $\mathcal{V}_{H,j0}$ of the lowest Goldstone (middle row) and Higgs (bottom row) excitations of a single disorder realization ($L = 128$, random-U disorder with $r = 1.0$, and different U).

quadruple precision real variables (16 byte) instead of double precision (8 bytes) alleviates this problem at the price of significantly slower performance. Moreover, the exact expression (57) for the ground state can be used to check the numerics. The iteration method, fulfilling the mean-field equations locally with higher accuracy, does not suffer from this effect but is very slow in the Griffiths phase.

To overcome these difficulties, we often compute the mean-field ground state using quadruple precision but perform the consecutive analysis of the excitations in double precision. In this way, the coupling matrices $X_{G,ij}$ and $X_{H,ij}$ in the eigenvalue problem for the excitations are effectively free of numerical errors (within double precision) which turns out to be sufficient for reliable results.

Appendix B. Local order parameters and eigenstates for the case of random U disorder

Figure B.14 presents the local order parameters ψ_j and the wave functions of the lowest Goldstone and Higgs excitations for a single disorder realization of a system with random-U disorder ($r = 1$). The qualitative features are similar to those of the diluted system shown in Fig. 3. The order parameter features superfluid puddles in an insulating bulk close to the onset of superfluidity. Deeper inside the superfluid phase , the order parameter is only weakly

inhomogeneous. The lowest Higgs excitation is strongly localized for all U whereas the lowest Goldstone excitation undergoes a delocalization transition when the system enters the superfluid phase.

References

[1] B. C. Crooker, B. Hebral, E. N. Smith, Y. Takano, J. D. Reppy, Superfluidity in a dilute bose gas, Phys. Rev. Lett. 51 (1983) 666–669. doi:10.1103/PhysRevLett.51.666.

[2] J. D. Reppy, ^{4}He as a dilute bose gas, Physica B+C 126 (1984) 335. doi:10.1016/0378-4363(84)90185-2.

[3] D. B. Haviland, Y. Liu, A. M. Goldman, Onset of superconductivity in the two-dimensional limit, Phys. Rev. Lett. 62 (1989) 2180–2183. doi:10.1103/PhysRevLett.62.2180.

[4] A. F. Hebard, M. A. Paalanen, Magnetic-field-tuned superconductor-insulator transition in two-dimensional films, Phys. Rev. Lett. 65 (1990) 927–930. doi:10.1103/PhysRevLett.65.927.

[5] H. S. J. van der Zant, F. C. Fritschy, W. J. Elion, L. J. Geerligs, J. E. Mooij, Field-induced superconductor-to-insulator transitions in josephson-junction arrays, Phys. Rev. Lett. 69 (1992) 2971–2974. doi:10.1103/PhysRevLett.69.2971.

[6] H. S. J. van der Zant, W. J. Elion, L. J. Geerligs, J. E. Mooij, Quantum phase transitions in two dimensions: Experiments in josephson-junction arrays, Phys. Rev. B 54 (1996) 10081–10093. doi:10.1103/PhysRevB.54.10081.

[7] M. White, M. Pasienski, D. McKay, S. Q. Zhou, D. Ceperley, B. DeMarco, Strongly interacting bosons in a disordered optical lattice, Phys. Rev. Lett. 102 (2009) 055301. doi:10.1103/PhysRevLett.102.055301.

[8] S. Krinner, D. Stadler, J. Meineke, J.-P. Brantut, T. Esslinger, Superfluidity with disorder in a thin film of quantum gas, Phys. Rev. Lett. 110 (2013) 100601. doi:10.1103/PhysRevLett.110.100601.

[9] C. D'Errico, E. Lucioni, L. Tanzi, L. Gori, G. Roux, I. P. McCulloch, T. Giamarchi, M. Inguscio, G. Modugno, Observation of a disordered bosonic insulator from weak to strong interactions, Phys. Rev. Lett. 113 (2014) 095301. doi:10.1103/PhysRevLett.113.095301.

[10] A. Oosawa, H. Tanaka, Random bond effect in the quantum spin system $(Tl_{1-x}K_x)CuCl_3$, Phys. Rev. B 65 (2002) 184437. doi:10.1103/PhysRevB.65.184437.

[11] T. Hong, A. Zheludev, H. Manaka, L.-P. Regnault, Evidence of a magnetic bose glass in $(CH_3)_2CHNH_3Cu(Cl_{0.95}Br_{0.05})_3$ from neutron diffraction, Phys. Rev. B 81 (2010) 060410. doi:10.1103/PhysRevB.81.060410.

[12] R. Yu, L. Yin, N. S. Sullivan, J. S. Xia, C. Huan, A. Paduan-Filho, N. F. Oliveira Jr, S. Haas, A. Steppke, C. F. Miclea, F. Weickert, R. Movshovich, E.-D. Mun, B. L. Scott, V. S. Zapf, T. Roscilde, Bose glass and mott glass of quasiparticles in a doped quantum magnet, Nature 489 (2012) 379. doi:10.1038/nature11406.

[13] D. Hüvonen, S. Zhao, M. Månsson, T. Yankova, E. Ressouche, C. Niedermayer, M. Laver, S. N. Gvasaliya, A. Zheludev, Field-induced criticality in a gapped quantum magnet with bond disorder, Phys. Rev. B 85 (2012) 100410. doi:10.1103/PhysRevB.85.100410.

[14] A. Zheludev, T. Roscilde, Dirty-boson physics with magnetic insulators, Comp. Ren. Phys. 14 (2013) 740 – 756. doi:https://doi.org/10.1016/j.crhy.2013.10.001.

[15] D. S. Fisher, Random transverse field ising spin chains, Phys. Rev. Lett. 69 (1992) 534–537. doi:10.1103/PhysRevLett.69.534.

[16] D. S. Fisher, Critical behavior of random transverse-field Ising spin chains, Phys. Rev. B 51 (1995) 6411. doi:10.1103/PhysRevB.51.6411.

[17] T. Vojta, Disorder-induced rounding of certain quantum phase transitions, Phys. Rev. Lett. 90 (2003) 107202. doi:10.1103/PhysRevLett.90.107202.

[18] J. A. Hoyos, T. Vojta, Theory of smeared quantum phase transitions, Phys. Rev. Lett. 100 (2008) 240601. doi:10.1103/PhysRevLett.100.240601.

[19] M. Thill, D. A. Huse, Equilibrium behaviour of quantum Ising spin glass, Physica A 214 (1995) 321. doi:10.1016/0378-4371(94)00247-Q.

[20] H. Rieger, A. P. Young, Griffiths singularities in the disordered phase of a quantum ising spin glass, Phys. Rev. B 54 (1996) 3328. doi:10.1103/PhysRevB.54.3328.

[21] O. Motrunich, S. C. Mau, D. A. Huse, D. S. Fisher, Infinite-randomness quantum Ising critical fixed points, Phys. Rev. B 61 (2000) 1160. doi:10.1103/PhysRevB.61.1160.

[22] T. Vojta, J. Schmalian, Quantum Griffiths effects in itinerant Heisenberg magnets, Phys. Rev. B 72 (2005) 045438. doi:10.1103/PhysRevB.72.045438.

[23] T. Vojta, J. A. Hoyos, Criticality and quenched disorder: Harris criterion versus rare regions, Phys. Rev. Lett. 112 (2014) 075702. doi:10.1103/PhysRevLett.112.075702.

[24] T. Vojta, Rare region effects at classical, quantum, and non-equilibrium phase transitions, J. Phys. A 39 (2006) R143. doi:10.1088/0305-4470/39/22/R01.
[25] T. Vojta, Quantum Griffiths effects and smeared phase transitions in metals: theory and experiment, J. Low Temp. Phys. 161 (2010) 299. doi:10.1007/s10909-010-0205-4.
[26] T. Vojta, Disorder in quantum many-body systems, Ann. Rev. Condens. Mat. Phys. 10 (2019) 233–252. doi:10.1146/annurev-conmatphys-031218-013433.
[27] E. Altman, A. Auerbach, Oscillating superfluidity of bosons in optical lattices, Phys. Rev. Lett. 89 (2002) 250404. doi:10.1103/PhysRevLett.89.250404.
[28] D. Pekker, B. Wunsch, T. Kitagawa, E. Manousakis, A. S. Sørensen, E. Demler, Signatures of the superfluid to mott insulator transition in equilibrium and in dynamical ramps, Phys. Rev. B 86 (2012) 144527. doi:10.1103/PhysRevB.86.144527.
[29] M. Vojta, Excitation spectra of disordered dimer magnets near quantum criticality, Phys. Rev. Lett. 111 (2013) 097202. doi:10.1103/PhysRevLett.111.097202.
[30] C. Burgess, Goldstone and pseudo-goldstone bosons in nuclear, particle and condensed-matter physics, Phys. Rep. 330 (2000) 193 – 261. doi:10.1016/S0370-1573(99)00111-8.
[31] D. Pekker, C. Varma, Amplitude/higgs modes in condensed matter physics, Ann. Rev. Condens. Mat. Phys. 6 (2015) 269–297. doi:10.1146/annurev-conmatphys-031214-014350.
[32] M. Puschmann, J. Crewse, J. A. Hoyos, T. Vojta, Collective modes at a disordered quantum phase transition, Phys. Rev. Lett. 125 (2020) 027002. doi:10.1103/PhysRevLett.125.027002.
[33] T. Giamarchi, H. J. Schulz, Anderson localization and interactions in one-dimensional metals, Phys. Rev. B 37 (1988) 325–340. doi:10.1103/PhysRevB.37.325.
[34] D. S. Fisher, M. P. A. Fisher, Onset of superfluidity in random media, Phys. Rev. Lett. 61 (1988) 1847–1850. doi:10.1103/PhysRevLett.61.1847.
[35] M. P. A. Fisher, P. B. Weichman, G. Grinstein, D. S. Fisher, Boson localization and the superfluid-insulator transition, Phys. Rev. B 40 (1989) 546–570. doi:10.1103/PhysRevB.40.546.
[36] P. B. Weichman, R. Mukhopadhyay, Critical dynamics of the dirty boson problem: Revisiting the equality $z = d$, Phys. Rev. Lett. 98 (2007) 245701. doi:10.1103/PhysRevLett.98.245701.
[37] T. Giamarchi, P. Le Doussal, E. Orignac, Competition of random and periodic potentials in interacting fermionic systems and classical equivalents: The mott glass, Phys. Rev. B 64 (2001) 245119. doi:10.1103/PhysRevB.64.245119.
[38] P. B. Weichman, R. Mukhopadhyay, Particle-hole symmetry and the dirty boson problem, Phys. Rev. B 77 (2008) 214516. doi:10.1103/PhysRevB.77.214516.
[39] C. Castellani, L. Peliti, Multifractal wavefunction at the localisation threshold, J. Phys. A 19 (1986) L429–L432. doi:10.1088/0305-4470/19/8/004.
[40] M. Schreiber, H. Grussbach, Multifractal wave functions at the anderson transition, Phys. Rev. Lett. 67 (1991) 607–610. doi:10.1103/PhysRevLett.67.607.
[41] L. J. Vasquez, A. Rodriguez, R. A. Römer, Multifractal analysis of the metal-insulator transition in the three-dimensional anderson model. i. symmetry relation under typical averaging, Phys. Rev. B 78 (2008) 1–10. doi:10.1103/PhysRevB.78.195106.
[42] A. Rodriguez, L. J. Vasquez, R. A. Römer, Multifractal analysis of the metal-insulator transition in the three-dimensional anderson model. ii. symmetry relation under ensemble averaging, Phys. Rev. B 78 (2008) 1–9. doi:10.1103/PhysRevB.78.195107.
[43] A. MacKinnon, The conductivity of the one-dimensional disordered anderson model: a new numerical method, J. Phys. C 13 (1980) L1031–L1034. doi:10.1088/0022-3719/13/35/002.
[44] A. MacKinnon, B. Kramer, The scaling theory of electrons in disordered solids: Additional numerical results, Z. Phys. B 53 (1983) 1. doi:10.1007/BF01578242.
[45] A. MacKinnon, The calculation of transport properties and density of states of disordered solids, Z. Phys. B 59 (1985) 385. doi:10.1007/BF01328846.
[46] D. Stauffer, A. Aharony, Introduction to Percolation Theory, CRC Press, Boca Raton, 1991.
[47] T. Vojta, J. Crewse, M. Puschmann, D. Arovas, Y. Kiselev, Quantum critical behavior of the superfluid-mott glass transition, Phys. Rev. B 94 (2016) 134501. doi:10.1103/PhysRevB.94.134501.
[48] C. Lerch, T. Vojta, Superfluid density and compressibility at the superfluid-mott glass transition, Eur. Phys. J. ST 227 (2019) 2275–2280. doi:10.1140/epjst/e2018-800002-2.
[49] T. Vojta, Smearing of the phase transition in Ising systems with planar defects, J. Phys. A 36 (2003) 10921–10935. doi:10.1088/0305-4470/36/43/017.
[50] M. Puschmann, T. Vojta, Superfluid-mott glass quantum multicritical point on a percolating lattice, J. Phys. Conf. Series 905 (2017) 012038. doi:10.1088/1742-6596/905/1/012038.
[51] F. Evers, A. D. Mirlin, Anderson transitions, Rev. Mod. Phys. 80 (2008) 1355–1417. doi:10.1103/RevModPhys.80.1355.

[52] H. Javan Mard, E. C. Andrade, E. Miranda, V. Dobrosavljević, Non-gaussian spatial correlations dramatically weaken localization, Phys. Rev. Lett. 114 (2015) 056401. doi:10.1103/PhysRevLett.114.056401.
[53] J. Crewse, C. Lerch, T. Vojta, Quantum critical behavior of a three-dimensional superfluid-mott glass transition, Phys. Rev. B 98 (2018) 054514. doi:10.1103/PhysRevB.98.054514.

3 CONCLUSION

In this work, we have presented many numerical results regarding two different random models, namely the random XX spin-1/2 chain and the random Bose-Hubbard model. Our results for random spin-1/2 chains are available in two papers that are closely related. In the first one, we focus more on the quantum information viewpoint of spin chains, by measuring entanglement properties and the violation of Bell inequalities. Our main result is that the correlated disorder case, i.e., the spin chain in which the odd and even sublattices are identical to each other, presents entangled spin pairs that do not violate the Bell inequality in the weak disorder regime. This feature contradicts the previously accepted concept that introducing any amount of disorder in spin chains should lead to a violation of the Bell inequality, which is indeed valid for the uncorrelated disorder case, as we have also shown.

Conversely, in the second paper, our goal was not only to report the exotic critical behavior of the correlated disorder case,[32,33] but also to confirm the strong-disorder renormalization group (SDRG) predictions for the uncorrelated case. We have shown that log-corrections to the scaling of spin-spin correlation functions may be related to system sizes below the crossover length, or due to a lack of numerical precision. Our results, however, do not refute what has been reported in Ref. (34) since the studied models are different from each other; we simply assume that the SDRG method is correct and, thus, the XX fixed point should govern the critical behavior of the random XXX spin-1/2 chain. Direct investigations on the XXX model require implementing other methods, such as the density-matrix renormalization group (DMRG). This has been accomplished in a separate project by our research group (soon to be published), in which our statements regarding the XX case remain valid for the XXX chain.

Our investigations on random spin chains have also been extended to evaluating dynamical transport properties. The motivation for this study comes from a prior work that has reported a so-called "metallic spin" behavior for the uncorrelated disordered model in the low-frequency limit.[38] This result, however, goes against what is known about the system ground state, either in the SDRG picture (i.e., the random singlet phase) or in the free fermions picture. Therefore, to show that the spin conductivity is truly zero for this system, we compute in our work both the geometric and arithmetic mean values of the conductivity, and we show that only the former, which is the relevant physical quantity, go to zero in the low-frequency limit. This work is in its final stages and should be published soon.

We are now interested in repeating these conductivity measurements for the correlated disorder case. This model, as we have shown in Chapter 2, has a much slower

decay for the spin-spin correlation functions than the uncorrelated case, which could be reflected in the behavior of the spin conductivity. There is even experimental evidence of a class of polymers exhibiting high conductivity, which can be described by a model with a correlated disorder, similar to the one used in this work.[39–41]

In the second model studied here, namely the two-dimensional (2D) random Bose-Hubbard model, we provided a more thorough analysis of the striking feature reported in Ref. (37): the existence of a delocalized lowest-energy state in a tight-binding-like Hamiltonian. Naively, one could imagine that this work questions the well-accepted result of the Anderson localization theory about the absence of extended states for noninteracting spinless systems.[17] However, we note that the variational mean-field method we employed, as explained in Chapter 2, indirectly introduces nontrivial correlations between the variables. This mean-field artifact, in principle, could be the one responsible for the delocalized Goldstone mode. Hence, a natural question that arises is to what extent are correlated variables relevant to the Anderson localization problem? This question (to the best of our knowledge) has not been as frequently investigated as other ones regarding the Anderson localization problem.

Instead of investigating the effects of correlation on the Anderson localization problem, we have been focusing on answering two more straightforward projects, which are: (*i*) measuring the localization properties of collective modes in the three-dimensional (3D) random system, and (*ii*) looking into the case where particle-hole symmetry is broken. For project (*i*) we have already gathered plenty of preliminary data; the lowest-energy modes behave similarly to what we have shown in this work for the 2D system. The higher energy states of the 3D system, however, can undergo a localization-delocalization transition, in which we have determined a critical behavior compatible with the usual noninteracting spinless problem. On the other hand, project (*ii*) is still in its beginning, but we have already verified that the computational effort should be greatly increased in comparison to the particle-hole symmetric case.

In summary, we have shown in this work that the introduction of randomness in condensed matter systems can lead to compelling and unexpected behavior. As one breaks translational invariance, however, most known analytical methods become inapplicable, thus requiring an unwelcome overreliance on numerical methods to study random systems. These studies have in general a high computational cost since the physical quantities are obtained by averaging over a relatively large number of samples. In addition, numerical methods are always prone to systematic measurement errors, given the inevitable rounding-off of floating-point operations. Nevertheless, research on random systems has shown to be very rewarding by the many novel features observed, and also by bringing the theoretical models closer to what real-world matter looks like.

REFERENCES

1 TAYLOR, P. L.; HEINONEN, O. **A quantum approach to condensed matter physics**. Cambridge: Cambridge University Press, 2002.

2 FETTER, A. L.; WALECKA, J. D. **Quantum theory of many-particle systems**. 2nd. ed. Mineola: Dover, 2003.

3 WEN, X.-G. **Quantum field theory of many-body systems:** from the origin of sound to an origin of light and electrons. Oxford: Oxford University Press, 2004.

4 SANDER, L. M. **Advanced condensed matter physics**. Cambridge: Cambridge University Press, 2009.

5 ALTLAND, A.; SIMONS, B. **Condensed matter field theory**. 2nd. ed. Cambridge: Cambridge University Press, 2010.

6 MAHAN, G. D. **Condensed matter in a nutshell**. Princeton: Princeton University Press, 2011.

7 SHANKAR, R. **Quantum field theory and condensed matter:** an introduction. Cambridge: Cambridge University Press, 2017.

8 EDIGER, M. D.; ANGELL, C. A.; NAGEL, S. R. Supercooled liquids and glasses. **The Journal of Physical Chemistry**, American Chemical Society, v. 100, n. 31, p. 13200–13212, 1996.

9 BERTHIER, L.; BIROLI, G. Theoretical perspective on the glass transition and amorphous materials. **Reviews of Modern Physics**, American Physical Society, v. 83, n. 2, p. 587–645, 2011.

10 BERTHIER, L.; EDIGER, M. D. Facets of glass physics. **Physics Today**, AIP Publishing, v. 69, n. 1, p. 40–46, 2016.

11 FOWLER, A. B. A semicentury of semiconductors. **Physics Today**, AIP Publishing, v. 46, n. 10, p. 59–62, 1993.

12 SEITZ, F. Research on silicon and germanium in world war II. **Physics Today**, AIP Publishing, v. 48, n. 1, p. 22–27, 1995.

13 ROSS, I. M. The foundation of the silicon age. **Physics Today**, AIP Publishing, v. 50, n. 12, p. 34–39, 1997.

14 RIORDAN, M.; HODDESON, L. The moses of silicon valley. **Physics Today**, AIP Publishing, v. 50, n. 12, p. 42–47, 1997.

15 ANDERSON, P. W. Absence of diffusion in certain random lattices. **Physical Review**, American Physical Society, v. 109, n. 5, p. 1492–1505, 1958.

16 EDWARDS, J. T.; THOULESS, D. J. Numerical studies of localization in disordered systems. **Journal of Physics C:** solid state physics, IOP Publishing, v. 5, n. 8, p. 807–820, 1972.

17 ABRAHAMS, E. *et al.* Scaling theory of localization: absence of quantum diffusion in two dimensions. **Physical Review Letters**, American Physical Society, v. 42, n. 10, p. 673–676, 1979.

18 EFETOV, K. B. Supersymmetry and theory of disordered metals. **Advances in Physics**, Taylor & Francis, v. 32, n. 1, p. 53–127, 1983.

19 KRAMER, B.; MACKINNON, A. Localization: theory and experiment. **Reports on Progress in Physics**, IOP Publishing, v. 56, n. 12, p. 1469–1564, 1993.

20 EVERS, F.; MIRLIN, A. D. Anderson transitions. **Reviews of Modern Physics**, American Physical Society, v. 80, n. 4, p. 1355–1417, 2008.

21 SACHDEV, S. **Quantum phase transitions**. Cambridge: Cambridge University Press, 2000.

22 VOJTA, T. Phases and phase transitions in disordered quantum systems. **AIP Conference Proceedings**, v. 1550, n. 1, p. 188–247, 2013.

23 HARRIS, A. B. Effect of random defects on the critical behaviour of ising models. **Journal of Physics C:** solid state physics, IOP Publishing, v. 7, n. 9, p. 1671–1692, 1974.

24 IMRY, Y.; MA, S.-k. Random-field instability of the ordered state of continuous symmetry. **Physical Review Letters**, American Physical Society, v. 35, n. 21, p. 1399–1401, 1975.

25 MA, S. K.; DASGUPTA, C.; HU, C. H. Random antiferromagnetic chain. **Physical Review Letters**, v. 43, n. 19, p. 1434, 1979.

26 DASGUPTA, C.; MA, S. K. Low-temperature properties of the random Heisenberg antiferromagnetic chain. **Physical Review B**, v. 22, n. 3, p. 1305, 1980.

27 FISHER, D. S. Random transverse field ising spin chains. **Physical Review Letters**, American Physical Society, v. 69, n. 3, p. 534–537, 1992.

28 FISHER, D. Random antiferromagnetic quantum spin chains. **Physical Review B**, v. 50, n. 6, p. 3799–3821, 1994.

29 FISHER, D. Critical behavior of random transverse-field Ising spin chains. **Physical Review B**, v. 51, n. 10, p. 6411–6461, 1995.

30 IGLÓI, F.; MONTHUS, C. Strong disorder RG approach of random systems. **Physics Reports**, v. 412, n. 5-6, p. 277, 2005.

31 IGLÓI, F.; MONTHUS, C. Strong disorder rg approach – a short review of recent developments. **The European Physical Journal B**, v. 91, n. 11, p. 290, 2018.

32 HOYOS, J. A. *et al.* Protecting clean critical points by local disorder correlations. **Europhysics Letters**, v. 93, n. 3, p. 30004, 2011.

33 GETELINA, J. C.; ALCARAZ, F. C.; HOYOS, J. A. Entanglement properties of correlated random spin chains and similarities with conformally invariant systems. **Physical Review B**, v. 93, n. 4, p. 045136, 2016.

34 SHU, Y. R. *et al.* Properties of the random-singlet phase: from the disordered Heisenberg chain to an amorphous valence-bond solid. **Physical Review B**, v. 94, n. 17, p. 1, 2016.

35 ALTMAN, E.; AUERBACH, A. Oscillating superfluidity of bosons in optical lattices. **Physical Review Letters**, American Physical Society, v. 89, n. 25, p. 250404, 2002.

36 PEKKER, D. *et al.* Signatures of the superfluid to mott insulator transition in equilibrium and in dynamical ramps. **Physical Review B**, American Physical Society, v. 86, n. 14, p. 144527, 2012.

37 PUSCHMANN, M. *et al.* Collective modes at a disordered quantum phase transition. **Physical Review Letters**, American Physical Society, v. 125, n. 2, p. 027002, 2020.

38 MOTRUNICH, O.; DAMLE, K.; HUSE, D. A. Dynamics and transport in random quantum systems governed by strong-randomness fixed points. **Physical Review B**, American Physical Society, v. 63, n. 13, p. 134424, 2001.

39 MACDIARMID, A. G. *et al.* Polyaniline: a new concept in conducting polymers. **Synthetic Metals**, v. 18, n. 1-3, p. 285–290, 1987.

40 DUNLAP, D. H.; WU, H.-L.; PHILLIPS, P. W. Absence of localization in a random-dimer model. **Physical Review Letters**, v. 65, n. 1, p. 88–91, 1990.

41 WU, H.-L.; PHILLIPS, P. Polyaniline is a random-dimer model: a new transport mechanism for conducting polymers. **Physical Review Letters**, v. 66, n. 10, p. 1366–1369, 1991.